AD_____

Award Number: DAMD17-98-C-8040

TITLE: Combinatorial Strategies and Hypothesis-Based Drug Design in Drug Discovery Targeted to the Protease and Channel Activities of Botulinum Toxin A

PRINCIPAL INVESTIGATOR: Mauricio Montal, M.D., Ph.D.

CONTRACTING ORGANIZATION: University of California, San Diego
La Jolla, California 92093-0934

REPORT DATE: January 2002

TYPE OF REPORT: Final

PREPARED FOR: U.S. Army Medical Research and Materiel Command
Fort Detrick, Maryland 21702-5012

REPORT DOCUMENTATION PAGE

Form Approved
OMB No. 074-0188

1. AGENCY USE ONLY (Leave blank)	2. REPORT DATE	3. REPORT TYPE AND DATES COVERED
	January 2002	Final (1 Jul 98 - 31 Dec 01)

4. TITLE AND SUBTITLE
Combinatorial Strategies and Hypothesis-Based Drug Design in Drug Discovery Targeted to the Protease and Channel Activities of Botulinum Toxin A

5. FUNDING NUMBERS
DAMD17-98-C-8040

6. AUTHOR(S)
Mauricio Montal, M.D., Ph.D.

7. PERFORMING ORGANIZATION NAME(S) AND ADDRESS(ES)
University of California, San Diego
La Jolla, California 92093-0934

E-Mail: mmontal@.ucsd.edu

8. PERFORMING ORGANIZATION REPORT NUMBER

9. SPONSORING / MONITORING AGENCY NAME(S) AND ADDRESS(ES)
U.S. Army Medical Research and Materiel Command
Fort Detrick, Maryland 21702-5012

10. SPONSORING / MONITORING AGENCY REPORT NUMBER

11. SUPPLEMENTARY NOTES
Report contains color

12a. DISTRIBUTION / AVAILABILITY STATEMENT
Approved for Public Release; Distribution Unlimited

12b. DISTRIBUTION CODE

13. ABSTRACT *(Maximum 200 Words)*

The ultimate goal of this program is to understand in detail the mechanisms by which botulinum neurotoxins (BoNT) abrogate neurotransmitter release. One facet is focused on the channel-forming domain of the heavy chain (HC). The aim is to identify open channel blockers as a single class of drugs that would be effective against all BoNT isoforms. A major objective is to seek direct demonstration that the HC acts as the molecular conduit for the light chain (LC) thereby allowing the protease activity to reach the cytosol where it acts. Accordingly, purified HC is first reconstituted in lipid bilayers and the direct translocation of isolated LC through the HC channel is measured by single channel recordings and also by direct analytical determination of the LC protease activity. A second facet of the program involves the concept that the peptide products of substrate proteolysis by BoNTs uncouple excitation from secretion pointing to new means of intervention. This notion, discovered for BoNT A, appears to be valid for other BoNT isoforms thereby yielding a diverse repertoire of peptide sequences that may provide insights into the molecular interactions between partner proteins involved in membrane fusion. It is anticipated that this concerted and focused approach will uncover lead compounds that may be developed into selective drugs targeted to prevent or relieve the neurotoxic actions of BoNT.

14. SUBJECT TERMS
Bothulinum neurotoxins; neurotoxicity; neurotransmission; ion channels; proteases; drug design

15. NUMBER OF PAGES
82

16. PRICE CODE

17. SECURITY CLASSIFICATION OF REPORT	18. SECURITY CLASSIFICATION OF THIS PAGE	19. SECURITY CLASSIFICATION OF ABSTRACT	20. LIMITATION OF ABSTRACT
Unclassified	Unclassified	Unclassified	Unlimited

FOREWORD

Opinions, interpretations, conclusions and recommendations are those of the author and are not necessarily endorsed by the U.S. Army.

MM Where copyrighted material is quoted, permission has been obtained to use such material.

___ Where material from documents designated for limited distribution is quoted, permission has been obtained to use the material.

___ Citations of commercial organizations and trade names in this report do not constitute an official Department of Army endorsement or approval of the products or services of these organizations.

N/A In conducting research using animals, the investigator(s) adhered to the "Guide for the Care and Use of Laboratory Animals," prepared by the Committee on Care and use of Laboratory Animals of the Institute of Laboratory Resources, national Research Council (NIH Publication No. 86-23, Revised 1985).

N/A For the protection of human subjects, the investigator(s) adhered to policies of applicable Federal Law 45 CFR 46.

N/A In conducting research utilizing recombinant DNA technology, the investigator(s) adhered to current guidelines promulgated by the National Institutes of Health.

N/A In the conduct of research utilizing recombinant DNA, the investigator(s) adhered to the NIH Guidelines for Research Involving Recombinant DNA Molecules.

N/A In the conduct of research involving hazardous organisms, the investigator(s) adhered to the CDC-NIH Guide for Biosafety in Microbiological and Biomedical Laboratories.

M. Monn 12/21/01

Award Number: DAMD17-98-C-8040

TITLE: Combinatorial Strategies and Hypothesis-Based Drug Design in Drug Discovery Targeted to the Protease and Channel Activities of Botulinum Toxin A

PRINCIPAL INVESTIGATOR: Mauricio Montal, M.D., Ph.D.

TABLE OF CONTENTS

INTRODUCTION AND SCOPE

The ultimate goal of this program is to understand in detail the mechanisms by which botulinum neurotoxins (BoNT) abrogate neurotransmitter release. *Clostridial* neurotoxins act as sequence specific endoproteases to cleave specific constituents of the synaptic vesicle docking/fusion complex [1-6]. A widely held view considers that BoNTs enter cells via receptor-mediated endocytosis. Exposure of the holotoxin to the acidic pH of the endosomal vesicles induces a conformational change of the dichain toxin allowing the heavy chain (HC) to insert into the membrane thereby forming a channel through which the light chain (LC) protease is translocated to the cytosol where it acts [3]. This model considers a tri-modular design of the neurotoxin protein with a receptor binding domain, a translocation domain and a catalytic domain. Indeed, the crystal structures of BoNT A [7,8] and BoNT E [9] have disclosed such organization of the holotoxin and have given impetus to dissect in molecular detail the steps involved in intoxication. We focused our efforts on two enigmatic aspects of the process: (1) The mechanism by which the HC forms the conduit for the translocation of the LC across a membrane; and (2) the contribution of the peptide products of BoNT protease activity on its substrates, namely, the components of the SNARE-complex [1-4].

That channels are formed by the HC has been surmised from evidence that the holotoxin forms channels in lipid bilayers, predominantly after exposure to an acidic pH [10-12; for review see ref. 13]. Further, a 23-mer peptide, patterned after the sequence of an amphipathic segment of the HC [659-681] predicted to self-assemble in membranes into a conductive oligomer, was shown to form channels in lipid bilayers [14]. Thus far, however, there is no evidence for the direct translocation of the LC through the putative channel and across the membrane. Several outstanding issues remain to be delineated. Key among these are the dissociation at acidic pH of the dichain toxin into its constituent LC and HC after breakdown of the disulfide bond linking them [Cys429-Cys453], the insertion of the HC monomers into the bilayer hydrophobic core, the oligomerization state of the HC when assembled into a conductive channel, the requirement of a pH gradient across the membrane, the unfolding of the LC in an acidic environment as a requirement for its passage through a narrow pore (the folded LC is 55 Å X 55 Å X 62 Å, too large to fit through a postulated tetrameric channel of ~12 Å

diameter at its widest extent), the refolding of the LC in the cytosol after its translocation. It is clear that a channel entity would constitute a critical target for intervention to abort the process of intoxication after internalization of the toxin. Screening for channel blockers was a dominant aspect of the program.

This brings us to the second facet of the program. The crystal structure of a SNARE complex, a key entity involved in the specific recognition and ultimately fusion of synaptic vesicles with the neuronal plasma membrane was described [2]. The complex is formed by the specific interaction between segments of three proteins: synaptobrevin-2, a vesicle associated protein, and syntaxin-1A and SNAP-25, two distinct proteins anchored to the plasma membrane. The SNARE complex folds into a parallel four-helical bundle with a left handed superhelical twist [2,4]: two helices are contributed by a molecule of the t-SNARE SNAP-25; the other two by synaptobrevin and syntaxin. We synthesized three peptides which correspond to sequences located in the syntaxin-1A H3 domain, the C-terminal domain of SNAP-25, and a conserved central domain of synaptobrevin-2, that exhibit a high propensity to form a minimal coiled-coil, and examined their ability to assemble into a coiled-coil using circular dichroism (CD) spectroscopy (Appendix #4) [15]. Our results with these synthetic peptides [15] are consistent with the high-resolution structure of the SNARE complex [2,4]. The four helical bundle structure of the SNARE complex may bring into juxtaposition the surfaces of the apposed vesicle and plasma membrane bilayers to facilitate fusion. How this may happen is not known, however, Ca^{2+} is required and other proteins may catalyze and confer additional specificity to the process (Appendices #2 and #3) [5,6].

BoNTs proteolytically cleave the three proteins of the SNARE complex, consequently preventing vesicle fusion and thereby abrogating transmitter release [3]. Our program focused on the cleavage fragments resulting from BoNT-mediated substrate proteolysis and the emerging hypothesis that the efficacy of BoNTs as inhibitors of neurosecretion may arise from the synergistic action of cleaving the substrate and releasing peptide products that disable the fusion process by blocking specific steps of the exocytotic cascade (Appendices # 1, #4 and #6)[16-18]. Indeed, synthetic peptides corresponding to the sequences of the cleavage products of BoNT A and E act as inhibitors of

neurosecretion, and mimic several aspects of the neurotoxin action *in vitro* [16-18]. Accordingly, effort was directed to achieve the stable expression of the SNAP-25 C-terminal cleavage product of BoNT E in mammalian neurosecretory cells and to compare its activity with that of the expressed LC of BoNT E. As summarized in the BODY of the report, we implemented a robust assay for basal and evoked exocytosis in PC-12 cells and demonstrated the inhibitory activity of expressed BoNT A, BoNT C and BoNT E LCs on secretion of human growth hormone, used as the marker for secretory granules. Further, structural dissection of syntaxin 1a revealed a minimal inhibitory construct containing the transmembrane domain and two of three helical subdomains of the H3 coil participating in SNARE complex formation. Structural dissection of SNAP-25 revealed that the large cleavage products of both LC A and E also inhibit regulated secretion in PC12 cells. And greater inhibitory activity was conferred to the full length SNARE motif of SNAP-25 by linking it to the transmembrane domain of syntaxin 1a. These results further elucidate the molecular interactions underlying the role of SNARE proteins in neurosecretion, pointing to the significance not only of protein sequence and structure, but also membrane localization in regulated exocytosis.

BODY

Task 1: Characterization of the ion channel of BoNT A and identification of open channel blockers.

During the tenure of the current contract (DAMD 17-98-C-8040), efforts were directed towards the elucidation of the steps involved in the translocation of the BoNT A LC through the HC channel. At present there is no compelling evidence to account for the molecular details of this elusive process. It is widely recognized that acidic pH, comparable to that present in endocytic vesicles (pH≤5.0), triggers a conformational change that drives the insertion of the HC into membranes and presumably allows the formation of a transmembrane channel for the transfer of the LC. There is biophysical evidence for the formation of channels with a conductance of ~100 pS in 0.5 M KCl or NaCl solutions. This conductance suggests a channel with a pore diameter of ~12 Å [19]. How does this model fit with the crystal structure of the holotoxin? The folded LC in the crystal structures obtained at pH 7.0 for BoNTA and pH 6.0 for BoNTB is ≥ 55 Å (55 Å X 55Å X 62 Å) if considered as a

globular structure; such dimensions would render it impermeant through a ~12 Å pore. These considerations imply that the LC may unfold and go through the channel presumably unstructured and, therefore, would have to refold after exiting the channel in the neutral pH of the cytosol, which would allow its ultimate release by reduction of the interchain disulfide linkage. At present, there is no high resolution structure for these two BoNTs at a pH lower than 6.0; and given the fact that the crystal structures of BoNTA (pH 7.0) and BoNTB (pH 6.0) are very similar it is reasonable to surmise that a pH<6 drives the structural switch. A striking feature of the the crystal structures of BoNTA and B is the translocation domain "belt", a ~50-residues long unstructured loop that wraps around the catalytic domain. This segment may undergo a structural transition that favors insertion of the translocation domain into the membrane and promotes its oligomerization to form a conductive channel.

Is there evidence for protein translocation across channels? The most persuasive data have been obtained for the translocation of the catalytic domain of diphteria toxin by its translocation domain [20,21] and for the protein conducting channels of the mitochondria [22-24] and the endoplasmic reticulum [25]. For the protein-conducting channel of the outer mitochondrial membrane -Tom40, there is evidence not only for the formation of channels but also for the translocation of peptides across the channel. Tom40, when purified and reconstituted in lipid bilayers, formed channels with conductances in the range 220 to 360 pS in 0.25 M KCl, and an estimated pore diameter of ~20 Å [22,25]. Significantly, the open channel probability of the Tom40 channel was drastically reduced by the addition of synthetic peptides with a sequence corresponding to the native mitochondrial preprotein sequences when added to the same side of the membrane (*cis*) as Tom40. This suppressive effect was sequence specific and could not be reproduced by peptides of similar hydrophobic and charge density. These findings suggest that the translocated peptide transiently occludes the channel during its transit across it. And, the data also constrain the secondary structure of the precursor polypeptides to be extended or as α-helical segments in order to fit into a channel of ~20 Å in diameter.

To address these questions, a functional strategy was designed which relied on the assay of the channel activity

of BoNTs holotoxin and the individual chains in lipid bilayers using single channel recordings as a sensitive readout to interrogate if the LC blocks the HC channel as it goes through. Both native and recombinant BoNTs holotoxin and the individual chains were used in the analysis.

Properties of native BoNTA holotoxin and HC channels

The properties of native BoNTA holotoxin and BoNTA HC single channels were studied according to the following protocol: After bilayer stabilization, the toxin samples were always added to *cis* solution and two min later, the *cis* solution was acidified to pH 5.5 with 2.5 mM citrate. The lipid composition of the bilayer was optimized to enhance the insertion of holotoxin and HC and consisted of diphytanoylphosphatidylethanolamine (PE), diphytanoylphosphatidylcholine (PC) and diphytanoylphosphatidylserine (PS) (Avanti Polar Lipids, Alabaster, AL), and GT1b gangliosides (Fidia Research Laboratories, Abano, Italy) at a weight ratio 2:2:1:0.125, as described in the Quarterly Reports for DAMD 17-98-C-8040 corresponding to period 7/1/00-10/1/00. Under these conditions, BoNTA holotoxin does not form channels. Notably, reduction of the holotoxin in the presence of 1 mM dithiothreitol (DTT), either by preincubation for 30 min at 37°C prior to the bilayer experiments or by direct addition of reductant to the aqueous compartments containing the holotoxin, elicits channel activity. The modified (reduced) BoNTA holotoxin forms channels with primary conductances (γ) in symmetric 0.5 M KCl of ~ 110 pS. A subconductance state is readily identifiable in the single channel recordings. The subconductane state has a γ ~ 20 pS. Transitions from the closed to the fully open state and from the substate to the closed and open state can be identified. These intermediate states are usually short lived, and the transitions between states are rather fast giving a flickery appearance to the records. At higher time resolution individual transitions are clearly discrete, square events. Discrete events with larger ($\geq$ 200 pS) conductances are also discerned. Their occurrence is sporadic and the channel open times are significantly shorter than those of the primary conductances. This pattern of channel activity is reminiscent of that recorded with tetanus holotoxin in lipid bilayers [26], and with BoNTA holotoxin in PC12 cells [27]. By contrast, native unmodified (unreduced) BoNTA HC forms channels similar to

those recorded with reduced holotoxin, under otherwise identical conditions. Representative segments of recordings obtained with native BoNTA holotoxin and HC are shown in Fig. 1A and 1B, respectively. The applied voltage was -100 mV and a downward deflection indicates channel opening. Corresponding cumulative current histograms and Gaussian fits for the primary conductances generated from continuous segments of recordings lasting several minutes are shown on the right panels. The peak of the currents of the closed (C) and open (O) states are indicated. The probability of the channel being open (P_o) is 0.56 for native holotoxin (Fig. 1A) and 0.55 for native HC (Fig. 1B). Note that for the HC, the calcualted γ = 128 pS includes the substate.

A salient aim of the current program has been to generate recombinant BoNT HC as a key tool to pursue a low resolution mapping of the relationship between the structure of the protein with its channel function. This requires demonstration of channel activity by recombinant BoNT HC and comparison of the channel properties with those of native HC. We succeeded in generating recombinant HC, as reported in the Quarterly Report for DAMD 17-98-C-8040 corresponding to period 4/1/00-7/1/00. The recombinant HC was purified, reconstituted into lipid bilayers and its properties compared with respect to those of native BoNT under otherwise identical conditions. Figure 1C shows a segment of a single channel record displaying the features of the recombinant HC channels and the corresponding current histogram. The pattern of activity of the recombinant HC is similar to that of the native reduced BoNT and native HC in terms of single channel conductance (γ = 96 pS), occurrence of substates (γ ~ 20 pS), bursting episodes of high channel activity interspersed between quiescent periods (P_o = 0.48). To the extent of the sensitivity of the assay the native and recombinant HC channels appear analogous; neither of them require reducing conditions to evoke channel activity. These findings set the stage for investigations on the role of the LC on HC channel activity and on the involvement of specific HC residues on the channel lining and, in due turn, on the structure of the binding pocket for blockers. Such analysis is feasible by site-directed mutagenesis on the recombinant BoNTA clone followed by expression of mutant proteins and reconstitution in lipid bilayers assayed by single channel recordings.

What is the influence of the light chain on the channels formed by heavy chain? Significantly, native or recombinant LC by itself does not form channels in lipid bilayers. In contrast, in the absence of reducing agent, the isolated BoNTA LC causes a change in the pattern of channel activity of BoNTA HC. This activity is elicited by both the native and recombinant LC on both the native and recombinant HC channels. We demonstrated blocking of the HC channels by addition of a 2-fold molar excess LC to the *trans*-compartment in the absence of reducing agent (Fig. 2). The pattern of channel activity of the HC in absence of the LC is characterized by the occurrence of frequent and fast transitions between open and closed states. A sample record obtained at V= -100 mV displayed in Fig. 2A. Corresponding cumulative current histograms and Gaussian fits for the primary conductance are shown on the right panels: γ = 124 pS with a subconductance state of γ ~ 20 pS and a P_o = 0.47. The presence of the LC in the *trans*-compartment (Fig. 2B) sharply attenuated the channel activity of HC both in terms of a reduction in single channel conductance (γ = 30 pS), and in the number of open channels at any given time. During the bursts of channel activity, the frequency of transitions between open and closed states increased and adopted a flickery pattern in which individual, discrete transitions were difficult to resolve. This pattern is characteristic of channel block and arises from frequent fast interruptions of the residence time in the open state leading to a blocked state. Furthermore, this silencing effect of the LC on the HC channels was independent of the polarity of the applied voltage. Thus, LCA attenuates and eventually silences the HCA channel.

Table 1 summarizes the experimental conditions used thus far to examine in detail the postulated mechanism for the translocation of LC through a HC channel. The model considers at least six independent steps, in the sequence: binding of holotoxin to gangliosides on bilayer surface → acidification-induced conformational change of holotoxin in the *cis*-compartment →insertion of the HC into the lipid bilayer →expression of channel activity → LC (presumably unfolded) translocation through the HC channel → enzymatic activity of the translocated (presumably refolded) LC in the *trans* compartment. The most telling results with the holotoxin emerge by examining the contrasting findings generated by the location of the membrane non-permeable reductant Tris-(2-carboxyethyl)phosphine (TCEP) in the *cis*

or the *trans* compartments, under otherwise identical conditions (Table 1, Conditions 4 and 5): binding, acidification, and insertion steps appear to proceed similarly; however, reduction in the *cis* compartment presumably allows the released LC to occlude the HC channel, whereas the reduction on the *trans* compartment leaves the HC channel activity unaltered. This model implies that free LC silences or blocks the HC channel. This prediction was tested using the isolated HC and LC and addressing the specific effect of the LC on HC channels depending on its location in the *cis* or the *trans* compartments (Table 1, Conditions 8, 9): A five-fold molar excess of LC present on the *cis* compartment, in the absence of reductant does not affect the HC channel activity. By contrast, a two-fold molar excess of LC present on the *trans* compartment attenuates and eventually silences the HC channel activity. The latter results imply that a unique orientation and probably open state of the HC channel provides an entryway for the LC to access the pore.

The picture that emerges from this systematic analysis is that the HC can be blocked by the free LC, consistent with the notion that the unfolded LC could be translocated through the HC channel. The most tempting explanation for these results is that the LC partially unfolds in the acidic vesicle environment, goes through the channel formed by the HC and is released on the other side of the membrane (cytosol) by reducing agents. The complete analysis requires the demonstration of the enzymatic activity of the LC protease after its translocation into the *trans* compartment from the *cis* compartment. This is currently under way.

Open channel blockers of the BoNT HC channel

Several "classes" of agents were surveyed based on their blockade efficacy of other cation-selective channels. Antimalarial agents such as chloroquine and quinacrine, known to affect intracellular processing of BoNTs by collapsing the pH gradient across endocytic vesicle, exert a direct blocking action on the HC channel [28] in the μM concentration range. A sample recording illustrating the effect of 10 μM quinacrine (6-chloro-9-([4-diethylamino]-1-methylbutyl)amino-2-methoxyacridine) is illustrated in Fig. 3. Figure 3A shows a segment of a single channel record displaying the features of the holotoxin channels; the corresponding single-channel current histogram shows the

fitted Gaussian distribution with a calculated γ = 112 pS and a P_o = 0.54. In contrast, in the presence of quinacrine, the pattern of channel activity is drastically altered: the frequency of openings is reduced and long quiescent periods dominate the records, as illustrated in the record shown in Fig. 3B. The corresponding conductance histogram displays a single distribution corresponding to the closed state. This is characteristic of channel block. Antiviral agents such as amantadine, an anti-influenza drug which acts by blocking the channels formed by the M2 protein of influenza virus [29-31], or its analogue -memantine (1-amino-3,5-dimethyladamantane)- a well known, clinically tolerated open channel blocker of the NMDA-subtype of glutamate receptor [32,33] also block the HC channel. Memantine, however, blocks the NMDA receptor channel with a Ki of 300 nM whereas it blocks the HC channel at concentrations $\geq$ 20 μM. Remarkably, a selectively guanidinylated memantine derivative, kindly synthesized for us by the group of Prof. Murray Goodman in the Chemistry and Biochemistry of UCSD, exerts blocking activity at 2 μM, suggesting that the increase in size and presence of the charged guanidinium group may promote the interaction of the blocker with the channel. By contrast, compounds such as 4-aminopyridine and 3,4-diaminopyiridine, known blockers of K^+ channels [cf. 34], did not affect the BoNT HC channel even in the mM concentration range. Interestingly, these aminopyridines transiently attenuate the channel conductance suggesting that they may even go through the channel and behave as permeant cations. QX-222, a trimethyl quaternary ammonium derivative of the ionizable amine local anesthetic lidocaine [cf. 34], is a blocker of voltage-gated cation-selective channels and also of the nicotinic cholinergic receptor channel [cf. 34]. QX-222 also blocks the BoNT HC channel in the μM concentration range. This is illustrated in Fig. 4. A segment of a continuous record displaying the activity of approximately five BoNT holotoxin channels with γ ~ 110 pS is shown in Fig. 4A. Note in the conductance histogram the occurrence of five discernible peaks, excluding the closed state. In contrast, in the presence of 40 μM QX-222 the channel activity is reduced to the extent that the channels appear to be primarily blocked giving rise to single distribution in the corresponding current histogram, as illustrated in Fig. 4B.

The information summarized establishes the feasibility of this strategy to discover novel and selective open channel blockers, which we intend to apply to the BoNT HC

channel. This is precisely what the new proposal submitted intends to achieve (See Reportable Outcomes).

Task 2: Role of the peptide products of BoNT protease activity on neurotransmitter release.

Many studies in the past three years have examined SNARE assembly and inhibition of complex formation by these toxins in relation to the kinetics and regulation of exocytosis [35-38]. In this laboratory, *in-vitro* studies were performed examining the activity of these toxin cleavage products as potential inhibitors of exocytosis (Appendices #1, #2, #4 and #6) [16-18]. The 26 amino acid C-terminal peptide released by cleavage of SNAP-25 with BoNT E was introduced into permeabilized chromaffin cells as well as *Aplysia* neurons to study the impact on neurotransmitter release. It was concluded that the peptide, termed ESUP, inhibits vesicle docking and thus exocytosis by competing with SNAP-25 for coil formation within the SNARE complex. From these studies the question arose: How does the stable expression of the SNAP-25 C-terminal cleavage product of BoNT E modulate neurosecretion in mammalian neurosecretory cells? As described in the Midterm Report, the 26-mer C-terminal fragment of SNAP-25 was subcloned into a mammalian expression vector, transfected into neurosecretory PC12 cells and the impact on exocytosis assessed [39]. The results indicate that in this mammalian expression system, BoNT LC A, LC C and LC E inhibit exocytosis, whereas the ESUPs tested have little if any effect.

This analysis was pursued by using transient overexpression of SNARE proteins, peptides and BoNT LCs in PC12 cells in order to examine the interactions of SNARE helices in a mammalian neurosecretory cell expression system. Using the published SNARE complex structure [2,4], we designed a series of partial syntaxin 1a and SNAP-25 constructs, one of which blocks secretion as effectively as BoNT LC C when overexpressed in PC12 cells. We also find that peptide sequences known to inhibit exocytosis when introduced as peptides into permeabilized cells do not display equivalent activity in this cell expression system. Interestingly, the transmembrane domain of syntaxin enhances inhibitory activity of a number syntaxin peptide constructs, and confers activity to inert SNAP-25 peptide fragments when linked as a fusion chimera. Localization studies indicate that the peptide fragments

alone are expressed in the cytosol, whereas those linked to the syntaxin transmembrane domain are targeted to the membrane compartments of the cell. These results further elucidate the role of the transmembrane domain of syntaxin in regulated exocytosis, and indicate that SNARE interactions *in vivo* may be subject to more complex regulation than those observed *in vitro*, relying on location as well as structural interactions to mediate membrane fusion.

Experimental Procedures:

The experimental procedures to generate the DNA constructs, for cloning, PC12 cell culture and transfection, the secretion and ELISA assays, were described in the Midterm Report. We proceed now to describe additional procedures used since the submission of the Midterm Report.

HEK-293 culture and transfection. HEK-293 cells (provided by William Romanov at UCSD) were plated at 50-80% confluency one day prior to transfection. Cells were transfected using GenePorter2 reagent according to manufacturer's instructions. For immunofluorescence studies, cells were plated onto poly-L-lysine/borate treated coverslips in 24-well culture plates and transfected with 0.5-1.0 μg/well of DNA. Cells were processed for immunofluorescence staining 48 hours after transfection. For Western blot studies, cells were plated into poly-D-lysine or poly-L-lysine/borate treated 12-well tissue culture plates and transfected with 1-2 μg/well of DNA. Cells were extracted for SDS-PAGE and Western blotting analysis 48 hours after transfection

Indirect immunofluorescence. Transfected HEK-293 cells were fixed in PFA (4% paraformaldehyde in phosphate buffer saline -PBS, pH 7.4) for 15-30 minutes at room temperature, washed three times in PBS, permeabilized in PBS/0.2% Triton-X 100/0.1M Glycine for 5-10 minutes, washed three times in PBS and then blocked for 1 hour in 10% Goat or Horse serum in PBS. Primary antibodies were applied in blocking buffer at 4°C overnight. After three washes in PBS, secondary antibodies were applied in blocking buffer for 1-2 hours at room temperature, washed three times in PBS, mounted onto slides using VectaShield and viewed using an Olympus Fluorescent microscope, 60X water immersible objective lens. Images were captured via a CCD camera and processed using MetaMorph and Photoshop software.

SDS-PAGE and Western blotting. Transfected HEK-293 cells were extracted in 0.1ml/well 1% SDS containing a protease inhibitor cocktail and boiled for 10 minutes. Laemmli sample buffer with β-mercaptoethanol was added and samples were boiled an additional 5 minutes, run on 12% Tris/Glycine gels and transferred to Immobilon PVDF membrane. Membranes were blocked in 5% nonfat milk in TBST (50mM Tris, 150mM NaCl, 0.1% Tween-20, pH 7.5) for one hour, primary antibodies were applied in blocking buffer at 4°C overnight, washed three times in TBST, then secondary antibodies were applied in blocking buffer for 1-2 hours at room temperature. After washing in TBST, blots were developed using the NBT/BCIP colorimetric reaction.

We turn now to summarize the new findings.

BoNT LCC is a more potent inhibitor of ATP-evoked hGH secretion in PC12 cells than LCE or LCA.

To compare the activities of BoNT A, E and C and to establish a positive control for inhibition of exocytosis in the PC12 cell secretion assay, constructs encoding the three toxin light chains were each transiently cotransfected into PC12 cells with the human growth hormone (hGH) marker plasmid. ATP-evoked hGH secretion was measured 72 hours later, as described. In this system using these clones, we found that LCC inhibited secretion most strongly (76.2% ± 7.7%, n=8 duplicates), followed by LCE (56.9% ± 14.6%, n=7 duplicates) and LCA (48.8% ± 10.3%, n=6 duplicates) in descending order of potency (Fig. 5). LCC was therefore established as the endpoint for inhibition for this assay, against which SNARE protein constructs were compared for their efficacy in suppressing secretion.

Syntaxin is the only SNARE protein which interferes with ATP-evoked exocytosis when overexpressed in PC12 cells.

To determine inhibitory activity of SNAREs and some of their associated proteins, whole protein-encoding constructs were tested for their ability to block ATP-evoked release of hGH from PC12 cells. Syntaxin 1a interferes with hGH release when coexpressed in PC12 cells, inhibiting secretion by nearly 75% (Figs. 6 and 7), in agreement with [40-42]. In contrast, SNAP-25, VAMP-2, Munc- 18 or synaptotagmin-1 (STG1) had no significant effect on regulated secretion (Fig. 6).

Structure-assisted molecular dissection of syntaxin 1a domains involved in SNARE complex formation.

Given the inhibitory activity of syntaxin 1a in this system, deletion constructs were designed based on the recent crystal structures of the SNARE core complex [2] and of syntaxin complexed with Nsec1 [43]. The latter structure discloses three subdomains a, b and c within the syntaxin SNARE motif. ST1-288 represents full length syntaxin 1a, ST251-288 encodes the transmembrane domain of syntaxin 1a, ST226-288 encodes the H3c plus transmembrane domains, ST211-288 encodes the H3b and c plus transmembrane domains, and ST191-288 encodes H3a, b, c and transmembrane domains. ST191-260 encodes the H3 coil alone, ST1-260 encodes cytosolic syntaxin 1a without the transmembrane domain, ST211-251 represents a minimal central coil spanning the Q226 residue, and ST191-218 encodes a component predicted to allow coil formation together with peptides representing the coil forming regions of SNAP-25 and VAMP2 (Appendix #4). While the syntaxin 1a SNARE motif alone (ST191-260) is not active in this expression system, robust inhibition of exocytosis is seen when the syntaxin 1a transmembrane domain is included (see ST191-288, Fig. 7). The transmembrane construct ST211-288 missing the H3a helix is also highly active, but subsequent deletions of helices H3b and H3c lead to a drastic drop in inhibition (see ST226-288 and ST251-288, Fig. 7). It is interesting to note that inhibitory activity is lost when the membrane attached SNARE motif no longer spans the zero layer Q226 residue [2]. As was shown previously, cytosolic syntaxin lacking a transmembrane domain (ST1-260) inhibits regulated secretion [41]. The SNARE motif region of syntaxin is known to interact with several proteins besides those involved directly in the SNARE coiled-coil, including Nsec1, calcium channels and several other proteins [44-50]. It is possible that the activity of our constructs reflect the importance of these interactions as well as the participation of syntaxin 1a in the SNARE core complex. Clearly, the syntaxin 1a SNARE motif coupled to the transmembrane domain embodies a minimum entity sufficient to compete with native syntaxin 1a for the assembly of a functional SNARE complex.

Structure-assisted molecular dissection of SNAP-25 domains involved in SNARE complex formation.

Helical regions of SNAP-25 were cloned using the polymerase chain reaction (PCR) as described and tested for their ability to inhibit secretion in PC12 cells (Fig. 8). SN1-82 represents the N-terminal coil (aa 1-82), SN1-141 encodes the N-terminal coil in addition to the membrane associated region of SNAP-25 , SN142-206 indicates the C-terminal coil, SN154-197 represents a minimal C-terminal coil spanning the central Q174 residue, SN82-206 includes the membrane-associated region and the C-coil, SN1-197 represents the larger cleavage product of BoNT A missing only the 9 C-terminal amino acids, and SN1-180 is the larger product of cleavage by BoNT E. SN172-206 and SN181-206 encode the C-terminal 35 and 26 amino acids of SNAP-25, respectively. Both the SN1-82 and SN142-206 constructs, expressing the N- and C-terminal SNARE motifs of SNAP-25 respectively, exhibit low to moderate inhibitory activity. Constructs SN1-197 and SN1-180 encoding the larger products of BoNT LCA and LCE cleavage, respectively, are clearly inhibitory, consistent with reports in chromaffin cells, suggesting that these cleavage products may contribute to the paralysis induced by BoNTs [51,52]. None of the SNAP-25 constructs tested matches the strong inhibitory activity displayed by the syntaxin construct ST191-288 (Fig. 7). Boosted expression of the 26 and 35 C-terminal SNAP-25 constructs using sodium butyrate and trichostatin A, agents known to drive expression of the CMV promoter of many mammalian expression vectors [53], did not result in increased inhibition with these clones.

SNARE chimeras.

Given the discrepancy between inhibition using peptide expression and direct peptide introduction into cells, it was hypothesized that the SN172-206 and SN181-206 encoding products may be degraded or relegated to compartments within the cell not involved in exocytosis. Based on the finding that the membrane anchored ST191-288 construct is inhibitory whereas the SNARE motif encoding ST191-260 construct is inactive under these conditions, chimeras were designed combining the transmembrane domain of syntaxin 1a (ST251-288) with both SN181-206 and SN172-206. Neither chimera acted as a potent inhibitor of secretion when compared to any toxin light chain or to the inhibitory syntaxin constructs (Figs. 7 and Table 2). However, a

chimera combining the full length C-terminal SNARE motif of SNAP-25 (SN142-206) with the syntaxin transmembrane domain demonstrated a two-fold increase in inhibitory activity over the SNAP-25 C-terminal coil alone (Table 2, 9A). These results indicate that the transmembrane domain of syntaxin may enhance the inhibitory effect of some SNARE helical constructs on ATP-evoked hGH secretion in transiently transfected PC12 cells. For the SNAP-25 chimeras, as for the syntaxin constructs, the central Q residue of the SNARE motif [2] is required to confer inhibitory activity to the construct. To localize expression of these protein products, HEK-293 cells transiently transfected with SNAP-25, syntaxin, the C-terminal coil of SNAP-25 and the chimera combining SN142-206 and ST251-288 were subjected to immunofluorescent staining. As shown in Fig. 9B, the SNARE proteins SNAP-25 and syntaxin 1a exhibit membrane-associated localization, whereas the peptide fragment SN142-206 is expressed throughout the cytosol. When this peptide fragment is linked to the syntaxin transmembrane domain, however, localization is again directed to the membrane (Fig. 9B, C). Immnunoblot analysis confirms expression and appropriate size of the transfected protein products (Fig. 9C).

These results provide novel information about the nature of the molecular interactions underlying the role of SNARE proteins in neurosecretion, pointing to the significance not only of protein sequence and structure, but also membrane localization in regulated exocytosis.

KEY RESEARCH ACCOMPLISHMENTS

- APPENDIX 1. Peptides that mimic the carboxy-terminal domain of SNAP-25 block acetylcholine release at an *Aplysia* synapse.

Botulinum neurotoxin serotypes A and E (BoNT/A and BoNT/E) block neurotransmitter release, presumably by cleaving SNAP-25, a protein involved in docking of synaptic vesicles with the presynaptic plasma membrane. Three excitation-secretion uncoupling peptides (ESUPs), which mimic the carboxy-terminal domain of SNAP-25 and span or adjoin the cleavage sites for BoNT/A and BoNT/E, also inhibit transmitter release from permeabilized bovine chromaffin cells. In this study, these peptides were tested for effects on acetylcholine (ACh) release at an identified cholinergic synapse in isolated buccal ganglia of *Aplyisia californica*. The presynaptic neuron was stimulated electrically to elicit action potentials. The postsynaptic neuron was voltage-clamped, and evoked inhibitory postsynaptic currents (IPSCs) were recorded. The ESUPs were pressure-injected into the presynaptic neuron, and their effects on the amplitude of the IPSCs were studied. Acetylcholine release from presynaptic cells, as measured by IPSC amplitudes, was gradually inhibited by the ESUPs. All three peptides caused ca. 40% reduction in IPSC amplitude in 2 h. Random-sequence peptides of the same amino acid composition had no effect. Injection of BoNT/E, in contrast, caused ca. 50% reduction in IPSC amplitude in 30 min and almost complete inhibition in 2 h. These results are the first demonstration that ESUPs block neuronal cholinergic synaptic transmission. They are consistent with the concept that ESUPs compete with the intact SNAP-25 for binding with other fusion proteins, thus inhibiting stimulus-evoked exocytosis of neurotransmitters.
J. Appl. Toxicol.19:S23-S26 (1999)

- APPENDIX 2. Activation of store-operated calcium-current in *Xenopus* oocytes requires SNAP-25 but not a diffusible messenger.

Depletion of Ca^{2+} stores in *Xenopus* oocytes activated entry of Ca^{2+} across the plasma membrane, which was measured as a current I_{SOC} in subsequently formed cell-attached patches. I_{SOC} survived excision into inside-out configuration. If cell-attached patches were formed before store depletion, I_{SOC} was activated outside but not inside the patches. I_{SOC} was potentiated by microinjection of *Clostridium* C3 transferase, which inhibits Rho GTPase, whereas I_{SOC} was

inhibited by expression of wild-type or constitutively active Rho. Activation of I_{SOC} was also inhibited by *Clostridium* BoNT A and dominant-negative mutants of SNAP-25 but was unaffected by brefeldin A. These results suggest that oocyte I_{SOC} is dependent not on aqueous diffusible messengers but on SNAP-25, probably via exocytosis of membrane channels or regulatory molecules.
Cell 98:475-485 (1999)

- APPENDIX 3. Electrostatic attraction at the core of membrane fusion.

SNARE proteins appear to be involved in homotypic and heterotypic membrane fusion events. The crystal structure of the synaptic SNARE complex exhibits a parallel four-helical bundle fold with two helices contributed by SNAP-25, a target SNARE (t-SNARE), and the other two by a different t-SNARE, syntaxin, and a donor vesicle SNARE (v-SNARE), synaptobrevin. The carboxy-terminal boundary of the complex, predicted to occur at the closest proximity between the apposed membranes, displays a high density of positively charged residues. This feature combined with the enrichment of negatively charged phospholipids in the cytosolic exposed leaflet of the membrane bilayer suggest that electrostatic attraction between oppositely charged interfaces may be sufficient to induce dynamic and discrete micellar discontinuities of the apposed membranes with the transient breakdown at the junction and subsequent reformation. Thus, the positively charged end of the SNARE complex in concert with Ca^{2+} may be sufficient to generate a transient "fusion pore".
FEBS Lett. 447:129-130 (1999)

- APPENDIX 4. Assembly of a ternary complex by the predicted minimal coiled-coil forming domains of syntaxin, SNAP-25 and synaptobrevin.

The assembly of target (t-SNARE) and vesicle-associated (v-SNARE) proteins is a critical step for the docking of synaptic vesicles to the plasma membrane. Syntaxin-1A, SNAP-25 and synaptobrevin-2 (VAMP-2) bind to each other with high affinity, and their binding regions are predicted to form a trimeric coiled-coil. We designed three peptides which correspond to sequences located in the syntaxin-1A H3 domain, the C-terminal domain of SNAP-25, and a conserved central domain of synaptobrevin-2, that exhibit a high propensity to form a minimal trimeric coiled-coil. The peptides were synthesized by solid phase methods and their interactions were studied by CD spectroscopy. In aqueous solution, the peptides

were unstructured and showed no interactions with each other. In contrast, upon addition of moderate amounts of trifluoroethanol (30%), the peptides adopted an α-helical structure and displayed both homomeric and heteromeric interactions. The interactions observed in ternary mixtures induce a stabilization of peptide structure that is greater than that predicted from individual binary interactions, suggesting the formation of a higher order structure compatible with the assembly of a trimeric coiled-coil.
J. Biol. Chem. 273:34214-34221 (1998)

- APPENDIX 5. The 26-mer peptide released from SNAP-25 by cleavage botulinum neurotoxin E inhibits vesicle docking.

BoNT E cleaves SNAP-25 at the C-terminal domain releasing a 26-mer peptide. This peptide product may act as an excitation-secretion uncoupling peptide (ESUP) to inhibit vesicle fusion and thus contribute to the efficacy of BoNT E in disabling neurosecretion. We have addressed this question using a synthetic 26-mer peptide which mimics the amino acid sequence of the naturally released peptide, and is hereafter denoted as ESUP E. This synthetic peptide is a potent inhibitor of Ca^{2+}-evoked exocytosis in permeabilized chromaffin cells and reduces neurotransmitter release from identified cholinergic synapses in *in vitro* buccal ganglia of *Aplysia californica*. In chromaffin cells, both ESUP E and BoNT E abrogate the slow component of secretion without affecting the fast, Ca^{2+}-mediated fusion event. Analysis of immunoprecipitates of the synaptic ternary complex involving SNAP-25, VAMP and syntaxin demonstrates that ESUP E interferes with the assembly of the docking complex. Thus, the efficacy of BoNTs as inhibitors of neurosecretion may arise from the synergistic action of cleaving the substrate and releasing peptide products that disable the fusion process by blocking specific steps of the exocytotic cascade.
FEBS Lett. 435:84-88 (1998)

- APPENDIX 6. Structural stabilization of botulinum neurotoxins by tyrosine phosphorylation.

Tyrosine phosphorylation of BoNTs augments their proteolytic activity and thermal stability, suggesting a substantial modification of the global protein conformation. We used Fourier-Transform Infrared (FTIR) spectroscopy to study the modulation of secondary structure and thermostability of tyrosine phosphorylated BoNT A and BoNT E. Changes in the conformationally-sensitive amide I band of the infrared spectra upon phosphorylation indicated alterations in the protein secondary structure; the α-helix content increased

with a concomitant decrease of less ordered structures such as turns and random coils, and without any change in β-sheet content. This change in secondary structure was accompanied by an increase in the amide II band absorbance remaining upon H-D exchange, suggesting tighter packing for the phosphorylated protein. FTIR and Differential Scanning Calorimetry (DSC) analyses of the denaturation process show that phosphorylated neurotoxins denaturated at temperatures higher than those required by nonphosphorylated species. These findings indicate that tyrosine phosphorylation induced transition to higher order and more compact structure probably imparts to the phosphorylated neurotoxins the higher catalytic activity and thermostability.
FEBS Lett. 429:78-82 (1998)

- Structural characteristics of a 23-mer channel forming peptide from botulinum neurotoxin type A.

A channel-forming peptide from the translocation domain of the HC of BoNTA has been examined by CD in order to probe transitions in secondary structure induced by environmental variables such as solvent polarity and pH. The secondary structure of the peptide is highly sensitive to solvent and pH. In aqueous solution at pH 7.0, the peptide was unstructured. In contrast, upon addition of trifluoroethanol (up to 60%), the peptide adopted a conformation compatible with a mixture of α-helix and β-sheets. At pH 3.3, the peptide exhibited primarily a β-sheet configuration at TFE concentrations below 30%, whereas it was primarily α-helical at TFE concentrations above 40%. This sensitivity to pH and solvent polarity are compatible with the requirement of an amphipathic segment to insert into the hydrophobic core of a bilayer. Such features are consistent with the channel forming activity recorded after reconstitution of the peptide in lipid bilayers and may reflect the key contribution of this segment of the HC towards the insertion of the translocation domain into the bilayer core.

Protein Sci. 7: p.116, Abst. 361- (1998)

REPORTABLE OUTCOMES:

- Research Articles and Abstracts

1. Apland, J.P., J.A. Biser, M. Adler, A.V. Ferrer-Montiel , M. Montal and M.G. Filbert.Peptides that mimic the carboxy-terminal domain of SNAP-25 block acetylcholine release at an Aplysia synapse.**J. Appl. Toxicol.** 19 Suppl 1:S23-6. (1999). Appendix #1.

2. Yao, Y., Ferrer-Montiel, A.V.F., Montal, M., and Tsien, R.Y. Activation of store-operated calcium-current in *Xenopus* oocytes requires SNAP-25 but not a diffusible messenger. **Cell** 98:475-485 (1999). Appendix #2.

3. M. Montal. Electrostatic attraction at the core of membrane fusion. **FEBS Lett.** 447: 129-130 (1999). Appendix #3.

4. J. M. Cànaves and M. Montal. Assembly of a Ternary Complex by the Predicted Minimal Coiled-coil-forming Domains of Syntaxin, SNAP-25, and Synaptobrevin. A circular dichroism study. **J. Biol. Chem.** 273: 34214-34221 (1998). Appendix #4.

5. Apland, J.P., Biser, J.A., Adler, M., Ferrer-Montiel, A.V., Montal, M. and Filbert, M.G. Peptides composed of carboxy-terminal domains of SNAP-25 block acetylcholine release at an *Aplysia* synapse. **Soc. Neurosci. Abstr.** 24 (Part 1) 73, 35.1 (1998).

6. Yao, Y., Ferrer-Montiel, A.V., Montal, M., and Tsien, R.Y., Botulinum neurotoxin A inhibits capacitative Ca^{2+} influx but not Ca^{2+} release in *Xenopus* oocytes. **Soc. Neurosci. Abstr.** 24 (Part 2) 2030, 812.4 (1998).

7. Ferrer-Montiel, A.V., J.M. Merino, R. Planells-Cases, W. Sun and M. Montal. Structural determinants of the blocker binding site in glutamate and NMDA receptor channels. **Neuropharmacology** 37:139-147. (1998).

8. Encinar, J.A., Fernandez, A., Ferragut, J.A., Gonzalez-Ros, J.M., DasGupta, B.R, Montal, M, and Ferrer-Montiel-A. Structural stabilization of botulinum neurotoxins by tyrosine phosphorylation. **FEBS Lett.** 429:78-82 (1998). Appendix #5.

9. Byrne, M.P., Montal, M., Canaves, J. and Lebeda, F.J. Conformational changes of a channel forming peptide from the translocation domain of botulinum neurotoxin as detected by circular dichroism. **Protein Sci.** 7: p.116, Abst. 361-T (1998)

10. Apland, J.P., Biser, J.A., Adler, M. Ferrer-Montiel, A.V., Montal, M., and Filbert, M.G.Peptides that mimic the carboxy-terminal domain of SNAP-25 block acetylcholine release at an *Aplysia* synapse. **Biosci. Rev.** p.184 (1998)

11. Ferrer-Montiel, A.V., Oblatt-Montal, M., Canaves, J., and Montal, M. Botulinum neurotoxins: Modulation of protease and channel activities by tyrosine phosphorylation. **Biosci. Rev.** p.190 (1998)

12. Ferrer-Montiel, A.V., Gutierrez, L.M., Apland, J.P., Canaves, J.M., Gil, A., Viniegra, S., Biser, J.A., Adler, M. and Montal, M. The 26-mer peptide released from SNAP-25 cleavage by botulinum neurotoxin E inhibits vesicle docking. **FEBS Lett.** 435:84-88 (1998). Appendix #6.

- Presentations:

1. Blanes-Mira, C., Gil, A., Llobregat, M., Fernandez-Ballester, G., Planells-Cases, R.,Perez-Paya, E., Canaves, J., Gutierrez, L.M., Montal, M. and Ferrer-Montiel, A. Modulation of SNAP-25-Syntaxin-VAMP complex formation and stability by small peptides. **Annual Meeting of the Spanish Biophysical Society.** Alicante, Spain (1998).

2. Apland, J.P., Biser, J.A., Adler, M. Ferrer-Montiel, A.V., Montal, M., and Filbert, M.G.Peptides that mimic the carboxy-terminal domain of SNAP-25 block acetylcholine release at an *Aplysia* synapse. **U.S. Army Medical Defense Bioscience Review.** Hunt Valley, Maryland, 31 May-4 June, 1998.

3. Ferrer-Montiel, A.V., Oblatt-Montal, M., Canaves, J., and Montal, M. Botulinum neurotoxins: Modulation of protease and channel activities by tyrosine phosphorylation. **U.S. Army Medical Defense Bioscience Review.** Hunt Valley, Maryland, 31 May-4 June, 1998.

4. Lebeda, F.J., Montal, M., Singh, B.R. and Byrne, M. Structural characteristics of a 23-mer channel forming

peptide from botulinum neurotoxin type A. **Interagency Botulism Research Coordinating Committee (IBRCC).** Philadelphia, Pennsylvania, November, 1998.

5. Montal, M. Modulation of botulinum neurotoxin protease activity by tyrosine phosphorylation. **Interagency Botulism Research Coordinating Committee (IBRCC).** Orlando, Florida November, 1999.

6. Yao, Y., Ferrer-Montiel, A.V.F., Montal, M., and Tsien, R.Y. Activation of store-operated calcium-current in *Xenopus* oocytes requires SNAP-25 but not a diffusible messenger. **U.S. Army Medical Defense Bioscience Review.** Hunt Valley, Maryland, 4 June-9 June, 2000.

- Patents and licenses applied for and/or issued:

1. U.S. Patent # 5,837,265.
Title: CHEMICALLY-MODIFIED CLOSTRIDIATOXIN WITH IMPROVED PROPERTIES
Inventors: Mauricio Montal, Antonio Ferrer-Montiel
University of California Reference: SD 96-036
Issue date: November 17, 1998

2. U.S. Patent Patent # 6,169,074B1.
Title: PEPTIDE INHIBITORS OF NEUROTRANSMITTER SECRETION BY NEURONAL CELLS.
Inventors: Mauricio Montal, Antonio Ferrer-Montiel and Jaume Canaves.
University of California Reference: SD 96-088
Issue date: January 2, 2001

- Degrees obtained: Not applicable.
- Development of cell lines: Not applicable.
- Informatics: Not applicable.
- Funding applied for based on work supported by this award: A new application entitled "Combinatorial Strategies And High Throughput Screening In Drug Discovery Targeted To The Channel Of Botulinum Neurotoxin" was submitted to Department of the Army, US Army Medical Research Acquisition Activity, and has been identified with Log. No. 01170001.
- Employment or research opportunities based on this award: Not applicable.

PERSONNEL RECEIVING PAY FROM THE RESEARCH EFFORT
Mauricio Montal, P.I.
Natalie Gude, Staff Research Associate
Lilia Koriazova, Postgraduate Researcher
Judy Moreen, Administrative Assistant
Lisa Parry, Laboratory Assistant
Jae-Young Seo, Laboratory Assistant
Doug Bei, Laboratory Assistant
Kay Chang, Laboratory Assistant

CONCLUSIONS

The thrust of this program aimed to identify the role of the channel-forming domain of the HC in the intoxication process and, ultimately, to provide a potential target for drug intervention in the management of botulism based on the development of BoNT-specific channel blockers. The contribution of the cleavage products of BoNTs activity on their substrates to the global intoxication efficacy was also evaluated. A patent, resulting from this analysis, has been awarded: it embodies the concept that the peptide products of substrate proteolysis by BoNTs can be developed into lead compounds acting as practical inhibitors of neurotransmitter secretion. Considerable progress was achieved in both fronts of the program, as summarized in the BODY of the report and ascertained by the published work. It is anticipated that this concerted and focused program will continue to uncover lead compounds that may be developed into selective drugs targeted to prevent, attenuate or relieve the neurotoxic action of BoNT.

REFERENCES

1. Söllner T, Whitehear, SW, Brunner M, Erdjument-Bromage H, Geromanos S, Tempst P, Rothman JE. 1993. *Nature 362*:318-324.
2. Sutton RB, Fasshauer D, Jahn R, Brunger AT. 1998. *Nature 395*:347-353
3. Montecucco C, Schiavo G. 1995.*Q Rev Biophys 28*:423-472.
4. Poirier M A, Xiao W, Macosko JC, Chan C, Shin Y-K, Bennett MK. 1998. *Nature Struct Biol 5:*765-769.
5. Shao X, Li C, Fernandez I, Zhang X, Südhof TC, Rizo J. 1997. *Neuron 18*:133-142.
6. Rettig J, Heinemann C, Ashery U, Sheng Z-H, Yokoyama CT, Catterall WA, Neher E. 1997. *J Neurosci 17*:6647-6656.

7. Lacy DB, Stevens RC. 1999. *J Mol Biol 291*:1091-104.
8. Lacy DB, Tepp W, Cohen AC, DasGupta BR, Stevens RC. 1998. *Nature Struct Biol 5*:898-902.
9. Swaminathan S, Eswaramoorthy S. 2000. *Nature Struct Biol* 7:693-699.
10. Donovan JJ, Middlebrook JL. 1986. *Biochemistry 25*: 2872-2876.
11. Hoch DH, Romero-Mira M, Ehrlich BE, Finkelstein A, DasGupta BR, Simpson L. 1985. *Proc Natl Acad Sci USA 82*:1692-1696.
12. Blaustein RO, Germann WJ, Finkelstein A, DasGupta BR. 1987. *FEBS Lett 226*:115-120.
13. Lebeda FJ, Singh BR. 1999. *J Toxicol-Toxin Reviews 18*:45-76.
14. Oblatt-Montal M, Yamazaki M, Nelson R, Montal M. 1995. *Protein Sci 4*:1490-1497.
15. Canaves JM, Montal M. 1998. *J Biol Chem 273*:34214-34221.
16. Gutierrez LM, Canaves JM, Ferrer-Montiel AV, Reig JA, Montal M, Viniegra S. 1995. *FEBS Lett 372*:39-43.
17. Gutierrez LM, Viniegra S, Rueda J, Ferrer-Montiel AV, Canaves JM, Montal M. 1997. *J Biol Chem 272*:2634-2639.
18. Ferrer-Montiel AV, Gutierrez LM, Apland JP, Canaves JM, Gil A,Viniegra S, Biser JA, Adler M, Montal M. 1998. *FEBS Lett 435*:84-88.
19. Smart OS, Breed J, Smith GR, Sansom MS. 1997. *Biophys J 72*:1109-1126.
20. Oh KJ, Senzel L, Collier RJ, Finkelstein A. 1999. *Proc Natl Acad Sci USA 96*:8467-8470.
21. Senzel L, Gordon M, Blaustein RO, Oh KJ, Collier RJ, Finkelstein A. 2000. *J Gen Physiol 115*:421-434.
22. Hill K, Model K, Ryan MT, Dietmeier K, Martin F, Wagner R, Pfanner N. 1998. *Nature 395*:516-521.
23. Kunkele KP, Heins S, Dembowski M, Nargang FE, Benz R, Thieffry M, Walz J, Lill R, Nussberger S, Neupert W. 1998. *Cell 93*:1009-1019.
24. Kunkele KP, Juin P, Pompa C, Nargang FE, Henry JP, Neupert W, Lill R, Thieffry M.1998. *J Biol Chem 273*:31032-31039.
25. Rapoport TA, Matlack KE, Plath K, Misselwitz B, Staeck O. 1999. *Biol Chem 380*:1143-1150.
26. Gambale F, Montal M. 1988. *Biophys J 53:*771-783.
27. Sheridan RE. 1998. *Toxicon 36*:703-717.
28. Schmid A, Benz R, Just I, Aktories K. 1994. *J Biol Chem 269:*16706-16711.
29. Holsinger LJ, Nichani D, Pinto LH, Lamb RA. 1994. *J Virol 68:*1551-1563.

30. Pinto LH, Holsinger LJ, Lamb RA. 1992. *Cell 69:*517-528.
31. Wang C, Takeuchi K, Pinto LH, Lamb RA.1993. *J Virol 67:*5585-5594.
32. Erdo SL, Schafer M. 1991. *Eur J Pharmacol 198:*215-217.
33. Chen HS, Lipton SA. 1997. *J Physiol 499*:27-46.
34. Montal M. 1995. *Annu Rev Biophys Biomol Struct 24:* 31-57.
35. Weber T, Zemelman BV, McNew JA, Westermann B, Gmachl M, Parlati F, Söllner TH, Rothman JE. 1998. *Cell 92*:759-772.
36. Rizo J, Südhof TC. 1998. *Nature Struct Biol 5*:839-842.
37. Chen YA, Scales SJ, Paytel SM, Doung Y-C, Scheller RH. 1999. *Cell 97*:165-174.
38. Xu T, Rammer B, Margittal M, Artalejo AR, Neher E, Jahn R. 1999. *Cell 99*:713-722.
39. Fisher RJ, Burgoyne RD. 1999. *Pflügers Arch-Eur J Physiol 437*:754-762.
40. Fujita-Yoshigaki J, Dohke Y,Hara-Yokoyama M, Furuyama S, Sugiya H.1998. *Eur J Morphol 36 Suppl*:46-49.
41. Dubulova I, Sugita S, Hill S, Hosaka M, Fernandez I, Sudhof TC, Rizo J. 1999. *EMBO J 18*:4372-2382.
42. Wu MN, Fergestad T, Lloyd TE, He Y, Broadie K, Bellen HJ. 1999. *Neuron 23*:593-605.
43. Misura KM, Scheller RH, Weis WI. 2000. *Nature 404*:355-362.
44. Bennett MK, Calakos N, Scheller RH. 1992. *Science 257*:255-259.
45. Hata Y, Slaughter CA, Sudhof TC. 1993. *Nature 366*:347-351.
46. Sollner T, Bennett MK, Whiteheart SW, Scheller RH, Rothman JE. 1993. *Cell 75*:409-418.
47. Chapman ER, Hanson PI, An S, Jahn R. 1995. *J Biol Chem 270*:23667-23671.
48. McMahon HT, Missler M, Li C, Sudhof TC. 1995. *Cell 83*:111-119.
49. Fujita Y, Shirataki H, Sakisaka T, Asakura T, OhyaT, Kotani H, Yokoyama S, Nishioka H, Matsura Y, Mizoguchi A, Scheller RH, Takai Y. 1998. *Neuron 20*:905-915.
50. Bezprozvanny I, Scheller RH, Tsien RW. 1995. *Nature 378*:623-626.
51. O'Sullivan GA, Mohammed N, Foran PG, Lawrence GW, Dolly OJ. 1999. *J Biol Chem 274*:36897-36904.
52. Keller JE, Neale EA. 2001. *J Biol Chem 276*:13476-13482.
53. Condreay JP, Witherspoon SM, Clay WC, Kost TA. 1999. *Proc Natl Acad Sci USA 96*:127-132.

FIGURES AND FIGURE LEGENDS

Fig. 1. BoNTA holotoxin and HC form channels in lipid bilayers. A. Single channel currents of reduced native BoNT holotoxin displaying the 110 pS channels. Records obtained at −100 mV in symmetric 0.5 M KCl, 1 mM $CaCl_2$, 2.5 mM citrate pH 5.5. Final protein concentration was 2.5 µg/ml. A downward deflection indicates channel opening. This segment illustrates the occurrence of two channels. A current amplitude histogram and Gaussian fit is shown on the right panel. This histogram was calculated for the initial section of the record in which a single channel underwent transitions between closed and open states. C and O denote closed and open states. The probability of the channel being open, P_O, or closed, P_C, is calculated from the area under the corresponding Gaussian curve. For this record, the cumulative P_O = 0.56. The single channel current is calculated as the difference between the peaks associated with the closed and open states. B. Single channel currents from bilayers containing native BoNTA HC. Currents were recorded at V= −100 mV. Final protein concentration was 0.5 µg/ml. A downward deflection indicates channel opening. Segments of a continuous record illustrate the occurrence of the 128 pS channels. Current histogram generated from a continuous segment of a record lasting several minutes and Gaussian fit are shown on the right panel. For this record, the cumulative P_O = 0.55. C. Single channel currents from bilayers containing recombinant BoNTA HC. Currents were recorded at V= −100 mV. Final protein concentration was 0.5 µg/ml. A downward deflection indicates channel opening. Segments of a continuous record illustrate the occurrence of the 96 pS channels. Current histogram generated from a continuous segment of a record lasting several minutes and Gaussian fit are shown on the right panel. For this record, the cumulative P_O = 0.48.

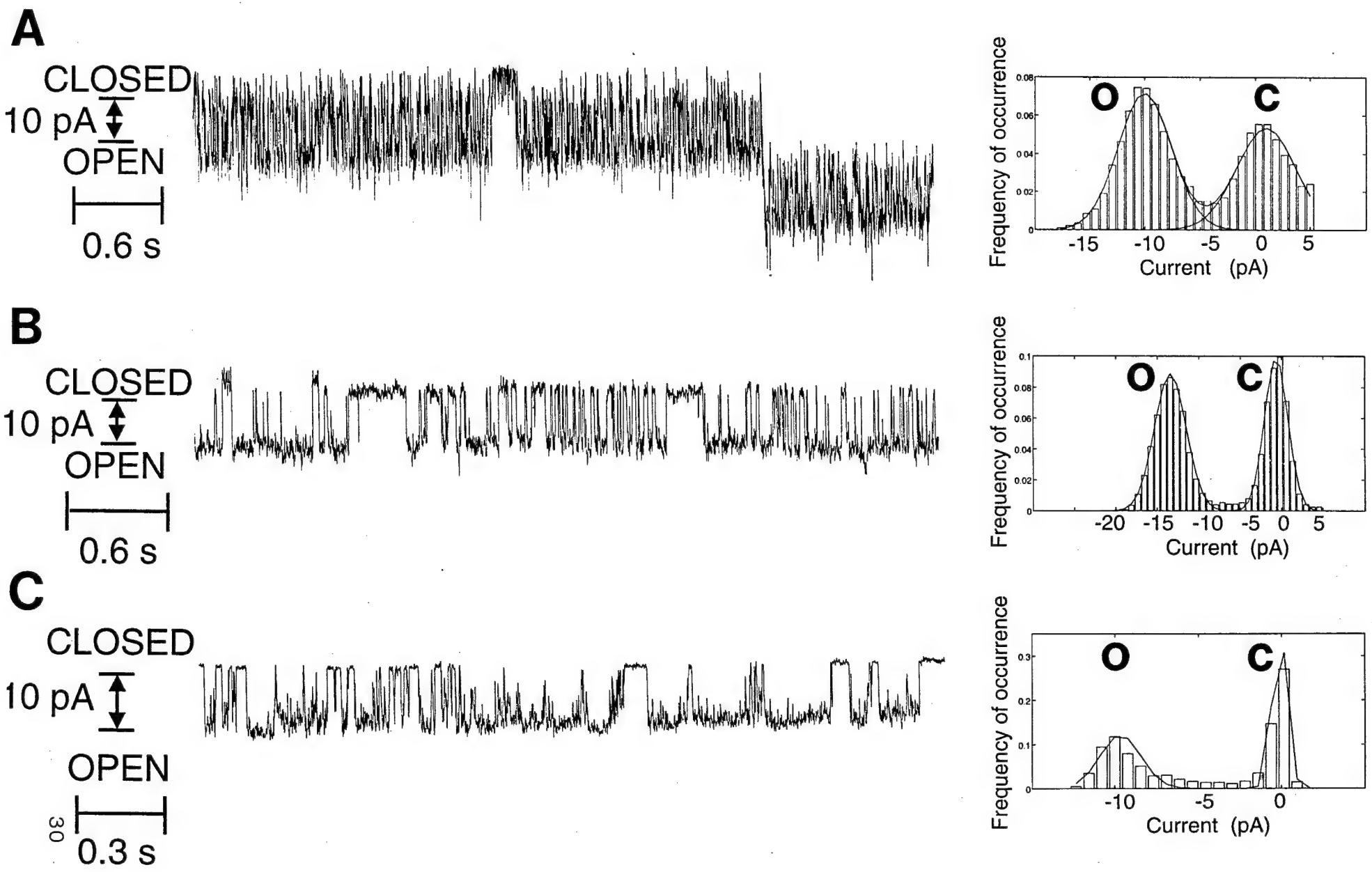
A
CLOSED
10 pA
OPEN
0.6 s
B
CLOSED
10 pA
OPEN
0.6 s
C
CLOSED
10 pA
OPEN
0.3 s
Frequency of occurrence
O
C
Current (pA)
-15 -10 -5 0 5
-20 -15 -10 -5 0 5
-10 -5 0

Figure 1

Fig. 2. BoNT LC blocks the HC channel. A. Single channel currents of native BoNT HC displaying the 124 pS channels. Records obtained at −100 mV in symmetric 0.5 M KCl, 1 mM $CaCl_2$, 2.5 mM citrate pH 5.5. Final protein concentration was 0.5 μg/ml. A downward deflection indicates channel opening. Current histogram and Gaussian fit are displayed in the right panel; for this record, the cumulative P_O = 0.47. B. Single channel currents from bilayers containing native BoNT HC in the presence of BoNT LC in the *trans*-compartment. Records obtained at −100 mV in symmetric 0.5 M KCl, 1 mM $CaCl_2$, 2.5 mM citrate pH 5.5. Final protein concentration was . 0.5 μg/ml for HC and 0.5 μg/ml for LC. Current histogram and Gaussian fit are displayed in the right panel; for this record, γ = 29.8 pS and the cumulative P_O = 0.51. Note the occurrence of fast transitions between open and blocked states. Other conditions as for Fig. 1.

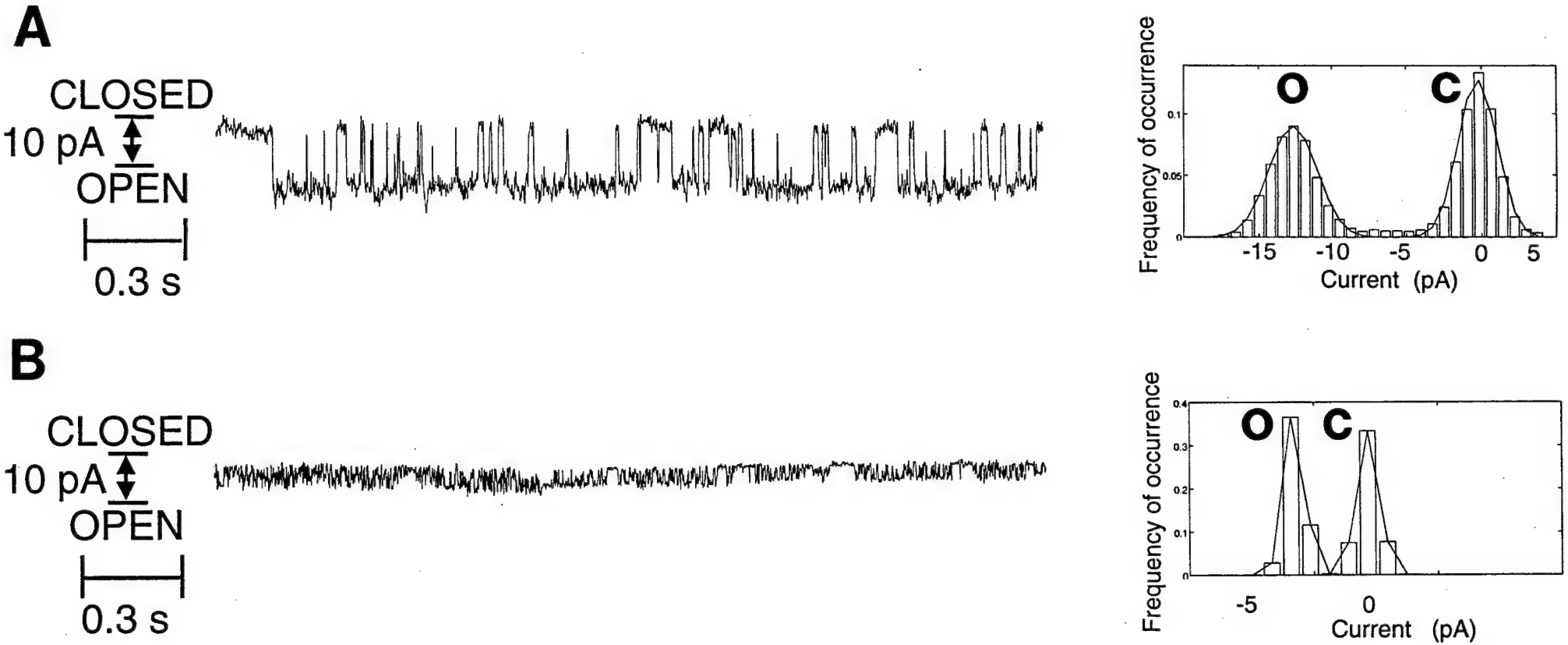
A
CLOSED
10 pA
OPEN
0.3 s
B
CLOSED
10 pA
OPEN
0.3 s
Frequency of occurrence
O
C
-15
-10
-5
0
5
Current (pA)
Frequency of occurrence
O
C
-5
0
Current (pA)

Figure 2

Fig. 3. Quinacrine blocks the BoNT holotoxin channel. Single channel recordings and current histograms of BoNT holotoxin in the absence (A) and presence (B) of 10 μM quinacrine. Records obtained at −100 mV in symmetric 0.5 M KCl, 1 mM $CaCl_2$, 2.5 mM citrate pH 5.5. Final protein concentration was 0.5 μg/ml. Current histogram and Gaussian fit are displayed in the right panel. For these records, in the absence of quinacrine γ = 112 pS and the cumulative P_O = 0.54; in contrast, in the presence of quinacrine the histogram can only be fitted with a single Gaussian corresponding to the closed state. Other conditions as for Fig. 1.

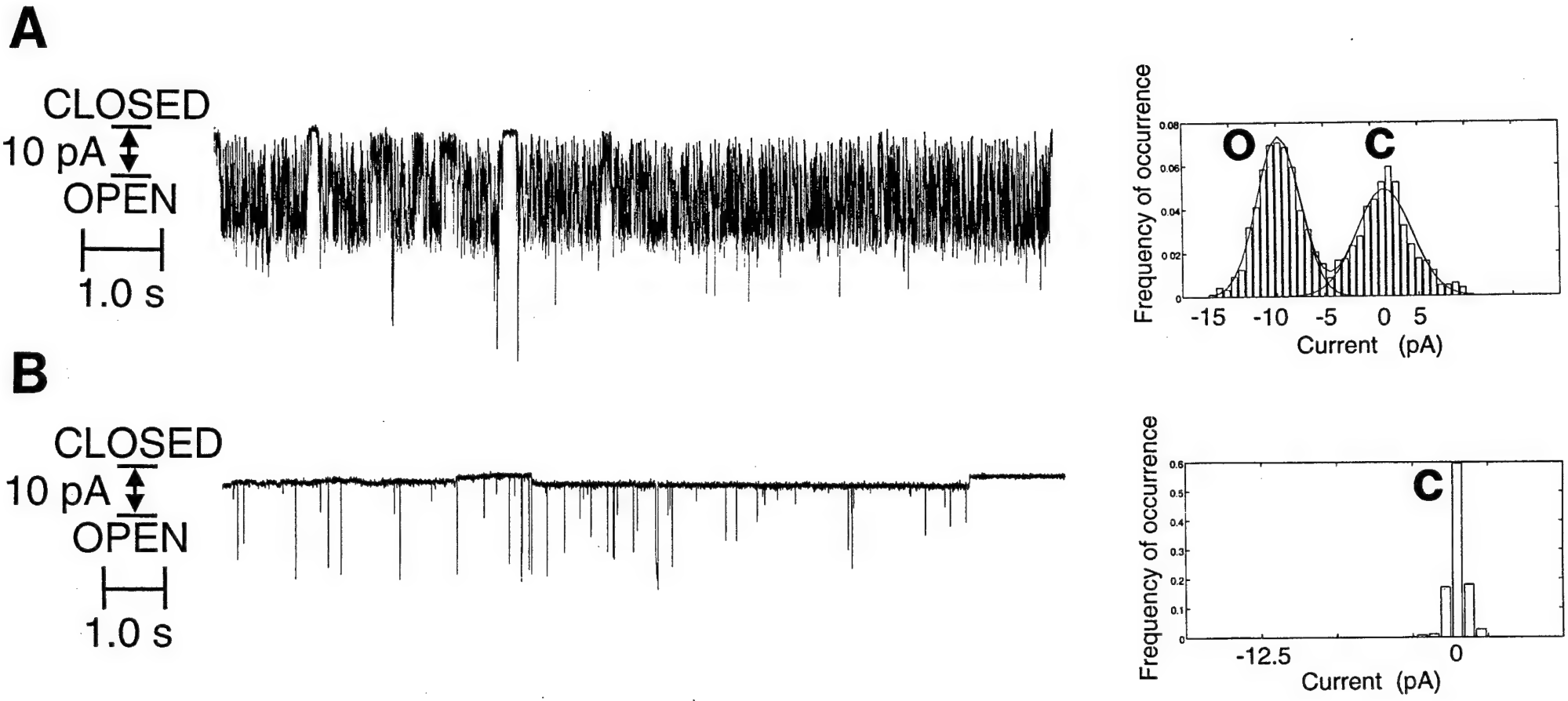
A
CLOSED
10 pA
OPEN
1.0 s
B
CLOSED
10 pA
OPEN
1.0 s
O
C
Frequency of occurrence
0.08
0.06
0.04
0.02
0
-15
-10
-5
0
5
Current (pA)
C
Frequency of occurrence
0.6
0.5
0.4
0.3
0.2
0.1
0
-12.5
0
Current (pA)

Figure 3

Fig. 4. QX-222 blocks the BoNT holotoxin channel. Single channel recordings and current histograms of BoNT holotoxin in the absence (A) and presence (B) of 40 μM QX-222. Records obtained at −100 mV in symmetric 0.5 M KCl, 1 mM $CaCl_2$, 2.5 mM citrate pH 5.5. Final protein concentration was 0.5 μg/ml. Current histogram and Gaussian fit are displayed in the right panel. For these records, in the absence of QX-222 the current histogram is fitted with the sum of five Gaussians (excluding the closed state) corresponding to the occurrence of five channels with a conductance of approximately 110 pS. In the presence of QX-222, there is a marked reduction in both γ and in the number of events. The open states are scarcely populated to allow a meaningful fit to the data point; the histogram is best fitted with a single Gaussian corresponding to the closed state. Other conditions as for Fig. 1.

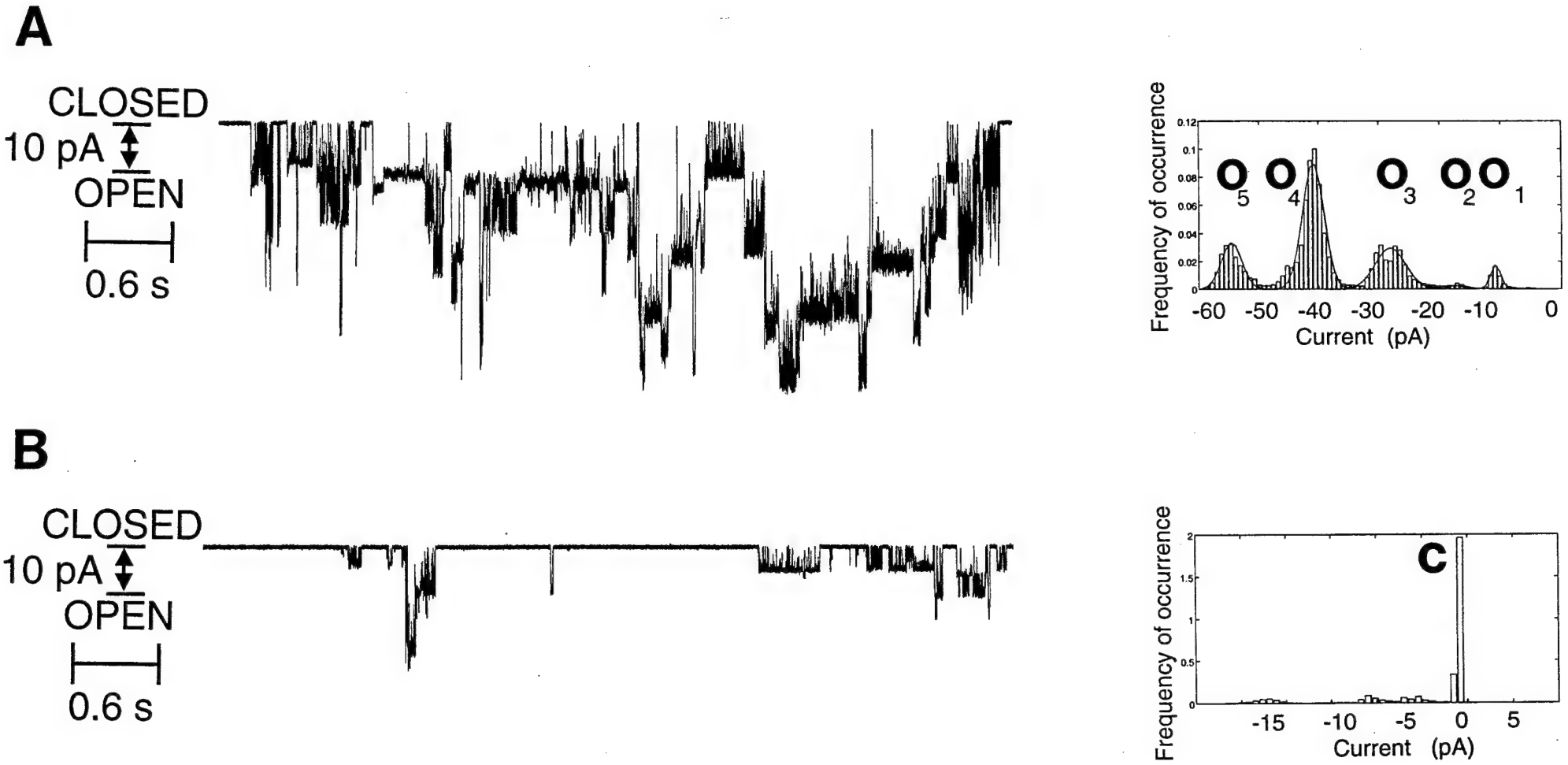
A
CLOSED
10 pA
OPEN
0.6 s
B
CLOSED
10 pA
OPEN
0.6 s
Frequency of occurrence
O5 O4 O3 O2 O1
-60 -50 -40 -30 -20 -10 0
Current (pA)
C
Frequency of occurrence
-15 -10 -5 0 5
Current (pA)

Figure 4

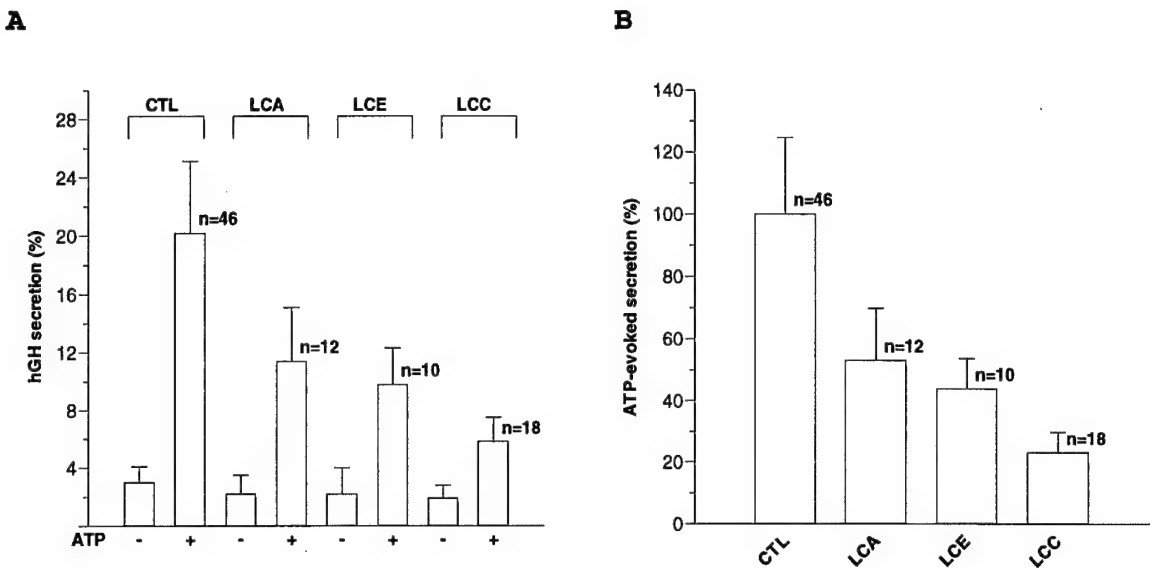

Fig. 5. Overexpression of BoNT LC A, E or C abrogates ATP-evoked secretion of hGH in PC12 cells. PC12 cells were transiently cotransfected with plasmids encoding hGH and pCDNA3.1+ for control (CTL) or BoNT LC A, E or C. After 72 hours in culture at 37°C, 5% CO_2, hGH secretion was induced using basal secretion medium with or without 300 μM ATP. A) Basal (-) and ATP-evoked (+) values are expressed as a percentage of the total cell hGH content (mean ± SD). B) ATP-evoked values are normalized to control and reflect ATP-stimulated levels minus the basal levels shown in A (mean ± SD). n denotes individual samples measured in multiple experiments. $P<0.001$ (Student's t test) for LCA, LCE and LCC.

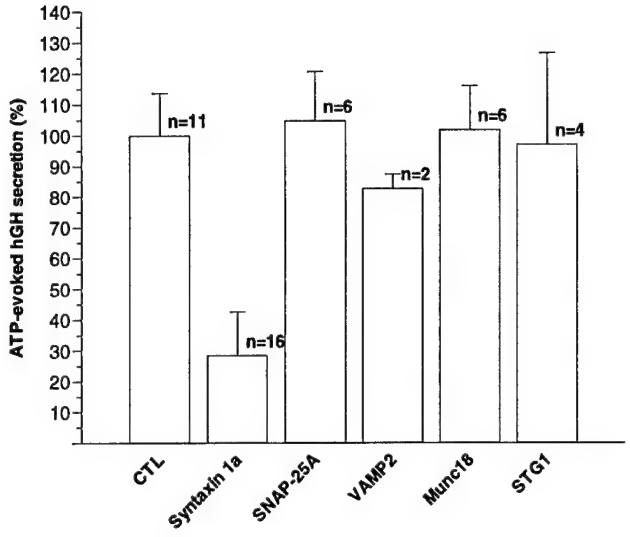

Fig. 6. Syntaxin 1a is the only SNARE protein which interferes with ATP-evoked exocytosis when overexpressed in PC12 cells. ATP-evoked hGH release was measured in PC12 cells transiently cotransfected for 72 hours with hGH-encoding plasmid and plasmids encoding proteins associated with the SNARE complex (mean ± SD). STG1 indicates synaptotagmin I. n denotes individual samples measured in various experiments. $P<0.001$ for syntaxin 1a (Student's *t* test). Other conditions are as described in the legend for Figure 5.

A

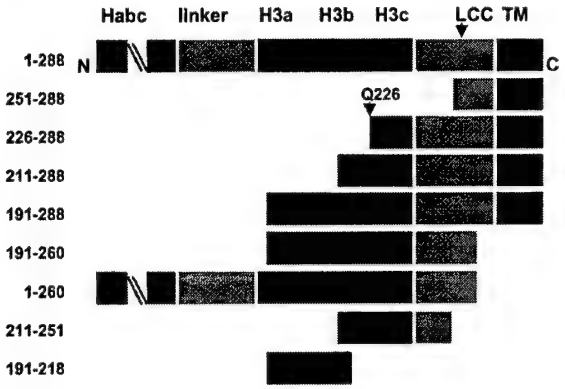

B

Syntaxin 1a constructs	% inhibition	n
ST1-288	74.0 ± 6.8 ***	9
ST251-288	-0.4 ± 5.1	3
ST226-288	0.6 ± 33.1	2
ST211-288	53.3 ± 30.2	2
ST191-288	85.8 ± 2.8 ***	4
ST191-260	-4.0 ± 9.1	2
ST1-260	62.7 ± 16.1	2
ST211-251	3.4 ± 26.6	5
ST191-218	4.8 ± 7.0	8

Fig. 7. Structure-assisted molecular dissection of syntaxin domains involved in regulated exocytosis. A) Plasmids encoding syntaxin 1a deletion constructs were cloned by the polymerase chain reaction (PCR) from PC12 cDNA and cotransfected into PC12 cells with hGH marker plasmid. Numbers denote the N- and C- terminal amino acids of the SNARE constructs: for example, ST1-288 represents full length syntaxin 1a. Habc denotes an abbreviated depiction of the three N-terminal coils of syntaxin 1a. H3a, H3b and H3c indicate the three helical subdomains of the syntaxin 1a SNARE motif [43]. LCC shows the cleavage site for BoNT LC C between amino acids K253 and A254, Q226 marks the location of the ionic layer glutamine residue [2], and TM denotes the transmembrane domain. B) The extent of inhibition effected by each construct on hGH release is tabulated and expressed with respect to pCDNA3.1+ control plasmid, defined as 0% (mean ± SD). n denotes duplicate samples from several experiments. ***, $P<0.001$ (Student's t test). Other conditions are as described in the legend for Figure 5.

A

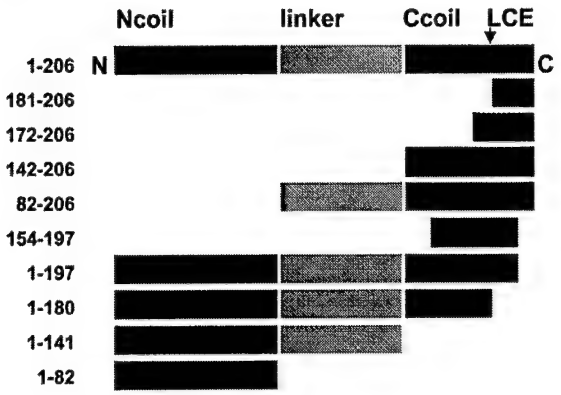

B

SNAP-25A constructs	% inhibition	n
SN1-206	1.7 ± 6.0	4
SN181-206	4.6 ± 5.4	7
SN172-206	1.8 ± 5.5	5
SN142-206	13.7 ± 3.2	5
SN82-206	25.9 ± 19.2	3
SN154-197	6.4 ± 11.0	5
SN1-197	45.4 ± 15.6	2
SN1-180	51.7 ± 10.8 **	4
SN1-141	2.4 ± 16.1	2
SN1-82	17.6 ± 13.6	3

Fig. 8. Structure-assisted molecular dissection of SNAP-25A domains involved in regulated exocytosis. A) Plasmids encoding SNAP-25A deletion constructs were cloned by PCR from PC12 cDNA and cotransfected into PC12 cells with hGH marker plasmid. Numbers denote the N- and C- terminal amino acids of the SNARE constructs: for example, SN1-206 stands for full length SNAP-25A. Ncoil and Ccoil depict the two SNARE motifs of SNAP-25A. LCE shows the cleavage site for BoNT LC E between amino acids R180 and I181. B) The extent of inhibition effected by each construct on hGH release is tabulated and expressed with respect to pCDNA3.1+ control plasmid, defined as 0% (mean ± SD). n denotes duplicate samples from at least two experiments. **, $P<0.01$ (Student's *t* test). Other conditions are as described in the legend for Figure 5.

Fig. 9. The syntaxin 1a transmembrane domain increases inhibitory activity of the SNAP-25A SNARE motif in PC12 cells and localizes it to to the plasma membrane of HEK-293 cells when expressed as the SN142-206$_{\cup}$**ST251-288** chimera. A) SN142-206 and SN142-206$_{\cup}$**ST251-288** (SN142-206/TM) constructs were cotransfected with hGH marker plasmid into PC12 cells. Inhibitory activity of SN142-206 compared with that of SN142-206$_{\cup}$**ST251-288** (SN142-206/TM) is expressed relative to pCDNA3.1+ control plasmid, defined as 0% (mean ± SD). n=5, the number of duplicate samples from 5 experiments. *, $P<0.05$ (Student's *t* test). B) SNAP-25A, SN142-206, the SN-142-206$_{\cup}$**ST251-288** chimera and syntaxin 1a were transiently transfected into HEK-293 cells and localized by immunofluorescence using goat anti-SNAP-25 C-terminal (Fig. 9Ba, 9Bb and 9Bc) or mouse anti-HPC-1 (Fig. 9Bd) antibodies. For Figures 9Ba-c, secondary antibody was fluorescently labeled with fluorescein (green); for Figure 9Bd, secondary antibody was fluorescently labeled with Texas Red (red). C) HEK-293 cells were transiently transfected with pCDNA3.1+ control (Figure 9C, lane 1), SNAP-25A (Figure 9C, lane 2) or the SN142-206$_{\cup}$**ST251-288** chimera (Fig. 9C, lane 3) plasmid, and subjected to immunoblotting using a goat anti-SNAP-25 C-terminal antibody.

A

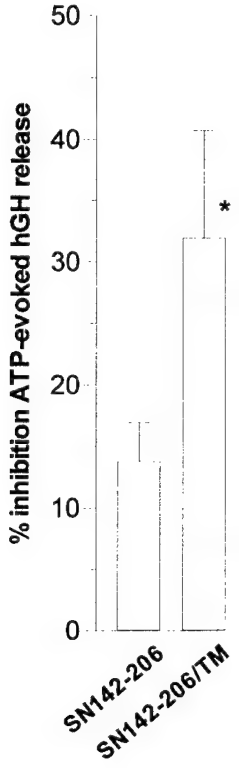
50
40
30
20
10
0
% inhibition ATP-evoked hGH release
*
SN142-206
SN142-206/TM

B

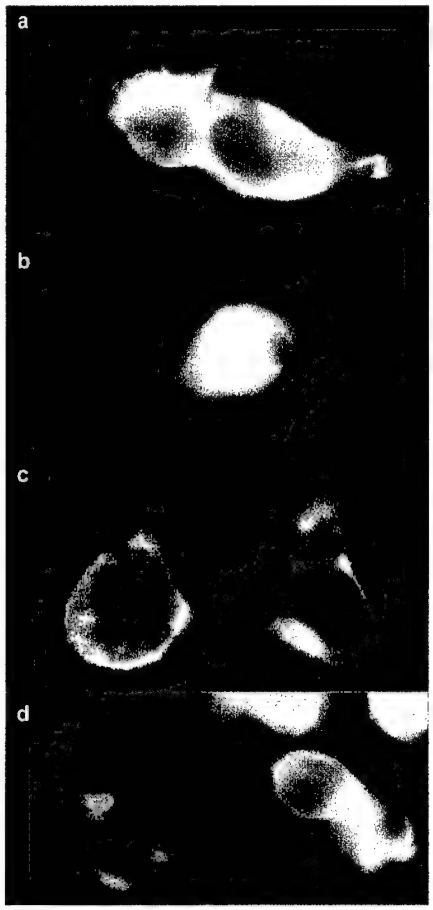
a
b
c
d
SNAP-25A
SNAP-25A 142-206
SNAP-25A 142-206 fused to Syntaxin 1a 251-288
Syntaxin 1a

C

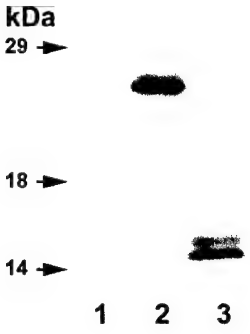
kDa
29
18
14
1
2
3

Table 1 Summary of the conditions tested to examine the postulated mechanism for the translocation of the LCA through the HC channel, and the results obtained

	CONDITION	ACIDIFICATION	INSERTION	CHANNEL ACTIVITY
1	BoNTA holotoxin reduced before experiment	–	–	–
2	BoNTA holotoxin – no reduction	+	+	–
3	BoNTA holotoxin + TCEP – *cis* before acidification	+	+	+
4	BoNTA holotoxin + TCEP – *cis* after acidification	+	+	–
5	BoNTA holotoxin + TCEP – *trans*	+	+	+
6	HCA – no reduction	+	+	+
7	HCA + LCA – *cis*, 5x molar excess before acidification, no reduction	+	+	–
8	HCA + LCA – *cis*, 5x molar excess after acidification, no reduction	+	+	+
9	HCA + LCA – *trans*, 2x molar excess, no reduction	+	+	–

Table 2. Inhibition of regulated exocytosis in PC12 cells by SNAP-25A/syntaxin 1a TM chimeras.

peptide and chimera constructs	% inhibition	n
SN172-206	6.1 ± 6.7	8
SN172-206∪**ST251-288**	10.6 ± 9.3	5
SN181-206	1.8 ± 5.5	5
SN181-206∪**ST251-288**	7.2 ± 10.4	6
SN154-197	6.4 ± 11.0	5
SN154-197∪**ST251-288**	14.8 ± 16.5	2
SN142-206	13.7 ± 3.2	5
SN142-206∪**ST251-288**	31.9 ± 8.8 ***	5

The extent of inhibition effected by SNAP-25A peptide and its corresponding chimeric construct on hGH release is tabulated and expressed with respect to pCDNA3.1+ control plasmid, defined as 0% (mean ± SD). n denotes duplicate samples from at least two experiments. ***, $P<0.001$ (Student's *t* test). Peptides are identified as described in Figure 8. Chimeric constructs are represented by using the symbol ∪ to join the SNAP-25A peptide (in regular type) with the syntaxin 1a TM segment (in bold type). Other conditions are as described in the legend for Figure 5.

APPENDICES #1 - #6

M. MONTAL

Appendices #1-#6

1. Apland, J.P., J.A. Biser, M. Adler, A.V. Ferrer-Montiel , M. Montal and M.G. Filbert.Peptides that mimic the carboxy-terminal domain of SNAP-25 block acetylcholine release at an Aplysia synapse.**J. Appl. Toxicol.** 19 Suppl 1:S23-6. (1999). Appendix #1.

2. Yao, Y., Ferrer-Montiel, A.V.F., Montal, M., and Tsien, R.Y. Activation of store-operated calcium-current in *Xenopus* oocytes requires SNAP-25 but not a diffusible messenger. **Cell** 98:475-485 (1999). Appendix #2.

3. M. Montal. Electrostatic attraction at the core of membrane fusion. **FEBS Lett.** 447: 129-130 (1999). Appendix #3.

4. J. M. Cànaves and M. Montal. Assembly of a Ternary Complex by the Predicted Minimal Coiled-coil-forming Domains of Syntaxin, SNAP-25, and Synaptobrevin. A circular dichroism study. J. Biol. Chem. 273: 34214-34221 (1998). Appendix #4.

5. Encinar, J.A., Fernandez, A., Ferragut, J.A., Gonzalez-Ros, J.M., DasGupta, B.R, Montal, M, and Ferrer-Montiel-A. Structural stabilization of botulinum neurotoxins by tyrosine phosphorylation. **FEBS Lett.** 429:78-82 (1998). Appendix #5.

6. Ferrer-Montiel, A.V., Gutierrez, L.M., Apland, J.P., Canaves, J.M., Gil, A., Viniegra, S., Biser, J.A., Adler, M. and Montal, M. The 26-mer peptide released from SNAP-25 cleavage by botulinum neurotoxin E inhibits vesicle docking. **FEBS Lett.** 435:84-88 (1998). Appendix #6.

JOURNAL OF APPLIED TOXICOLOGY
J. Appl. Toxicol. **19**, S23–S26 (1999)

Peptides that Mimic the Carboxy-terminal Domain of SNAP-25 Block Acetylcholine Release at an *Aplysia* Synapse†‡

J. P. Apland,[1]* J. A. Biser,[1] M. Adler,[1] A. V. Ferrer-Montiel,[2] M. Montal[2] and M. G. Filbert[1]
[1]Neurotoxicology Branch, US Army Medical Research Institute of Chemical Defense, 3100 Ricketts Point Road, Aberdeen Proving Ground, MD 21010–5400, USA [2]Department of Biology, University of California at San Diego, La Jolla, CA 92083–0366, USA

Key words: botulinum; toxin; synaptic protein; neurotransmitter release.

Botulinum neurotoxin serotypes A and E (BoNT/A and BoNT/E) block neurotransmitter release, presumably by cleaving SNAP-25, a protein involved in docking of synaptic vesicles with the presynaptic plasma membrane. Three excitation–secretion uncoupling peptides (ESUPs), which mimic the carboxy-terminal domain of SNAP-25 and span or adjoin the cleavage sites for BoNT/A and BoNT/E, also inhibit transmitter release from permeabilized bovine chromaffin cells. In this study, these peptides were tested for effects on acetylcholine (ACh) release at an identified cholinergic synapse in isolated buccal ganglia of *Aplysia californica*. The presynaptic neuron was stimulated electrically to elicit action potentials. The postsynaptic neuron was voltage-clamped, and evoked inhibitory postsynaptic currents (IPSCs) were recorded. The ESUPs were pressure-injected into the presynaptic neuron, and their effects on the amplitude of the IPSCs were studied. Acetylcholine release from presynaptic cells, as measured by IPSC amplitudes, was gradually inhibited by the ESUPs. All three peptides caused ca. 40% reduction in IPSC amplitude in 2 h. Random-sequence peptides of the same amino acid composition had no effect. Injection of BoNT/E, in contrast, caused ca. 50% reduction in IPSC amplitude in 30 min and almost complete inhibition in 2 h. These results are the first demonstration that ESUPs block neuronal cholinergic synaptic transmission. They are consistent with the concept that ESUPs compete with the intact SNAP-25 for binding with other fusion proteins, thus inhibiting stimulus-evoked exocytosis of neurotransmitter.

INTRODUCTION

The botulinum neurotoxins (BoNTs), of which there are seven serotypes (A–G), are the most poisonous substances known. These toxins have a molecular weight of ca. 150 kDa and are composed of two polypeptide chains linked by a disulfide bond and non-covalent interactions.[1] The toxin dichain consists of a heavy chain (ca. 100 kDa) and a light chain (ca. 50 kDa). Poisoning by BoNT involves four sequential steps: binding by the toxin heavy chain to a serotype-specific receptor on the presynaptic neuronal membrane; internalization of the toxin by an endocytotic process; release of the light chain into the cytosol; and enzymatic cleavage of a target protein.[2] The BoNTs are zinc-dependent endopeptidases[3] having a high specificity for proteins that are associated with the docking and fusion of synaptic vesicles. Each of the serotypes has been shown to cleave a protein that is essential for exocytotic release of neurotransmitter.[4] Botulinum neurotoxin A cleaves the presynaptic plasma membrane protein known as SNAP-25 (synaptosomal-associated protein of 25 kDa) at a site near the C-terminus (Gln^{197}-Arg^{198}), and BoNT/E cleaves SNAP-25 at the Arg^{180}-Ile^{181} site.[5,6] Recently, Gutierrez *et al.*[7] synthesized a 20-amino acid (aa) peptide with the same sequence as the C-terminal domain of SNAP-25 (aa 187–206: SNKTRIDEANQRATKMLGSG), which spans the cleavage site for BoNT/A and was designated ESUP/A (excitation–secretion uncoupling peptide). The authors focused on the C-terminal domain of SNAP-25 because it is a target of BoNT/A and BoNT/E and it has been shown to interact with synaptobrevin and syntaxin.[4] They found that ESUP/A blocked Ca^{2+}-dependent catecholamine release from permeabilized bovine chromaffin cells,[7] apparently by blocking vesicle docking.[8] Shorter peptides and one mimicking an N-terminal motif were inactive.[7] Gutierrez *et al.*[9] more recently have synthesized a second 20-amino acid peptide called ESUP/E (aa 170–189: EIDTQNRQIDRIMEKADSNK), which spans the cleavage site for BoNT/E, and a 26-amino acid

* Correspondence to: J. P. Apland, US Army Medical Research Institute of Chemical Defense, 3100 Ricketts Point Rd, Aberdeen Proving Ground, MD 21010–5400, USA.
† The opinions or assertions contained herein are the private views of the author(s) and are not to be construed as official or as reflecting the views of the Department of the Army or the Department of Defense. In conducting the research described in this report, the investigators adhered to the Guide for the Care and Use of Laboratory Animals of the Institute of Laboratory Animal Resources, National Research Council.

Published in 1999 by John Wiley & Sons, Ltd.

Received 26 January 1999
Accepted 4 May 1999

peptide corresponding to the sequence of the peptide cleaved from SNAP-25 by BoNT/E. The latter peptide is designated ESUP/E26 (aa 181–206: IMEKADSNKTRIDEANQRATKMLGSG) and was expected to be more effective in inhibiting transmitter release. To determine whether ESUPs inhibit transmitter release at neuronal synapses, the effect of these peptides on ACh release at identified cholinergic synapses[10] of *Aplysia californica* was investigated and compared with the effect of BoNT/E application. We found that ESUPs cause ca. 40% inhibition of acetylcholine (ACh) release in 2 h, compared with nearly complete inhibition by BoNT/E.

EXPERIMENTAL

Experiments were performed with neuronal preparations from the marine mollusc *Aplysia californica*. Inhibition of nerve-evoked release of ACh was measured at identified cholinergic synapses in buccal ganglia[10] using procedures similar to those described by Poulain *et al.*[11] The buccal ganglia were surgically removed and pinned to the Sylgard® (Dow Corning, Midland, MI)-lined bottom of an acrylic chamber, and the connective tissue capsule was surgically removed. The soma of identified pre- and postsynaptic cholinergic neurons (Fig. 1) were impaled with glass microelectrodes (2–4 MΩ filled with 2 M potassium acetate. Action potentials were evoked in presynaptic neurons by suprathreshold depolarizing stimuli applied once every 10 s. Neurotransmitter release was assessed by measuring the amplitude of the inhibitory postsynaptic current (IPSC) recorded in a voltage-clamped follower neuron. Presynaptic potentials and postsynaptic currents were digitized and stored on a laboratory computer using pClamp software (Axon Instruments, Inc., Foster City, CA). Responses were analyzed only if they were not obscured by spontaneous IPSCs, which were frequent in some preparations. The preparation was superfused continuously at a rate of 1 ml min^{-1} with artificial seawater (ASW) containing the following (in mM): NaCl, 480; KCl, 10; $CaCl_2$, 10; $MgCl_2$, 20; $MgSO_4$, 30; $NaHCO_3$, 2.5; HEPES, 10; at pH 7.8. The ganglia were maintained at room temperature during the experiments.

Excitation-secretion uncoupling peptides (5 mM) were dissolved in a 600 mM NaCl/10 mM HEPES solution (pH 7.8) containing 1% (w/v) Fast Green FCF dye (Sigma Chemical Company, St. Louis, MO) to aid in visualizing the injected solution.[12] Random-sequence peptides of the same amino acid composition as ESUP/A (ESUP/A Random: TDSSGREMIKANKQLANGTR) or ESUP-E26 (ESUP-E26 Random: ESDNDTRAIKITQAGSMKRMGLNAKE) were synthesized and used as controls. Randomized sequences were generated, their secondary structures were predicted using improved self-optimized prediction method analysis (SOPMA)[13] and the sequences with an α-helical content similar to the original sequence were run against the Prosite database. Peptides were air pressure-injected into the presynaptic cell by micropipette. The volume of solution injected was less than 10% of the estimated cell volume, yielding a final intracellular peptide concentration ≤100 μM.

Pure BoNT/E was purchased from Drs E. A. Johnson and M. Goodnough, Food Research Institute, University of Wisconsin-Madison. The single-chain neurotoxin was converted to the 'nicked' dichain form by treatment with 0.3 mg ml^{-1} trypsin XI for 30 min at 37°C, followed by incubation with 0.5 mg ml^{-1} soybean trypsin inhibitor for 15 min at room temperature.[14] Aliquots of the nicked toxin were frozen at −80°C and then thawed and treated with 1 mM dithiothreitol for 30 min

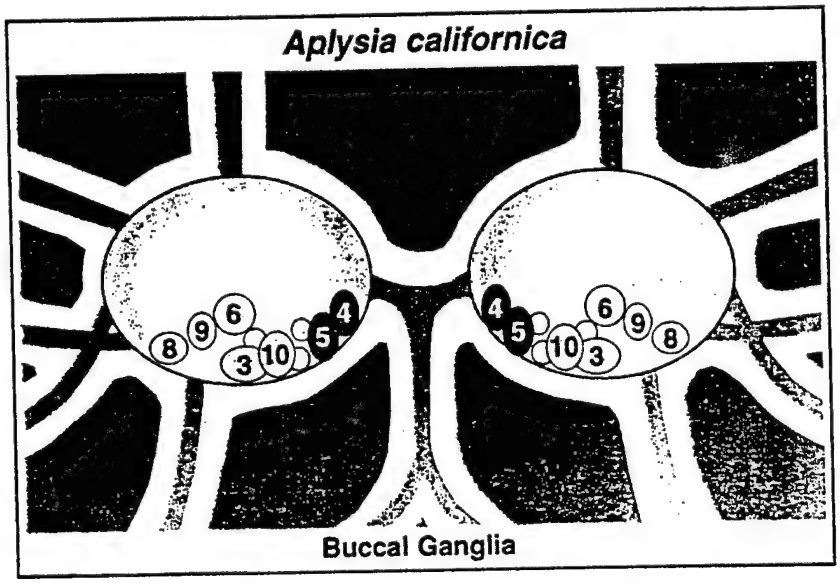

Figure 1. Schematic diagram of the cephalic surface of the paired buccal ganglia. Numbered presynaptic (dark)- and postsynaptic (light)-shaded cells are indicated. Within each hemiganglion, each presynaptic neuron projects to all of the indicated postsynaptic neurons. (Modified from Gardner and Kandel.[10])

Published in 1999 by John Wiley & Sons, Ltd.

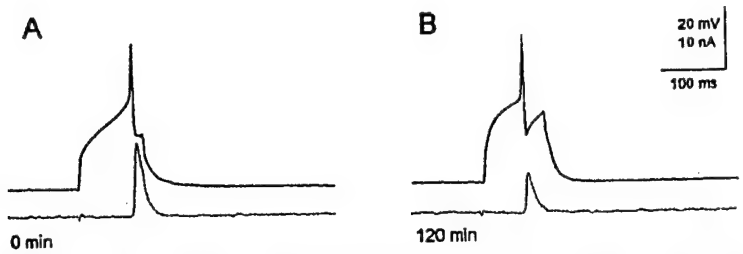

Figure 2. Excitation–secretion uncoupling peptide A blocks synaptic transmission in an *Aplysia* buccal ganglion cholinergic synapse. Acetylcholine release was monitored as the amplitude of the IPSC (dotted trace) elicited by an evoked action potential (solid trace) in the presynaptic neuron. Recordings show the decrease in IPSC amplitude 120 min (B) after injection of ESUP/A into the presynaptic neuron at time zero (A). Injection of other active ESUPs produced similar effects.

at room temperature before use[15] to enhance the enzymatic activity of the toxin light chain. The BoNT/E concentration in the micropipette was 3.3 μM.

RESULTS

Release of ACh by the presynaptic neuron in response to electrically evoked action potentials was assessed by measuring the amplitude of the evoked IPSCs in a voltage-clamped postsynaptic neuron. Figure 2 shows superimposed action potentials and IPSCs in a typical experiment. The ESUP/A was injected at time zero (A) and the resultant decline of IPSC amplitude is shown at 120 min (B). The IPSC amplitude declined to 55% of the control value 120 min after injection of ESUP/A. The decline of IPSC amplitude caused by ESUP/A was gradual and incomplete, typically requiring 2 h to reach a stable level of 55.1% (±4.5; $n = 8$) of the control value.

The time-course of the effect of peptide injection on IPSC amplitude is shown in Fig. 3. Peptide (either active ESUPs or random-sequence control peptides) was injected at time zero. The large increase in IPSC amplitude following injection was a frequent consequence of pressure injection of any compound. The rise in IPSC amplitudes after injection of active ESUPs was partially masked by a peptide-induced reduction in amplitude and typically returned to control values within 30 min. No further decline of responses occurred in cells injected with the random-sequence control peptides, whereas IPSCs in cells injected with active ESUPs declined to a stable level over the ensuing 120 min and changed very little thereafter. Similar results were obtained with all three active peptides.

Injection of BoNT/E also produced inhibition of evoked IPSC amplitudes in this preparation. However, the extent and time-course were different from that produced by injection of ESUPs (Fig. 4). The IPSC amplitude was inhibited by ca. 50% in 30 min and inhibition was nearly complete within 120 min. A transient increase in IPSC amplitude was observed within the first 20 min following injection of BoNT/E, similar to that seen following injection of ESUPs. However, IPSC amplitudes exhibited net inhibition within 30 min.

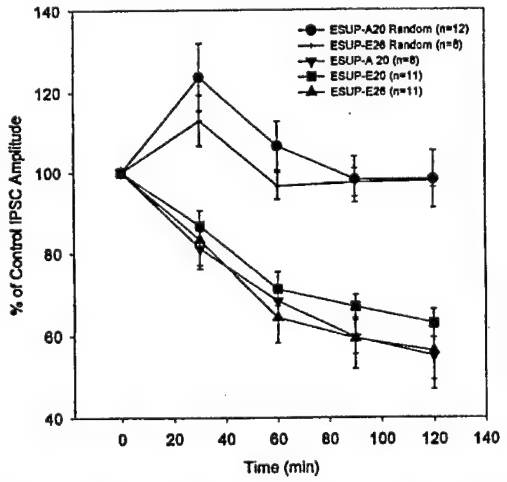

Figure 3. Excitation–secretion uncoupling peptides (ESUPs) inhibit IPSC amplitudes in *Aplysia* buccal ganglion synapses. Either active ESUPs or the inactive random-sequence ESUP/A20 or ESUP/E26 analogs were injected into the presynaptic neuron at time zero. The IPSC amplitude was inhibited after injection of active ESUPs, whereas injection of the inactive analogs did not inhibit IPSCs. Values are means ± SEM; n = number of pre- and postsynaptic cell pairs.

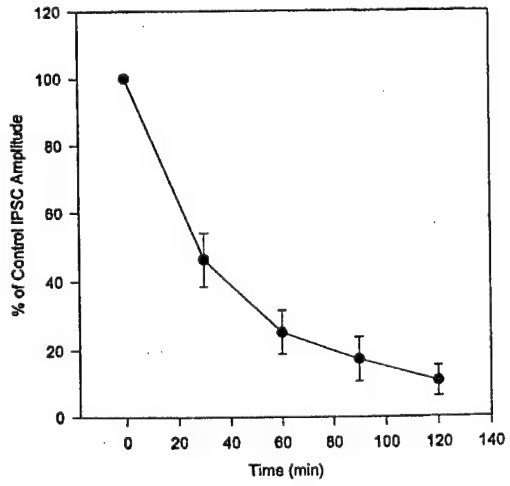

Figure 4. Botulinum neurotoxin E inhibits IPSC amplitudes in *Aplysia* buccal ganglion synapses. Botulinum neurotoxin E was injected at time zero. The IPSC amplitude was decreased by ca. 50% in 30 min, and inhibition was nearly complete in 2 h. Values are means ± SEM; $n = 7$.

Published in 1999 by John Wiley & Sons, Ltd.

DISCUSSION

In this investigation, ESUP injection did not cause complete inhibition of the evoked IPSC, which differs from the nearly complete inhibition in neuronal cells caused by injection of BoNT/E in this study and injection or bath application of BoNT in other laboratories (e.g. Poulain *et al.*[11]). These results are consistent with those of Gutierrez *et al.*,[7,8] who found that ESUP/A and ESUP/E26 produce at maximum 60–70% inhibition of Ca^{2+}-stimulated catecholamine release from permeabilized bovine chromaffin cells. The SNAP-25 cleavage sites for both BoNT/A (Gln^{197}-Arg^{198}) and BoNT/E (Arg^{180}-Ile^{181}) are near the C-terminus.[6] A recent study[16] has demonstrated that both C-terminal and N-terminal domains of SNAP-25 are involved in forming the core synaptic fusion complex with synaptobrevin II and syntaxin-1A. Our results, and those of Gutierrez *et al.*,[7,8] suggest that ESUPs compete with intact SNAP-25 for binding with other fusion proteins, thus inhibiting docking and exocytosis of synaptic vesicles. Production of cleavage products of SNAP-25 by BoNT/A and BoNT/E may therefore contribute indirectly to decreased neurotransmitter exocytosis.[9] Inhibition of neurotransmitter release by BoNTs would be expected to be more complete than that caused by treatment with ESUPs because the toxins would decrease the supply of synaptic proteins in the active zone of the neuron, in addition to generating cleavage products. Peptide fragments of other synaptic proteins such as synaptobrevin and syntaxin, produced by the other BoNT serotypes, may similarly interfere with synaptic vesicle docking and exocytosis. However, this prediction has not yet been verified. It is possible that removal or inactivation of cleavage products may provide a means of treating BoNT poisoning. These results provide further insight into the mechanisms of BoNT intoxication and ultimately may lead to new approaches to its treatment.

REFERENCES

1. G. Sakaguchi, *Clostridium botulinum* toxins. *Pharmacol. Ther.* **19**, 165–194 (1983).
2. L. L. Simpson, Molecular pharmacology of botulinum toxin and tetanus toxin. *Annu. Rev. Pharmacol. Toxicol.* **26**, 427–453 (1986).
3. G. Schiavo, O. Rossetto, A, Santucci, B. R. DasGupta and C. Montecucco, Botulinum neurotoxins are zinc proteins. *J. Biol. Chem.* **267**, 23479–23483 (1992).
4. H. Niemann, J. Blasi and R. Jahn, Clostridial neurotoxins: new tools for dissecting exocytosis. *Trends Cell Biol.* **4**, 179–185 (1994).
5. T. Binz, J. Blasi, S. Yamasaki, A. Baumeister, E. Link, T. Sudhof, R. Jahn and H. Niemann, Proteolysis of SNAP-25 by types E and A botulinal neurotoxins. *J. Biol. Chem.* **269**, 1617–1620 (1994).
6. G. Schiavo, A. Santucci, B. R. DasGupta, P. P. Metha, J. Jontes, F. Benfenati, M. C. Wilson and C. Montecucco, Botulinum neurotoxin serotypes A and E cleave SNAP-25 at distinct COOH-terminal peptide bonds. *FEBS Lett.* **335**, 99–103 (1993).
7. L. M. Gutierrez, J. M. Canaves, A. V. Ferrer-Montiel, J. A. Reig, M. Montal and S. Viniegra, A peptide that mimics the carboxy-terminal domain of SNAP-25 blocks Ca^{2+}-dependent exocytosis in chromaffin cells. *FEBS Lett.* **372**, 39–43 (1995).
8. L. M. Gutierrez, S. Viniegra, J. Rueda, A. V. Ferrer-Montiel, J. M. Canaves and M. Montal, A peptide that mimics the C-terminal sequence of SNAP-25 inhibits secretory vesicle docking in chromaffin cells. *J. Biol. Chem.* **272**, 2634–2639 (1997).
9. A. V. Ferrer-Montiel, L. M. Gutiérrez, J. P. Apland, J. M. Canaves, A. Gil, S. Viniegra, J. A. Biser, M. Adler and M. Montal, The 26-mer peptide released from SNAP-25 cleavage by botulinum neurotoxin E inhibits vesicle docking. *FEBS Lett.* **435**, 84–88 (1998).
10. D. Gardner and E. R. Kandel, Physiological and kinetic properties of cholinergic receptors activated by multiaction interneurons in buccal ganglia of *Aplysia*. *J. Neurophysiol.* **40**, 333–348 (1977).
11. B. Poulain, L. Tauc, E. A. Maisey, J. D. F. Wadsworth, P. M. Mohan and J. O. Dolly, Neurotransmitter release is blocked intracellularly by botulinum neurotoxin, and this requires uptake of both toxin polypeptides by a process mediated by the larger chain. *Proc. Natl. Acad. Sci. USA* **85**, 4090–4094 (1988).
12. S. Mochida, B. Poulain, U. Eisel, T. Binz, H. Kurazono, H. Niemann and L. Tauc, Exogenous mRNA encoding tetanus or botulinum neurotoxins expressed in *Aplysia* neurons. *Proc. Natl. Acad. Sci. USA* **87**, 7844–7848 (1990).
13. C. Geourjon and G. Deleage, SOPMA: significant improvements in protein secondary structure prediction by consensus prediction from multiple alignments. *Comput. Appl. Biosci.* **11**, 681–684 (1995).
14. D. M. Evans, R. S. Williams, C. C. Shone, P. Hambleton, J. Melling and J. O. Dolly, Botulinum neurotoxin type B. Its purification, radioiodination and interaction with rat-brain synaptosomal membranes. *Eur. J. Biochem.* **154**, 409–416 (1986).
15. M. Wictome, O. Rosetto, C. Montecucco and C. C. Shone, Substrate residues N-terminal to the cleavage site of botulinum type B neurotoxin play a role in determining the specificity of its endopeptidase activity. *FEBS Lett.* **386**, 133–136 (1996).
16. R. B. Sutton, D. Fasshauer, R. Jahn and A. T. Brunger, Crystal structure of a SNARE complex involved in synaptic exocytosis at 2.4 Å resolution. *Nature (London)* **395**, 347–353 (1998).

Published in 1999 by John Wiley & Sons, Ltd.

Cell, Vol. 98, 475–485, August 20, 1999, Copyright ©1999 by Cell Press

Mauricio Montal
Appendix #2

Activation of Store-Operated Ca^{2+} Current in *Xenopus* Oocytes Requires SNAP-25 but Not a Diffusible Messenger

Yong Yao,* Antonio V. Ferrer-Montiel,†‖ Mauricio Montal,† and Roger Y. Tsien*‡§
*Department of Pharmacology
†Department of Biology
‡Howard Hughes Medical Institute
University of California, San Diego
La Jolla, California 92093-0647

Summary

Depletion of Ca^{2+} stores in *Xenopus* oocytes activated entry of Ca^{2+} across the plasma membrane, which was measured as a current I_{soc} in subsequently formed cell-attached patches. I_{soc} survived excision into inside-out configuration. If cell-attached patches were formed before store depletion, I_{soc} was activated outside but not inside the patches. I_{soc} was potentiated by microinjection of *Clostridium* C3 transferase, which inhibits Rho GTPase, whereas I_{soc} was inhibited by expression of wild-type or constitutively active Rho. Activation of I_{soc} was also inhibited by botulinum neurotoxin A and dominant-negative mutants of SNAP-25 but was unaffected by brefeldin A. These results suggest that oocyte I_{soc} is dependent not on aqueous diffusible messengers but on SNAP-25, probably via exocytosis of membrane channels or regulatory molecules.

Introduction

Ca^{2+} influx across the plasma membrane can be activated by depletion of intracellular Ca^{2+} stores in many nonexcitable cells, and it is important in activation of lymphocytes, exocytosis of mast cells, and other Ca^{2+}-dependent physiological events (for recent reviews, Berridge, 1995; Lewis and Cahalan, 1995; Favre et al., 1996; Parekh and Penner, 1997; Holda et al., 1998; Putney and McKay, 1999). The mechanism by which such "capacitative" Ca^{2+} entry is activated remains controversial. Major proposals include direct interaction ("conformational coupling") between proteins in organellar and plasma membranes (Berridge, 1995), diffusible messengers or calcium influx factors (CIFs) generated by store depletion (Parekh et al., 1993; Randriamampita and Tsien, 1993; Csutora et al., 1999), metabolites of phosphoinositides, phosphorylation cascades, heterotrimeric or small G proteins (Bird and Putney, 1993; Fasolato et al., 1993), and exocytotic insertion of vesicular channels into the plasma membrane. Previous arguments for exocytosis have included inhibition of capacitative Ca^{2+} entry by intracellular GTPγS (Bird and Putney, 1993; Fasolato et al., 1993), primaquine (Somasundaram et al., 1995), and the actin-depolymerizing drug cytochalasin D (Holda and Blatter, 1997). Each of these observations is controversial. Petersen and Berridge (1995) and Gregory and Barritt (1996) showed that the GTPγS inhibition of Ca^{2+} influx into oocytes could be prevented by staurosporine. They concluded that the GTPγS effect was mediated via stimulation of kinases. The effect of primaquine has been reinterpreted as direct inhibition of the Ca^{2+} influx channels (Gregory and Barritt, 1996). Cytochalasin D has no effect on capacitative Ca^{2+} entry in NIH3T3 cells, even though it blocks agonist-dependent Ca^{2+} release (Ribeiro et al., 1997). Furthermore, none of these pharmacological interventions is particularly diagnostic for exocytosis or takes advantage of our increased understanding of the macromolecules involved in membrane trafficking. Unfortunately, the channels that mediate capacitative Ca^{2+} influx have not yet been definitively identified at the molecular level.

This study began as a reexamination of the diffusible messenger hypothesis. Channels gated directly by diffusible messengers should be activatable in cell-attached configuration, lost in excised patches, and reactivated upon cramming those inside-out patches into the cytosol of preactivated cells, as first shown for cyclic-nucleotide-gated cation channels by Kramer (1990). Parekh et al. (1993) reported analogous behavior for capacitative Ca^{2+} entry into *Xenopus* oocytes, though Ca^{2+} entry was not directly monitored but only surmised from currents of uncertain ionic basis. Recently, we showed that store-operated, capacitative Ca^{2+} currents (I_{soc}) into whole oocytes could be directly measured by buffering cytosolic Ca^{2+} to prevent secondary currents, perfusing extracellularly with isotonic Ca^{2+} and Mg^{2+} alternately, and quantitating the difference in currents (Yao and Tsien, 1997). We have now extended this protocol to cell-attached and excised patches, hoping to solidify the evidence of Parekh et al. (1993) for a diffusible messenger. In addition, inside-out patches would be useful online detectors for the diffusible messenger(s) and would facilitate chromatographic purification and chemical identification. To our surprise, our patch-clamp findings (see Results) argued against simple mechanisms involving reversible binding of diffusible messengers.

We therefore sought experimental approaches that would be more diagnostic for an exocytotic coupling mechanism than those employed previously. We tried modulation of the small G protein Rho, because *Clostridium botulinum* C3 transferase, which specifically inactivates Rho through ADP ribosylation of Rho at Asn-41, was shown to increase insertion of the insulin-sensitive glucose transporter GLUT4 into the plasma membrane in 3T3-L1 adipocytes (Van den Berghe et al., 1996). C3 transferase also increases membrane capacitance and externalization of sodium pumps in *Xenopus* oocytes, possibly by blockade of constitutive endocytosis (Schmalzing et al., 1995).

We tested botulinum neurotoxins (BoNTs), a group of zinc endoproteases produced by bacteria of the genus *Clostridium*, because they display specific activity for a triad of protein components of the exocytic apparatus:

§To whom correspondence should be addressed (e-mail: rtsien@ucsd.edu).
‖Present address: Centro de Biologia Molecular y Celular, Universidad Miguel Hernández, C/ Monóvar s/n, 03206 Elche, Spain.

Cell, Vol. 98, 475–485, August 20, 1999, Copyright ©1999 by Cell Press

Activation of Store-Operated Ca^{2+} Current in *Xenopus* Oocytes Requires SNAP-25 but Not a Diffusible Messenger

Yong Yao,* Antonio V. Ferrer-Montiel,†‖ Mauricio Montal,† and Roger Y. Tsien*‡§
*Department of Pharmacology
†Department of Biology
‡Howard Hughes Medical Institute
University of California, San Diego
La Jolla, California 92093-0647

Summary

Depletion of Ca^{2+} stores in *Xenopus* oocytes activated entry of Ca^{2+} across the plasma membrane, which was measured as a current I_{soc} in subsequently formed cell-attached patches. I_{soc} survived excision into inside-out configuration. If cell-attached patches were formed before store depletion, I_{soc} was activated outside but not inside the patches. I_{soc} was potentiated by microinjection of *Clostridium* C3 transferase, which inhibits Rho GTPase, whereas I_{soc} was inhibited by expression of wild-type or constitutively active Rho. Activation of I_{soc} was also inhibited by botulinum neurotoxin A and dominant-negative mutants of SNAP-25 but was unaffected by brefeldin A. These results suggest that oocyte I_{soc} is dependent not on aqueous diffusible messengers but on SNAP-25, probably via exocytosis of membrane channels or regulatory molecules.

Introduction

Ca^{2+} influx across the plasma membrane can be activated by depletion of intracellular Ca^{2+} stores in many nonexcitable cells, and it is important in activation of lymphocytes, exocytosis of mast cells, and other Ca^{2+}-dependent physiological events (for recent reviews, Berridge, 1995; Lewis and Cahalan, 1995; Favre et al., 1996; Parekh and Penner, 1997; Holda et al., 1998; Putney and McKay, 1999). The mechanism by which such "capacitative" Ca^{2+} entry is activated remains controversial. Major proposals include direct interaction ("conformational coupling") between proteins in organellar and plasma membranes (Berridge, 1995), diffusible messengers or calcium influx factors (CIFs) generated by store depletion (Parekh et al., 1993; Randriamampita and Tsien, 1993; Csutora et al., 1999), metabolites of phosphoinositides, phosphorylation cascades, heterotrimeric or small G proteins (Bird and Putney, 1993; Fasolato et al., 1993), and exocytotic insertion of vesicular channels into the plasma membrane. Previous arguments for exocytosis have included inhibition of capacitative Ca^{2+} entry by intracellular GTPγS (Bird and Putney, 1993; Fasolato et al., 1993), primaquine (Somasundaram et al., 1995), and the actin-depolymerizing drug cytochalasin D (Holda and Blatter, 1997). Each of these observations is controversial. Petersen and Berridge (1995) and Gregory and Barritt (1996) showed that the GTPγS inhibition of Ca^{2+} influx into oocytes could be prevented by staurosporine. They concluded that the GTPγS effect was mediated via stimulation of kinases. The effect of primaquine has been reinterpreted as direct inhibition of the Ca^{2+} influx channels (Gregory and Barritt, 1996). Cytochalasin D has no effect on capacitative Ca^{2+} entry in NIH3T3 cells, even though it blocks agonist-dependent Ca^{2+} release (Ribeiro et al., 1997). Furthermore, none of these pharmacological interventions is particularly diagnostic for exocytosis or takes advantage of our increased understanding of the macromolecules involved in membrane trafficking. Unfortunately, the channels that mediate capacitative Ca^{2+} influx have not yet been definitively identified at the molecular level.

This study began as a reexamination of the diffusible messenger hypothesis. Channels gated directly by diffusible messengers should be activatable in cell-attached configuration, lost in excised patches, and reactivated upon cramming those inside-out patches into the cytosol of preactivated cells, as first shown for cyclic-nucleotide-gated cation channels by Kramer (1990). Parekh et al. (1993) reported analogous behavior for capacitative Ca^{2+} entry into *Xenopus* oocytes, though Ca^{2+} entry was not directly monitored but only surmised from currents of uncertain ionic basis. Recently, we showed that store-operated, capacitative Ca^{2+} currents (I_{soc}) into whole oocytes could be directly measured by buffering cytosolic Ca^{2+} to prevent secondary currents, perfusing extracellularly with isotonic Ca^{2+} and Mg^{2+} alternately, and quantitating the difference in currents (Yao and Tsien, 1997). We have now extended this protocol to cell-attached and excised patches, hoping to solidify the evidence of Parekh et al. (1993) for a diffusible messenger. In addition, inside-out patches would be useful online detectors for the diffusible messenger(s) and would facilitate chromatographic purification and chemical identification. To our surprise, our patch-clamp findings (see Results) argued against simple mechanisms involving reversible binding of diffusible messengers.

We therefore sought experimental approaches that would be more diagnostic for an exocytotic coupling mechanism than those employed previously. We tried modulation of the small G protein Rho, because *Clostridium botulinum* C3 transferase, which specifically inactivates Rho through ADP ribosylation of Rho at Asn-41, was shown to increase insertion of the insulin-sensitive glucose transporter GLUT4 into the plasma membrane in 3T3-L1 adipocytes (Van den Berghe et al., 1996). C3 transferase also increases membrane capacitance and externalization of sodium pumps in *Xenopus* oocytes, possibly by blockade of constitutive endocytosis (Schmalzing et al., 1995).

We tested botulinum neurotoxins (BoNTs), a group of zinc endoproteases produced by bacteria of the genus *Clostridium*, because they display specific activity for a triad of protein components of the exocytic apparatus:

§To whom correspondence should be addressed (e-mail: rtsien@ucsd.edu).
‖Present address: Centro de Biologia Molecular y Celular, Universidad Miguel Hernández, C/ Monóvar s/n, 03206 Elche, Spain.

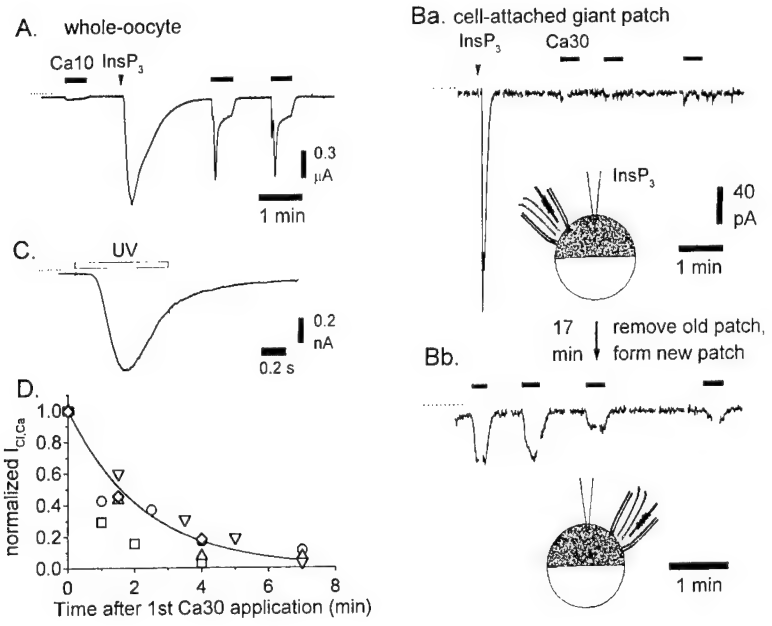

Figure 1. Blockade of Activation of Store-Operated Ca^{2+} Influx by GΩ Sealing Procedure

(A) Ca^{2+} release activated Ca^{2+} influx in oocyte recorded with two-electrode voltage clamp. Ca^{2+} influx was monitored by switching bath from Mg70 to Ca10 where indicated by heavy bars. Dotted lines in this and subsequent panels indicate zero current levels.

(Ba) Ca^{2+} release failed to activate Ca^{2+} influx in preformed cell-attached giant patch. Solution inside patch pipette was alternately changed between Mg70 and Ca30 Ringer.

(Bb) A new cell-attached giant-patch recording was made about 17 min after $InsP_3$ injection from the same oocyte. Note that the Ca^{2+} influx was recorded now in the patch formed after activation of the capacitative Ca^{2+} influx. $InsP_3$ (2 mM of 25 nl) was injected in both recordings from whole oocyte and patch as indicated by arrow heads in (A) and (B). Voltage ramps were repetitively applied during the patch recording to monitor the I-V curve. The corresponding transient currents have been blanked for clarity.

(C) $I_{Cl,Ca}$ was elicited by uncaging caged $InsP_3$ in a cell-attached giant patch. Oocyte had been loaded with 30 nl of 10 mM caged $InsP_3$.

(D) Deactivation of store-operated Ca^{2+} influx in cell-attached giant patches from $InsP_3$-loaded oocytes. Ca^{2+} influx–induced $I_{Cl,Ca}$ was measured at $V_m \approx +50$ mV and normalized to the first current amplitude. Data from five patch recordings were plotted against the time after first exposure to Ca30, among which three were made subsequently from a same oocyte. The smooth curve was a single exponential fit with a decay time constant of around 2 min.

a vesicle-associated membrane protein (VAMP or synaptobrevin), and two plasma membrane–attached proteins, SNAP-25 and syntaxin (Montecucco and Schiavo, 1995). BoNT B, D, F, and G recognize and cleave VAMP specifically. BoNT A and E cleave SNAP-25 specifically. BoNT C1 cleaves syntaxin. Binding of VAMP to syntaxin is facilitated by SNAP-25, which leads finally to fusion of vesicles with plasma membrane (Calakos and Scheller, 1996). BoNTs are widely used to block regulated exocytosis in secretory cells. Finally, dominant-negative mutants of SNAP-25 provided a molecularly independent confirmation of the BoNT A results. The combined results argue that SNAP-25 and presumably membrane trafficking play essential roles in the activation of oocyte I_{SOC}.

Results

Prior Gigaseal Formation Prevents Store Depletion from Activating Ca^{2+} Entry inside but Not outside the Patch

As well-established in two-electrode voltage clamp recording (Yao and Tsien, 1997), Ca^{2+} release due to injection of $InsP_3$ invariably led to Ca^{2+} influx, which caused a Ca^{2+}-activated Cl^- current $I_{Cl,Ca}$ whenever external Ca^{2+} was present (solid horizontal bars in Figure 1A). In these cells, we did not inject Ca^{2+} chelators to buffer cytosolic Ca^{2+}, so that $I_{Cl,Ca}$ could be a maximally sensitive monitor of Ca^{2+} entry. In contrast, when currents were recorded in cell-attached giant patches, injection of a saturating dose of $InsP_3$ activated only a transient $I_{Cl,Ca}$ mediated by Ca^{2+} release, but not Ca^{2+} influx (Figure 1Ba, typical of 10 of 11 patches). Interestingly, Ca^{2+} influx could be recorded subsequently in cell-attached patches at different spots from the same oocyte (Figure 1Bb). This indicated that prior formation of a gigaohm seal blocked the coupling mechanism between store depletion and Ca^{2+} entry within the pipette, whereas Ca^{2+} entry outside the pipette activated normally.

In a separate group of experiments, TPEN (Hofer et al., 1998) was used as an independent activator to confirm the above curious finding. In two-electrode voltage clamp recordings from whole oocytes, application of 5 mM TPEN induced Ca^{2+} influx-mediated $I_{Cl,Ca}$ of 200 to 600 nA in 10 mM extracellular Ca^{2+}. This much whole-cell current should give 31–94 pA $I_{Cl,Ca}$ in giant patches of 30 μm diameter given the ratio of giant-patch to whole-cell areas, 1/6400. However, there was no detectable Ca^{2+} influx-mediated $I_{Cl,Ca}$ in 12 of 14 cell-attached giant patches under similar stimuli measured with pipettes filled with 10 mM Ca^{2+}. In the remaining two patches, the $I_{Cl,Ca}$ mediated by Ca^{2+} influx was only −3 and −5 pA, approximately one order of magnitude less than predicted from the ratio of membrane areas. This result confirmed that most cell-attached giant patches did not respond to stimuli that normally activate store-operated Ca^{2+} influx.

The plasma membrane in cell-attached patches was visibly somewhat invaginated into the patch pipette, as is common in patch clamping (Sokabe and Sachs, 1990). To estimate the diffusional distance between the stores and plasma membrane patch, oocytes were loaded with caged $InsP_3$, and the latency of $I_{Cl,Ca}$ in giant patches after UV flash was measured (Figure 1C). This latency resulted mainly from the delay time of $InsP_3$-evoked Ca^{2+} release plus time for Ca^{2+} to diffuse from the stores to plasma membrane (Parker and Ivorra, 1993). Hot spots of $InsP_3$-evoked Ca^{2+} release are normally located about 5 μm deep under the plasma membrane in oocytes (Yao et al., 1995). This distance (d) corresponds well with 30

ms latency (t) between the Ca^{2+} fluorescence signal and $I_{Cl,Ca}$, a Ca^{2+} diffusion coefficient (D) of 140 $\mu m^2 s^{-1}$, and the equation $d^2 = 6Dt$ (Allbritton et al., 1992; Parker and Ivorra, 1993). The latency of $I_{Cl,Ca}$ in giant patches after UV uncaging of $InsP_3$ was 210 ± 30 ms (n = 3). This 7-fold increase in latency corresponds to a mean effective distance of 13 μm between stores and plasma membrane. The modest increase in distance from 5 to 13 μm should not be enough to prevent diffusion of a small molecule activator.

Maintenance of Store-Operated Ca^{2+} Influx in Whole Cells, Cell-Attached, and Excised Patches

When oocytes were injected with a saturating dose of $InsP_3$, about 0.2 mM, the Ca^{2+} influx assayed by two-electrode voltage clamp recording of $I_{Cl,Ca}$ or whole-cell recording of I_{SOC} lasted >0.5 hr. However, once a patch was formed on an activated cell, $I_{Cl,Ca}$ measured from the enclosed patch as the difference of currents with 30 mM versus 0 Ca^{2+} in the pipette declined with a time constant of about 2 min. Figure 1Bb shows one example, while Figure 1D shows the pooled data from five recordings. This decay probably represented unmasking of deactivation after gigaseal formation had blocked any further activation within the patch.

The above experiments were performed with $I_{Cl,Ca}$ as the most sensitive index of Ca^{2+} entry to maximize its likelihood of detection within the patch. We were also able to detect the much smaller Ca^{2+} current itself, I_{SOC}, in similar patches if cytosolic Ca^{2+} was well buffered by EGTA injection and store depletion preceded gigaseal formation (Figure 2A). The intrapipette solution was perfused alternately with 70 mM Mg^{2+} (Mg70) and 70 mM Ca^{2+} (Ca70), and the difference of currents $I_{Ca70} - I_{Mg70}$ was taken as I_{SOC} (Yao and Tsien, 1997). In average, I_{SOC} measured in cell-attached giant membrane patches was −22.1 ± 2.7 pA (n = 32) in oocytes depleted with ionomycin, versus −3.6 ± 0.5 pA (n = 13) from control oocytes. The amplitude of I_{SOC} in preactivated patches corresponded well with that predicted from 1/6400 of the area of a whole oocyte. Ramp current traces a and b were obtained, respectively, in Mg70 and Ca70 (Figure 2Ba) and showed an I-V relation similar to that measured in whole oocytes with two-electrode voltage clamp (Yao and Tsien, 1997).

After excision of the patch into a mock intracellular Ringer with 0 Ca^{2+} and 5 mM EGTA, I_{SOC} was constant or increased with time (Figure 2A) in 12 out of 15 patches, unlike the rapid decay of Ca^{2+} entry in patches left attached to unbuffered cells (Figures 1Bb and 1D). In the other three patches, I_{SOC}-like current decayed to baseline after a few minutes. On average, this inward current was sustained for at least 4 min after patch excision (Figure 2C). In our longest recording, lasting 8 min after excision, I_{SOC} was sustained throughout. I_{SOC} in excised patches was larger and noisier at negative membrane potentials but otherwise had much the same I-V relationship (Figure 2Bb) as before excision. To verify that the former cytosolic face of the patch was truly exposed to the bath, the external solution was briefly switched to a buffer with 0.2 μM [Ca^{2+}], which activated $I_{Cl,Ca}$ as expected (Figure 2A shaded bar and I-V relation in Figure 2Bc). In oocytes without ionomycin incubation, the residual currents measured by the usual protocol ($I_{Ca70} - I_{Mg70}$) were small and not significantly affected by excision, 4.7 ± 0.7 pA (n = 6) before versus 4.8 ± 1.0 pA (n = 6) after excision.

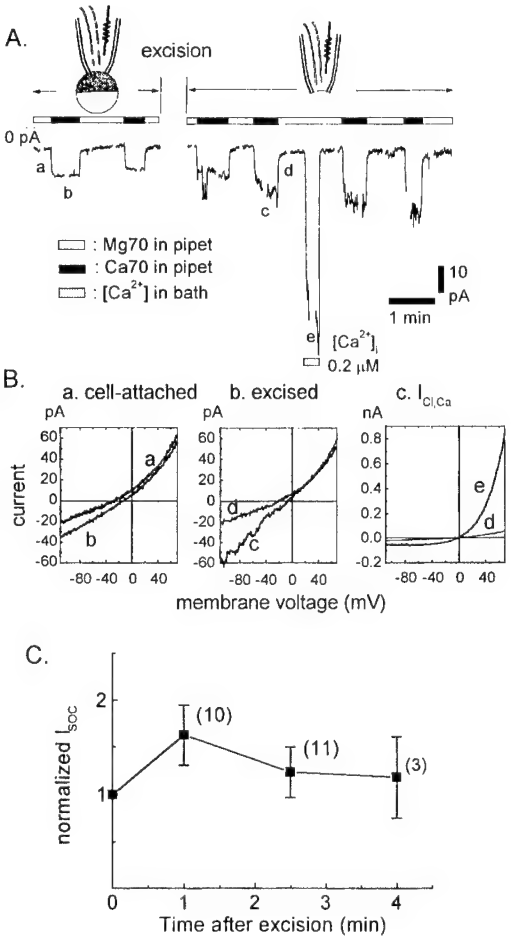

Figure 2. Survival of I_{SOC} in Inside-Out Giant Patches

(A) Store-operated Ca^{2+} current in cell-attached and inside-out giant patch. Oocyte was treated with ionomycin and injected with EGTA before patching. Pipette solution was alternately perfused with Mg70 (indicated with open bar) and Ca70 (solid bar). Voltage ramps were applied periodically to obtain the I-V curves shown in (B). The evoked current transients have been blanked for clarity.

(B) I-V curves were obtained respectively in Mg70 and Ca70 in cell-attached patch (measured at time a and b in [A]; shown in [Ba]), and in inside-out patch (c and d in [Bb]). $I_{Cl,Ca}$ was activated in excised patch by a transient increase of bath [Ca^{2+}] (e).

(C) Average of normalized I_{SOC}-like current after patch excision. The number in parentheses indicates number of patch recordings made.

Thus, seal formation on the outside of the plasma membrane inhibited activation of new I_{SOC} inside the patch but allowed preactivated I_{SOC} to continue; maintenance of such I_{SOC} did not require presence of cytosolic substances and was actually enhanced by excision. These results suggest that activation of I_{SOC} is rather localized, sensitive to membrane deformation, and unlikely to result from simple diffusion of an activator molecule. Furthermore, activation and deactivation seem to be separate processes not linked by a simple equilibrium, because different orders of manipulation can give very different results.

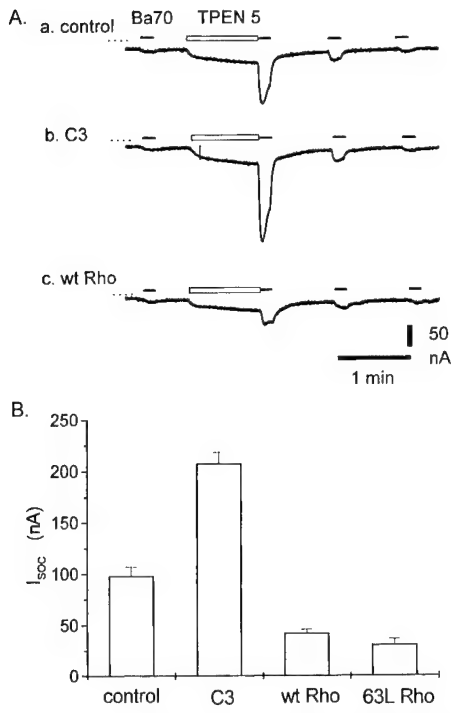

Figure 3. I_{soc} Was Potentiated by Injection of C3 Transferase and Inhibited by Expression of Rho A

(A) I_{soc} was induced by TPEN 5 mM in bath (open bars) and monitored by switching from Mg70 to Ba70 (solid bars). I_{soc} evoked by TPEN was rapidly reversible. Recordings were made, respectively, in native oocyte (Aa), oocyte 1 hr after injection of C3 transferase 0.4 μM (Ab), and oocyte 6 hr after injection of 20 ng Rho A cRNA (Ac).

(B) Summary of effects on I_{soc} of microinjected C3 transferase, expression of wild-type Rho A, and its constitutively active mutant 63L.

Regulation of Store-Operated Ca^{2+} Influx by Rho A

To examine whether the store-operated Ca^{2+} influx was affected by Rho, C3 transferase was microinjected into oocytes. In recordings illustrated in Figure 3A, Ba^{2+} current was measured to quantitate effects of C3 and Rho. Injection of Ca^{2+} chelators was omitted because activation of $I_{Cl,Ca}$ by Ba^{2+} was negligible. I_{soc} induced by 5 mM TPEN was 98 ± 9 nA (n = 9) in control oocytes and 207 ± 11 nA (n = 7) in oocytes measured about 1–2 hr after injection of C3 (3 ng/oocyte, or 120 nM assuming uniform distribution in 1 μl cytosol), an increase of 2.1-fold ($p < 0.01$). In complementary experiments, Rho A, its constitutively active mutant (63L), and dominant-negative mutant (19N) were expressed in oocytes by injection of 20 ng of their respective cRNAs about 5 hr before recordings started. I_{soc} was 42 ± 4 nA (n = 4) in oocytes expressed with wild-type Rho and 31 ± 6 (n = 6) with constitutively active mutant (63L), corresponding to 57% ($p < 0.01$) and 68% ($p < 0.01$) inhibition, respectively (Figure 3B). I_{soc} remained unchanged in oocytes expressing dominant-negative mutant 19N Rho A, suggesting a large pool of endogenous Rho A existed to maintain basal activity. Injection of C3 also induced an increase of membrane capacitance. Membrane capacitance increased by about 41% in 2 hr after injection of C3 (3 ng/oocyte) (n = 7, $p < 0.01$). In contrast, no significant decrease in membrane capacitance was found to accompany inhibition of I_{soc} in oocytes expressed with wt Rho (n = 4) and 63 L Rho (n = 6). Amplitude of I_{soc} activated by 5 mM TPEN in the above experiments was about half of the maximum. Maximal I_{soc} induced by a saturating dose of ionomycin (10 μM) was also enhanced about 46% (n = 9, $p < 0.01$) by C3 transferase. Oocytes from five of six animals showed a similar extent of potentiation by C3 transferase but not in the remaining one frog. This suggested that Rho played a modulatory rather than an indispensable role in activation of I_{soc}.

Because one of the many effects of active Rho is to promote assembly of actin-myosin filaments (stress fibers), we examined whether the potentiation of I_{soc} by C3 might simply result from the disruption of the actin-myosin assembly. Oocytes were treated with cytochalasin D (20 μg/ml) for 17 hr, at which time oocytes appeared mottled as an indication of actin depolymerization and had relative low input resistance. I_{soc} was 118 ± 14 nA (n = 7) in control oocytes and 93 ± 17 nA (n = 7) in oocytes treated with cytochalasin D. Thus, destruction of the actin cytoskeleton by cytochalasin D slightly reduced I_{soc}, probably by nonspecific mechanisms rather than mimicking C3 transferase, which greatly potentiated I_{soc}. We also tried 5 μM jasplakinolide, which solidifies the actin cytoskeleton (Shurety et al., 1998). I_{soc} was reduced from its control value of 87 ± 9.5 nA (n = 4) to 64 ± 3 nA (n = 6) during drug exposures of 0.5 or 2 hr, which were equivalent. This small reduction was significant at the p = 0.026 level and was in the same direction as, but much weaker than, the complete inhibition by 3 μM jasplakinolide of store-operated Ca^{2+} entry in cultured mammalian cells (Patterson et al., 1999 [this issue of *Cell*]).

BoNT A Inhibits Activation of Store-Operated Ca^{2+} Influx

Preinjection with 100 nM BoNT A reduced I_{soc} by about 50% (Figures 4Aa and 4Ba) without any effect on the inward rectification or the leak current, as shown by the I-V curves in Mg70 and Ca70 (Figures 4Ab and 4Bb). BoNT A also reduced Ca^{2+} influx-dependent $I_{Cl,Ca}$ induced by ionomycin, $InsP_3$, and TPEN in 10 mM Ca_o by 89% (n = 11, $p < 0.01$), 86% (n = 4, $p < 0.01$), and 86% (n = 6, $p < 0.01$), respectively (data not shown). The more dramatic reduction in the $I_{Cl,Ca}$ compared to I_{soc} probably reflects the nonlinear relation of the former with I_{soc} (Yao and Tsien, 1997). No significant change in the resting potential, input resistance, and membrane capacitance were found by BoNT A. Also, BoNT A did not alter the $I_{Cl,Ca}$ transients elicited by ionomycin, $InsP_3$, or TPEN in calcium-free medium, showing that the release of Ca^{2+} from stores and the properties of $I_{Cl,Ca}$ were unaltered.

The kinetics of BoNT A action are shown in Figure 4C. The inhibition developed with an apparent single exponential time constant of 1.1 hr and reached maximum about 4 hr after BoNT A administration. I_{soc} was 141 ± 9 nA (n = 9) in control oocytes and 72 ± 3 nA (n = 7, $p < 0.01$) in oocytes about 4 hr after injection of BoNT A. The inhibition was long-lasting and still apparent after 2 days. In a separate double-blind experiment, various doses of BoNT A were injected into oocytes. I_{soc} was measured 4 to 7 hr after injection of 20 nl BoNT A of different concentrations. The inhibition of

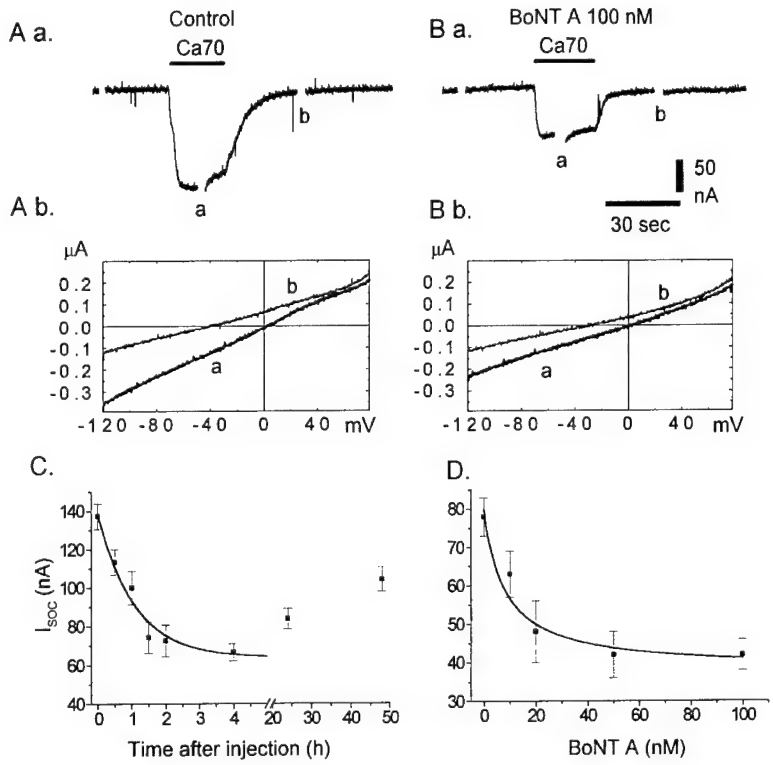

Figure 4. Inhibition of I_{SOC} by BoNT A

I_{SOC} was activated by 5 μM ionomycin followed by injection of EGTA to a final internal concentration of about 10 mM and was recorded by switching from Mg70 to Ca70 (solid bars) in a control oocyte (Aa) and an oocyte injected 4 hr earlier with 100 nM BoNT A (Ba). (Ab and Bb) The I-V relations obtained in Ca70 (a) and Mg70 (b). (C) Kinetics of BoNT A action. I_{SOC} was activated as above at different times after injection of BoNT A 100 nM. The smooth curve was the best fit to a single exponential decay with a time constant of 1.1 hr. Each data point was from more than three oocytes. (D) Dose dependence of BoNT A action. Oocytes were injected with different concentrations of BoNT A as indicated. Recordings were made 4 to 7 hr after the injections. Each data point was the average of more than four oocytes. Smooth curve was a fit to equation $(I - I_{min})/(I_{max} - I_{min}) = K_i/(K_i + [BoNT])$, with I_{max} = 80 nA, I_{min} = 38 nA, K_i = 8 nM.

I_{SOC} was found to be dose dependent on BoNT A with an apparent $K_i \approx 8$ nM (Figure 4D).

In contrast to BoNT A, BoNT B, E, and tetanus toxin had no significant effects on I_{SOC} measured about 6–8 hr after injection to final concentrations of 200 nM each. I_{SOC} was 93 ± 4 nA (n = 6) in control oocytes versus 74 ± 4 nA (n = 4), 78 ± 5 (n = 5), and 73 ± 8 (n = 6) in oocytes injected with BoNT B, E, and tetanus toxin, respectively. Unfortunately, we cannot yet test biochemically whether our toxin samples could cleave *Xenopus* oocyte SNAREs because the latter have not yet been cloned, and the antibodies we had against the mammalian proteins did not recognize their oocyte counterparts.

Blockade of I_{SOC} by Dominant-Negative Mutants of SNAP-25

Because the usual target of BoNT A is SNAP-25, we examined whether I_{SOC} activation could be similarly inhibited by dominant-negative mutants of SNAP-25. It was shown in yeast that sec9-Δ17, a C-terminal truncation of a SNAP-25 homolog, was a dominant-negative mutant (Rossi et al., 1997). According to sequence alignment (Weimbs et al., 1998) supported recently by crystal structure data (Sutton et al., 1998), yeast sec9-Δ17 corresponds to deletion of C-terminal 20 amino acids of mouse SNAP-25 (Δ20). BoNT A cleavage of mammalian SNAP-25 causes C-terminal truncation of nine amino acids (Δ9). Therefore, we made a series of C-terminal truncated SNAP-25 mutants spanning between Δ9 and Δ20 to examine whether they would have any inhibitory action on I_{SOC}. A truncated mutant SNAP-25 Δ41 was also made that corresponded to sec9-Δ38, which did not show dominant-negative effects in yeast (Rossi et al., 1997). The SNAP-25 mutants were expressed in oocytes by injection of their cRNA. I_{SOC} activated by TPEN was measured in oocytes about 14 hr after injection of 3 ng cRNA per oocyte of full-length, Δ9, Δ20, or Δ41, respectively (Figure 5). TPEN 5 mM induced about 100 nA I_{SOC} in uninjected oocytes and oocytes expressing full-length (Figure 5Aa) and Δ41 SNAP-25 (Figure 5Ac), but no I_{SOC} in oocytes expressing Δ20 (Figure 5Ab). I_{SOC} activation was inhibited by about half in oocytes expressing Δ9 cRNA. I_{SOC} activated by ionomycin was similarly inhibited by the expression of dominant-negative SNAP-25 mutants (Figure 5B). Oocytes were injected with 1 ng cRNA of each mutant per cell and recorded in 15 hr after the injection. I_{SOC} activated by 10 μM ionomycin was not affected by expression of full-length SNAP-25, but almost completely abolished by expression of Δ11, Δ14, Δ17, and Δ20 mutants. The inhibitory kinetics could be speeded up by injection of larger amounts of cRNA to express more proteins in shorter time. Thus, after injection of 30 ng of SNAP-25-Δ20, inhibition of I_{SOC} activated by ionomycin started in 2 hr and reached maximum within 4 hr after the injection (Figure 5C). While I_{SOC} was totally abolished, $I_{Cl,Ca}$ activated by ionomycin in calcium-free medium was unaffected in peak amplitude and more prolonged in oocytes expressing the dominant-negative mutant of SNAP-25, showing that inhibition of I_{SOC} was not due to any interference with Ca^{2+} release from stores. Furthermore, $I_{Cl,Ca}$ elicited by membrane depolarization (Barish, 1983) was not reduced by the dominant-negative mutants of SNAP-25. The effect of SNAP-25 on membrane turnover was assessed by capacitance measurements. A reduction of about 50% of total membrane capacitance was observed in oocytes injected with SNAP-25-Δ20 (189 ± 3 nF in control oocytes versus 96 ± 11 nF in SNAP-25-Δ20-expressed oocytes). This confirmed that the dominant-negative mutants of SNAP-25 were affecting plasma membrane turnover.

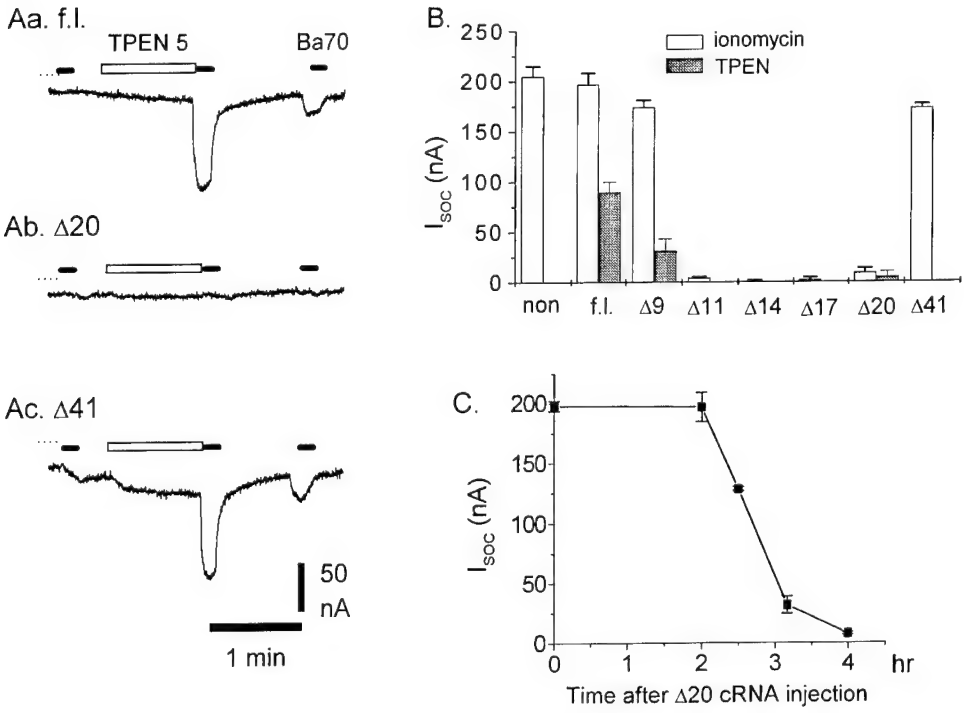

Figure 5. Prevention of I_{SOC} by C-Terminal Truncated Mutants of SNAP-25

(A) Activation of I_{SOC} by TPEN was not affected in oocytes expressing full-length (f.l.) SNAP-25 (Aa) and SNAP-25-Δ41 (Ac), but it was completely absent in oocytes expressing Δ20.

(B) Summary of inhibition of I_{SOC} by expressing SNAP-25 mutants. Activation of I_{SOC} by ionomycin (open columns) was totally abolished by expression of SNAP-25-Δ11, Δ14, Δ17, and Δ20 4 hr after injection of 30 ng cRNA, respectively. Activation of I_{SOC} by TPEN (filled columns) was inhibited by about half by expressing SNAP-25-Δ9 and was almost totally blocked by expressing Δ20 in 17 hr after injection of 3 ng cRNA each.

(C) Kinetics of I_{SOC} inhibition by expression of SNAP-25-Δ20. I_{SOC} was activated by ionomycin and measured at various times after the injection of 30 ng cRNA.

Activation of I_{SOC} Is Not Inhibited by Brefeldin A

To distinguish whether inhibition of I_{SOC} by BoNT A and dominant-negative mutants of SNAP-25 was mediated by interference with constitutive versus regulated exocytosis, we compared the effects of brefeldin A (BFA) with those of BoNT A and SNAP-25 Δ20. BFA blocks constitutive exocytosis by inhibiting protein exit from Golgi apparatus, which possibly results from BFA inhibition of guanine nucleotide exchange for ARF, a small G protein that is involved in coatomer-mediated vesicle budding from ER (Peyroche et al., 1999). Wild-type amiloride-sensitive epithelial sodium current (ENaC) expressed in *Xenopus* oocytes is inhibited by 5 μM BFA with a time constant of 3.6 hr due to blockade of constitutive insertion of ENaC channels while clathrin-mediated endocytosis remains active (Shimkets et al., 1997). We confirmed such downregulation of ENaC in oocytes by BFA as a positive control for BFA efficacy. I_{ENaC} was reduced by about 86% ($p < 10^{-10}$) by incubation of oocytes with BFA 5 μM for 7 hr. I_{SOC}, however, remained unchanged after incubation of oocytes in 5 μM BFA for 7 to 20 hr in the same batch of oocytes (Figure 6). In complete contrast to BFA, BoNT A inhibited I_{SOC} ($p < 10^{-28}$) but not I_{ENaC}. A dominant-negative SNAP-25 mutant slightly inhibited I_{ENaC} ($p = 0.014$), but to a much lesser extent than did BFA (Figure 6). In addition to the exogenous Na^+ channels, the endogenous voltage-operated Ca^{2+} channels and Ca^{2+}-activated Cl^- channels were not reduced by BoNT A and SNAP-25-Δ20 but were inhibited by BFA, though the BFA block was statistically significant only at the $p = 0.06$ level (Figure 6). These results indicated that blockade by BFA of constitutive traffic to the plasma membrane for up to 24 hr did not reduce the cells' ability to activate I_{SOC}, and inhibition of I_{SOC} by BoNT A and SNAP-25 mutants did not result from disruption of constitutive trafficking.

Discussion

Activation of the Store-Operated Ca^{2+} Current Is a Local Process that Can Show Hysteresis

Our patch-clamp experiments showed that store-operated Ca^{2+} entry was highly localizable, required store depletion to precede patch isolation, and yet survived patch excision. Thus, depletion of Ca^{2+} stores could activate Ca^{2+} influx outside but not inside a preformed gigaseal onto a 30 μm diameter patch pipette (Figures 1A and 1B). Therefore, the ability of store depletion to trigger Ca^{2+} current within the patch was disrupted by some aspect of seal formation, such as the visible invagination of the plasma membrane into the lumen of the pipette. Meanwhile, the $InsP_3$-induced increase in cytosolic [Ca^{2+}] was still able to activate $I_{Cl,Ca}$ within the cell-attached patch with slightly greater latency than normal (Figure 1C). This finding showed that Ca^{2+} was still able to diffuse from the internal stores to the plasma membrane inside the gigaseal, though the mean diffusion distance had apparently been increased from the normal

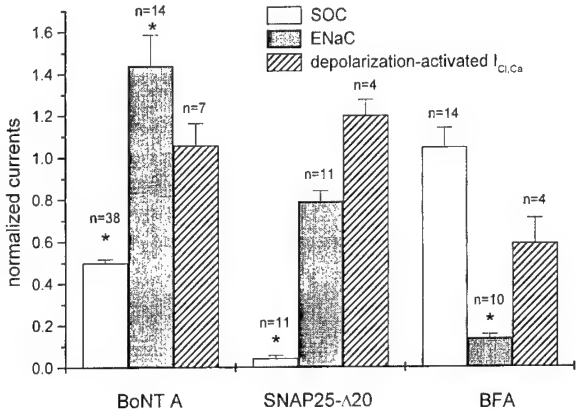

Figure 6. Comparison of Effects on I_{SOC}, I_{ENaC}, and Depolarization-Activated $I_{Cl,Ca}$ by BoNT A, SNAP-25-Δ20, and BFA

All current values measured were normalized to mean values of control groups of the same donor. The normalized currents from separate donors were averaged for statistical analysis. Groups significantly different ($p < 0.01$) from control are marked with an asterisk. Number of oocytes measured in each group is indicated on the column. I_{SOC} was activated by ionomycin and measured in Ba70. I_{ENaC} was measured in calcium-free Ringer at holding $V_m = -30$ mV as the difference in currents before and after 1 μM amiloride. Peak values of depolarization-activated $I_{Cl,Ca}$ were measured by stepping V_m to +40 mV in Ca10. It represents endogenous voltage-gated Ca^{2+} channel activity evoking $I_{Cl,Ca}$ (Barish, 1983). BoNT A was injected into oocytes to a 100–200 nM final concentration, waiting for 4 to 7 hr before recording. SNAP-25-Δ20 cRNA (30 ng) was injected into oocytes to allow protein expression for 4–6 hr. Incubations with 5 μM BFA lasted 5–20 hr before recording.

5 μm to 13 μm. Once Ca^{2+} influx was activated in the absence of or outside a gigaseal, it was readily detectable in a new cell-attached patch, showing that patch formation only obstructed initial activation rather than maintenance of the influx. Furthermore, I_{SOC} survived without diminution for minutes after excision of the patch into the inside-out configuration (Figure 2). Although one of us helped launch the idea of a diffusible CIF (Randriamampita and Tsien, 1993), we must admit that these findings argue against mediation by a CIF freely diffusible through the cytosol, because such a factor should have easily reached the plasma membrane inside the gigaseal but should have washed out immediately after excision of the patch. In a "conformational coupling" hypothesis, one would need to postulate that the protein–protein contact between the stores and plasma membrane would be easily disrupted or prevented before store depletion, but it would become robust enough after I_{SOC} activation to survive invagination and excision of the patch. In an exocytosis model, one would assume that exocytosis is locally prevented by bulging of the plasma membrane into the gigaseal. Indeed, exocytosis in mast cells is reported to be reversibly blocked by inflating the plasma membrane (Solsona et al., 1998). Whatever the model, the gigaseal results show that activation of Ca^{2+} influx can vary over distances of only a few microns, even more spatially confined than those of Petersen and Berridge (1996) or Jaconi et al. (1997), where localization was reported over distances of hundreds of microns.

These results would seem to conflict with a previous report (Figure 2, Parekh et al., 1993) in which a depletion-activated current in cell-attached patches was immediately quenched by excision from the oocyte and could be reactivated by cramming back into a stimulated cell. This current had a linear I-V curve with a reversal potential of −30 mV, was recorded in the presence of niflumic acid to block $I_{Cl,Ca}$, and had amplitudes of 10–20 pA with pipettes of ordinary micron diameters. I_{SOC} was characterized in recent two-electrode voltage clamp recording studies (Hartzell, 1996; Yao and Tsien, 1997), in which Ca^{2+} chelators instead of niflumic acid were used to abolish $I_{Cl,Ca}$ because niflumic acid was found to inhibit I_{SOC}. As expected for a highly Ca^{2+}-selective current, I_{SOC} has an inwardly rectifying I-V curve with a reversal potential $>+40$ mV. Giant-patch recording (Hilgemann, 1995) with 30 μm diameter pipettes and intrapipette perfusion was required to increase detection sensitivity and to record ~10 pA of I_{SOC} directly as the difference in currents between 70 and 0 mM extracellular Ca^{2+}. Therefore, the current that was quenched by excision and restored by cramming in the experiment of Parekh et al. (1993) was dominated by components other than Ca^{2+} influx.

Mechanisms of Rho A Action on I_{SOC}

Up- and downregulation of RhoA, by expression of excess Rho A or injection of *Clostridium* C3 transferase, respectively, decreased and increased the amplitude of I_{SOC} (Figure 3). Rho A is known to regulate many cell events, including cytoskeletal rearrangement and membrane trafficking (Van Aelst and D'Souza-Schorey, 1997; Hall, 1998). Because RhoA may affect both constitutive and regulated membrane trafficking, our results with C3 and RhoA provide only general evidence for the importance of trafficking in modulating capacitative Ca^{2+} entry.

Mechanisms of Action of Botulinum Neurotoxin A and SNAP-25

In this study, I_{SOC} was found to be inhibited by about 50% by BoNT A (Figures 4 and 6). This inhibition was relatively specific as endogenous $I_{Cl,Ca}$, voltage-gated Ca^{2+} current, and transfected epithelial Na^+ channels were not reduced. The time course and potency of the inhibitory action on I_{SOC} by BoNT A were similar to that described in blockade of neurotransmission of *Aplysia* synapses (Rossetto et al., 1994). Recently BoNTs have also been shown to block insulin-stimulated translocation of GLUT4 in adipocytes (Cheatham et al., 1996). The maximum inhibition of insulin-stimulated glucose uptake was 43%–51% (Tamori et al., 1996; Chen et al., 1997), quite similar to the maximal reduction of I_{SOC} in our experiments. Likewise BoNT A causes only a partial block and slowing of catecholamine release from chromaffin cells (Xu et al., 1998).

The complete inhibition of I_{SOC} by dominant-negative mutants of SNAP-25 and the biphasic length dependence of the effective truncations strongly complement the evidence from BoNT A for a crucial role for a SNAP-25 homolog in oocytes. The length dependence fits well with multiple studies showing the critical importance of the region corresponding to 9 to 26 residues from the C terminus of mammalian SNAP-25 for exocytosis and its triggering by calcium sensors (Gutierrez et al., 1995;

Rossi et al., 1997; Ferrer-Montiel et al., 1998; Huang et al., 1998; Xu et al., 1998). The partial inhibition by the Δ9 truncation fits well with the similarly partial inhibition by BoNT A, which should cut SNAP-25 at the corresponding location. The inhibition of I_{SOC} is not explainable by general interference with constitutive insertion of channels into the plasma membrane, because currents through Ca^{2+}-activated Cl^- channels, voltage-gated Ca^{2+} channels, or transfected epithelial Na^+ currents remained undiminished (Figure 6). Conversely, constitutive insertion, for example of epithelial Na^+ channels, can be inhibited by brefeldin A without any effect on I_{SOC} (Figure 6). Therefore, SNAP-25 and, presumably, regulated exocytosis are important in the process for activating I_{SOC}. We did not see any change in the I-V relation of I_{SOC} after partial inhibition by BoNT A, so we could find no evidence that SNAP-25 modifies the conductance properties of the Ca^{2+} entry channels in the way that syntaxin modulates the gating of voltage-activated Ca^{2+} channels (Bezprozvanny et al., 1995). Instead, loss of functional SNAP-25 simply reduces the amplitude of the residual I_{SOC}.

Conclusions regarding the Mechanism of Coupling

Ca^{2+} entry into oocytes can be activated by microinjection of extracts from lymphocytes or yeast in which Ca^{2+} stores have been pharmacologically or genetically depleted (Csutora et al., 1999). However, those authors acknowledged that oocytes themselves produce relatively low levels of calcium influx factor, and that the evoked influx had different properties from endogenously stimulated capacitative Ca^{2+} entry, especially in lanthanide sensitivity. Our present results come entirely from oocytes and do not rule out the potential importance of diffusible factors in other cell types. A conformational coupling hypothesis could be compatible with our data if one assumes that the link between the stores and the plasma membrane is mechanically weak before store depletion and strong afterward, and that SNAP-25 or a homolog is important for the linkage. Our results are somewhat more naturally accommodated within a model in which the channels themselves or membrane-bound activator molecules are exocytotically incorporated into the plasma membrane upon store depletion. We would argue that inhibitions by BoNT A and dominant-negative SNAP-25 are far more likely to be pharmacologically specific for SNAP-25 and exocytosis than the previous controversial effects of GTP-γS, primaquine, and cytoskeletal inhibitors. Furthermore, new experiments with cytoskeletal modulation have provided fresh evidence for secretion-like coupling (Patterson et al., 1999). The major arguments against exocytosis are the lack of measurable increases in membrane capacitance before or during store-operated Ca^{2+} entry in oocytes (<1% change; preliminary data of Y. Y.) and other cell types (e.g., Fomina and Nowycky, 1999), and the lack of effect of BoNT B and E and tetanus toxin. However, the negligible capacitance increases could reflect the minuscule amount of membrane required to accommodate the channels or activators, swamped by the huge amount of concurrent exo- and endocytosis, sufficient to replace the entire oocyte plasma membrane once every day if all components mixed freely (Zampighi et al., 1999). The lack of inhibition by certain toxins might be due to imperfect homology of the relevant oocyte components to the better-studied mammalian SNAREs; we had no positive control that our toxin samples had any effect in oocytes. Nevertheless, the involvement of proteins extensively studied in exocytosis opens up many possible testable hypotheses and experiments for the future.

Experimental Procedures

Cell Preparation and Electrophysiology

Oocytes were cultured in Barth's medium supplemented with 5% horse serum to increase viability of the cells (Quick et al., 1992). Recordings were taken at least 2 hr after removal of the serum. Oocytes used to assess drug action were obtained from the same frog to reduce variability in I_{SOC}. Extracellular solution compositions and recording of whole-oocyte membrane currents with a conventional two-electrode voltage clamp were as described by Yao and Tsien (1997). Membrane potential was held at −60 mV unless otherwise specified. Capacitance of whole-oocyte plasma membrane was determined by $C_m = \int i_C\, dt/\Delta V$, where C_m is membrane capacitance, i_C capacitance current transient, ΔV membrane voltage step. C_m was averaged from ΔV of 5, 10, and 15 mV, respectively.

Giant-patch glass pipettes (#7052, O. D./I. D. 1.65/1.1, WPI, FL or borosilicate glass, O. D./I. D. 1.5/0.86 Warner Instrument Corp., Hamden, CT) were pulled to have tip openings of around 40 μm with a horizontal electrode puller (P-80/PC, Sutter Instrument Co., Novato, CA). The pipette tips were then heat-polished to give final openings of about 30 μm, which should encompass about 1/6400 of the total surface of an oocyte of 1.2 mm diameter. Thus, an oocyte with a total I_{SOC} of 100 nA should give about 16 pA through the patch assuming the channels are evenly distributed. Patch recordings made from various sites on the animal hemisphere showed no significant variation in current amplitudes. In some experiments (e.g., Figure 1), $I_{Cl,Ca}$ was measured as a more sensitive monitor of Ca^{2+} influx, because its amplitude is about an order of magnitude larger than I_{SOC} (Yao and Tsien, 1997). For intrapipette perfusion, quartz capillaries (O. D./I. D. 150/75 μm, Polymicro Technologies Inc., Phoenix, AZ) were pulled and the tips cut to about 15 to 20 μm diameter. Two capillaries were bundled with glue and inserted to within 100–200 μm of the patch pipette tip under a stereo microscope. Perfusates were passed through a 2 μm filter. Perfusates in quartz capillaries were held by suction (typically −10 mm Hg) to prevent leakage and were ejected by a positive pressure (typically 150 mm Hg). Turnover of intrapipette solutions at the membrane was typically within a few seconds. Oocyte vitelline membranes were removed in a hyperosmotic solution that contained (mM): KCl 200, $MgCl_2$ 2, KCl 1, and HEPES 5, titrated to pH 7.2 with NaOH, supplemented with EGTA 5 mM for measuring I_{SOC} or 40 μM for measuring $I_{Cl,Ca}$. Current was recorded with an Axopatch 200B amplifier (Axon Instruments, Inc., Foster City, CA), whose range of the fast capacitance compensation was expanded to 20 pF by the manufacturer. Membrane seal resistance were larger than 1 GΩ. Bath solution for excised patch recordings was a mock intracellular Ringer (IR), containing (mM): 95 KCl, 1 NaCl, 5 $MgCl_2$, 5 HEPES, titrated to pH 7.2 with NaOH, plus EGTA 5 mM and 40 μM, respectively, for recording I_{SOC} and $I_{Cl,Ca}$. Membrane potentials of the oocytes were measured to be −8.8 ± 0.5 mV (n = 4) in IR. The pipette potential was held at 50 mV after a GΩ seal was formed. A voltage ramp command from 50 to −130 mV with a duration of 0.5 s was repetitively applied at 30 s intervals to allow rapid collection of I-V relations of the current. This resulted in a final membrane potential ramp from −109 to 71 mV after summing pipette holding potential, oocyte membrane potential, and the ramp command.

All recordings were performed at room temperature (22°C ± 2°C). Data points are expressed as mean ± SE. Statistical significance of drug actions was evaluated with two-tailed Student's t test using Origin software (Microcal, Northampton, MA).

Use of TPEN to Activate Store-Operated Ca^{2+} Influx in *Xenopus* Oocytes

The usual means for dumping Ca^{2+} stores and activating I_{SOC}, such as ionomycin administration or metabolic production or microinjection of $InsP_3$, were poorly reversible. A rapidly reversible agent not requiring microinjection would be very helpful. A membrane-permeant chelator of divalent cations, TPEN, was shown recently to induce store-operated Ca^{2+} influx in mammalian cells (Hofer et al., 1998). TPEN has a low affinity for Ca^{2+} (K_D = 40 μM; Arslan et al., 1985) suitable for buffering the relatively high free Ca^{2+} concentrations in the lumen of Ca^{2+}-accumulating organelles while exerting little effect on cytosolic free Ca^{2+} (Hofer et al., 1998). The total Ca^{2+} inside the stores is conserved during application of TPEN because the TPEN–Ca^{2+} complex is impermeant (Arslan et al., 1985). When free extracellular TPEN is removed, the intraluminal TPEN–Ca^{2+} dissociates and rapidly restores intraluminal free Ca^{2+} so that deactivation of influx can be studied.

TPEN had not been previously tested in *Xenopus* oocytes but proved very useful in activating I_{SOC} because of the above advantages. TPEN was dispersed in nominally Ca^{2+}-free media and applied extracellularly to load the oocytes before restoration of normal Ca^{2+} to measure the influx. The minimum TPEN concentrations required to activate the Ca^{2+} influx varied from 0.1 to 1 mM in different batches of oocytes. Ca^{2+} influx reversed quickly after washout of TPEN from bath and could be reactivated repeatedly. Maximal Ca^{2+} influx was activated by preincubation of oocyte with TPEN for 1 min. Longer incubations with TPEN slowed the deactivation time course of the Ca^{2+} influx. An additional inward nonspecific current was present during the TPEN loading, which was not inhibited by injection of EGTA. To test whether the action of TPEN was additive to that of ionomycin, Ca^{2+} influx was first induced by TPEN and then ionomycin to obtain their individual activities in the same oocyte. Ca^{2+} influx induced by ionomycin was long-lasting. Application of TPEN after ionomycin did not induce additional Ca^{2+} influx (data not shown). Such occlusion indicates that Ca^{2+} influx induced by TPEN is through the store-operated Ca^{2+} influx pathway.

One concern with TPEN is its very high binding affinity for Zn^{2+} ($K_D = 2.63 \times 10^{-16}$ M) (Arslan et al., 1985). Also, even 5 mM TPEN only activated I_{SOC} to about half the maximal amplitude obtainable with other means for depleting stores. A new membrane-permeable Ca^{2+} chelator that has a higher affinity to Ca^{2+} and lower affinity to Zn^{2+} than TPEN would be yet better. Fortunately, inhibition of BoNTs by TPEN's chelation of Zn^{2+} is irrelevant because TPEN is only applied well after BoNT injection.

Materials

Botulinum toxin A, B, and E were kindly supplied by Dr. B. R. DasGupta (University of Wisconsin, Madison). They were dissolved at 1 mg/ml in buffer containing (mM): 150 NaCl, 10 HEPES, titrated to pH 7.0, maintained at −80°C. BoNTs were reduced with 10 or 20 mM DTT at room temperature for 1 hr before injection. Activity of BoNT A was assessed by in vitro cleavage assay of SNAP-25 (Ferrer-Montiel et al., 1996). Cytochalasin D was from Sigma. C3 transferase, amiloride, and brefeldin A were from Calbiochem Novabiochem (La Jolla, CA). One side effect of C3 transferase was a spontaneous current, dependent on extracellular Ca^{2+}, which usually developed about 1 hr or longer after the injection of C3. Intracellular injection of EGTA or exposure to TPEN suppressed the current, so it did not interfere with measurement of I_{SOC}. The origin of this curious current remained to be further characterized.

Expression Vector Construction and In Vitro Transcription

cDNAs of wild-type Rho A, its constitutively active mutant 63L, and dominant-negative mutant 19N in plasmid pCMV5 were kind gifts of Dr. G. Bokoch (Scripps Research Institute, San Diego, CA). Rho and its mutant cDNA inserts were released from pCMV5 with HindIII digestion and subcloned into pSGEM at the HindIII site. Vector pSGEM was obtained from Dr. Philipp and Dr. Flockerzi (Universität des Saarlandes, Homburg/Saar, Germany), which derived from a popular oocyte expression vector pGEMHE that contained *Xenopus* β-hemoglobin untranslated regions flanking the multiple cloning site (Liman et al., 1992). The orientation of the cDNA inserts was checked by gel electrophoresis after EcoRV digestion.

C-terminal truncated mutants of mouse SNAP-25 were created by PCR using a forward primer paired with various reverse primers that introduced a stop codon to terminate translation at different C-terminal sites of SNAP-25. The forward primer in PCR reaction had the sequence 5′-CGGGATCCGCCACCATGGCCGAGGACGCA GACATG, which contained a BamHI site and a Kozak sequence at the 5′ end of SNAP-25. The reverse primers for CΔ9, CΔ11, CΔ14, CΔ17, CΔ20, and CΔ41 were, respectively, 5′-CGGAATTCTTATTGG TTGGCTTCATCAAT, 5′-CGGAATTCTTAGGCTTCATCAATTCTGGT, 5′-CGGAATTCTTAAATTCTGGTTTTGTTGGA, 5′-CGGAATTCTTATT TGTTGGAGTCAGCCTT, 5′-CGGAATTCTTAGTCAGCCTTCTCCAT GAT, and 5′-CGGAATTCTTATAGGGCCATATGACGGAG. All reverse primers incorporated an EcoRI site and a stop codon at the 3′-end of SNAP-25. Following PCR amplification, the PCR products were gel-separated and digested with BamHI and EcoRI. The resulting PCR frgments were subcloned into the vector pSGEM between the 5′ UTR and the 3′UTR of *Xenopus* β-globin. All C-terminal truncation mutants of SNAP-25 were verified by DNA sequencing.

cDNAs of three subunits of epithelial sodium channel, α, β, γ, in plasmids pSPORT (α and γ) and pSD5 (β), were kind gifts of Dr. C. Canessa (Yale University). pSPORT-α and γ were linearized by NotI and RNA synthesized by T7 polymerase, whereas BglII and SP6 polymerase were used for pSD5-β. A mixture of the three cRNAs (0.1 or 1 ng each) was injected into each oocyte, and I_{ENaC} was measured 1–3 days later.

Capped cRNAs were synthesized using mMESSAGE mMACHINE kits from Ambion (Austin, TX). Synthetic cRNAs were resuspended in water. Aliquots of 2 μl each were stored at −80°C until injection. Typically, 20 nl RNA solution was injected into each oocyte. Concentrations of RNA were adjusted to reach the final desired mass.

Acknowledgments

We thank Dr. J. Llopis and Dr. J. Garcia-Sancho for their unpublished data and discussion, Dr. D. Hilgemann and Dr. C. C. Lu for discussion of the giant-patch recording technique, and Ms. Q. Xiong for technical assistance. This study was supported by grants to R. Y. T. from the Human Frontier Science Program (RG520/1995-M), National Institutes of Health (NS27177), and Howard Hughes Medical Institute, and a Department of the Army Medical Research Grant DAMD17-C-98-C-8040 to M. M.

Received June 8, 1999; revised July 21, 1999.

References

Allbritton, N.L., Meyer, T., and Stryer, L. (1992). Range of messenger action of calcium ion and inositol 1,4,5-trisphosphate. Science *258*, 1812–1815.

Arslan, P., Di Virgilio, F., Beltrame, M., Tsien, R.Y., and Pozzan, T. (1985). Cytosolic Ca^{2+} homeostasis in Ehrlich and Yoshida carcinomas. A new, membrane-permeant chelator of heavy metals reveals that these ascites tumor cell lines have normal cytosolic free Ca^{2+}. J. Biol. Chem. *260*, 2719–2727.

Barish, M.E. (1983). A transient calcium-dependent chloride current in the immature *Xenopus* oocytes. J. Physiol. (Lond.). *342*, 309–325.

Berridge, M.J. (1995). Capacitative calcium entry. Biochem. J. *312*, 1–11.

Bezprozvanny, I., Scheller, R.H., and Tsien, R.W. (1995). Functional impact of syntaxin on gating of N-type and Q-type calcium channels. Nature *378*, 623–626.

Bird, G.S., and Putney, J.W., Jr. (1993). Inhibition of thapsigargin-induced calcium entry by microinjected guanine nucleotide analogues. Evidence for the involvement of a small G protein in capacitative Ca^{2+} entry. J. Biol. Chem. *268*, 21486–21488.

Calakos, N., and Scheller, R.H. (1996). Synaptic vesicle biogenesis, docking, and fusion: a molecular description. Physiol. Rev. *76*, 1–29.

Cheatham, B., Volchuk, A., Kahn, C.R., Wang, L., Rhodes, C.J., and Klip, A. (1996). Insulin-stimulated translocation of GLUT4 glucose transporters requires SNARE-complex proteins. Proc. Natl. Acad. Sci. USA *93*, 15169–15173.

Chen, F., Foran, P., Shone, C.C., Foster, K.A., Melling, J., and Dolly, J.O. (1997). Botulinum neurotoxin B inhibits insulin-stimulated glucose uptake into 3T3-L1 adipocytes and cleaves cellubrevin unlike type A toxin which failed to proteolyze the SNAP-23 present. Biochemistry *36*, 5719–5728.

Csutora, P., Su, Z., Kim, H.K., Bugrim, A., Cunningham, K.W., Nuccitelli, R., Keizer, J.E., Hanley, M.R., Blalock, J.E., and Marchase, R.B. (1999). Calcium influx factor is synthesized by yeast and mammalian cells depleted of organellar calcium stores. Proc. Natl. Acad. Sci. USA *96*, 121–126.

Fasolato, C., Hoth, M., and Penner, R. (1993). A GTP-dependent step in the activation mechanism of capacitative Ca^{2+} influx. J. Biol. Chem. *268*, 20737–20740.

Favre, C.J., Nusse, O., Lew, D.P., and Krause, K.H. (1996). Store-operated Ca^{2+} influx: what is the message from the stores to the membrane? J. Lab. Clin. Med. *128*, 19–26.

Ferrer-Montiel, A.V., Canaves, J.M., DasGupta, B.R., Wilson, M.C., and Montal, M. (1996). Tyrosine phosphorylation modulates the activity of clostridial neurotoxins. J. Biol. Chem. *271*, 18322–18325.

Ferrer-Montiel, A.V., Gutierrez, L.M., Apland, J.P., Canaves, J.M., Gil, A., Viniegra, S., Biser, J.A., Adler, M., and Montal, M. (1998). The 26-mer peptide released from SNAP-25 cleavage by botulinum neurotoxin E inhibits vesicle docking. FEBS Lett. *435*, 84–88.

Fomina, A.F., and Nowycky, M.C. (1999). A current activated on depletion of intracellular Ca^{2+} stores can regulate exocytosis in adrenal chromaffin cells. J. Neurosci. *19*, 3711–3722.

Gregory, R.B., and Barritt, G.J. (1996). Store-activated Ca^{2+} inflow in *Xenopus laevis* oocytes: inhibition by primaquine and evaluation of the role of membrane fusion. Biochem. J. *319*, 755–760.

Gutierrez, L.M., Canaves, J.M., Ferrer-Montiel, A.V., Reig, J.A., Montal, M., and Viniegra, S. (1995). A peptide that mimics the carboxy-terminal domain of SNAP-25 blocks Ca^{2+}-dependent exocytosis in chromaffin cells. FEBS Lett. *372*, 39–43.

Hall, A. (1998). Rho GTPases and the actin cytoskeleton. Science *279*, 509–514.

Hartzell, H.C. (1996). Activation of different Cl currents in *Xenopus* oocytes by Ca liberated from stores and by capacitative Ca influx. J. Gen. Physiol. *108*, 157–175.

Hilgemann, D.W. (1995). The giant membrane patch. In Single-Channel Recording (2nd edition), B. Sakmann and E. Neher, eds. (New York: Plenum Press), pp. 307–327.

Hofer, A.M., Fasolato, C., and Pozzan, T. (1998). Capacitative Ca^{2+} entry is closely linked to the filling state of internal Ca^{2+} stores: a study using simultaneous measurements of I_{CRAC} and intraluminal $[Ca^{2+}]$. J. Cell Biol. *140*, 325–334.

Holda, J.R., and Blatter, L.A. (1997). Capacitative Ca^{2+} entry is inhibited in vascular endothelial cells by disruption of cytoskeletal microfilaments. FEBS Lett. *403*, 191–196.

Holda, J.R., Klishin, A., Sedova, M., Huser, J., and Blatter, L.A. (1998). Capacitative calcium entry. News Physiol. Sci. *13*, 157–163.

Huang, X., Wheeler, M.B., Kang, Y.-h., Sheu, L., Lukacs, G.L., Trimble, W.S., and Gaisano, H.Y. (1998). Truncated SNAP-25 (1–197), like botulinum neurotoxin A, can inhibit insulin secretion from HIT-T15 insulinoma cells. Mol. Endocrinol. *12*, 1060–1070.

Jaconi, M., Pyle, J., Bortolon, R., Ou, J., and Clapham, D. (1997). Calcium release and influx colocalize to the endoplasmic reticulum. Curr. Biol. *7*, 599–602.

Kramer, R.H. (1990). Patch cramming: monitoring intracellular messengers in intact cells with membrane patches containing detector ion channels. Neuron *4*, 335–341.

Lewis, R.S., and Cahalan, M.D. (1995). Potassium and calcium channels in lymphocytes. Annu. Rev. Immunol. *13*, 623–653.

Liman, E.R., Tytgat, J., and Hess, P. (1992). Subunit stoichiometry of a mammalian K+ channel determined by construction of multimeric cDNAs. Neuron *9*, 861–871.

Montecucco, C., and Schiavo, G. (1995). Structure and function of tetanus and botulinum neurotoxins. Quart. Rev. Biophys. *28*, 423–472.

Parekh, A.B., and Penner, R. (1997). Store depletion and calcium influx. Physiol. Rev. *77*, 901–930.

Parekh, A.B., Terlau, H., and Stühmer, W. (1993). Depletion of $InsP_3$ stores activates a Ca^{2+} and K^+ current by means of a phosphatase and a diffusible messenger. Nature *364*, 814–818.

Parker, I., and Ivorra, I. (1993). Confocal microfluorimetry of calcium signals evoked in *Xenopus* oocytes by photoreleased inositol trisphosphate. J. Physiol. *461*, 133–165.

Patterson, R.L., van Rossum, D.B., and Gill, D.L. (1999). Store-operated Ca^{2+} entry: evidence for a secretion-like coupling model. Cell *98*, this issue, 487–499.

Petersen, C.C.H., and Berridge, M.J. (1995). G-protein regulation of capacitative Ca^{2+} entry may be mediated by protein kinases A and C in *Xenopus* oocytes. Biochem. J. *307*, 663–668.

Petersen, C.C.H., and Berridge, M.J. (1996). Capacitative calcium entry is colocalised with calcium release in *Xenopus* oocytes: evidence against a highly diffusible calcium influx factor. Pflug. Arch. Eu. J. Physiol. *432*, 286–292.

Peyroche, A., Antonny, B., Robineau, S., Acker, J., Cherfils, J., and Jackson, C.L. (1999). Brefeldin A acts to stabilize an abortive ARF-GDP-Sec7 domain protein complex: involvement of specific residues of the Sec7 domain. Mol. Cell *3*, 275–285.

Putney, J.W., Jr., and McKay, R.R. (1999). Capacitative calcium entry channels. BioEssays *21*, 38–46.

Quick, M.W., Naeve, J., Davidson, N., and Lester, H.A. (1992). Incubation with horse serum increases viability and decreases background neurotransmitter uptake in *Xenopus* oocytes. Biotechniques *13*, 357–361.

Randriamampita, C., and Tsien, R.Y. (1993). Emptying of intracellular Ca^{2+} stores releases a novel small messenger that stimulates Ca^{2+} influx. Nature *364*, 809–814.

Ribeiro, C.M.P., Reece, J., and Putney, J.W., Jr. (1997). Role of the cytoskeleton in calcium signaling in NIH 3T3 cells: an intact cytoskeleton is required for agonist-induced $[Ca^{2+}]_i$ signaling, but not for capacitative calcium entry. J. Biol. Chem. *272*, 26555–26561.

Rossetto, O., Schiavo, G., Montecucco, C., Poulain, B., Deloye, F., Lozzi, L., and Shone, C.C. (1994). SNARE motif and neurotoxins. Nature *372*, 415–416.

Rossi, G., Salminen, A., Rice, L.M., Brünger, A.T., and Brennwald, P. (1997). Analysis of a yeast SNARE complex reveals remarkable similarity to the neuronal SNARE complex and a novel function for the C terminus of the SNAP-25 homolog, Sec9. J. Biol. Chem. *272*, 16610–16617.

Schmalzing, G., Richter, H.P., Hansen, A., Schwarz, W., Just, I., and Aktories, K., (1995). Involvement of the GTP binding protein Rho in constitutive endocytosis in *Xenopus laevis* oocytes. J. Cell Biol. *130*, 1319–1332.

Shimkets, R.A., Lifton, R.P., and Canessa, C.M. (1997). The activity of the epithelial sodium channel is regulated by clathrin-mediated endocytosis. J. Biol. Chem. *272*, 25537–25541.

Shurety, W., Stewart, N.L., and Stow, J.L. (1998). Fluid-phase markers in the basolateral endocytic pathway accumulate in response to the actin assembly-promoting drug jasplakinolide. Mol. Biol. Cell *9*, 957–975.

Sokabe, M., and Sachs, F. (1990). The structure and dynamics of patch-clamped membranes: a study using differential interference contrast light microscopy. J. Cell Biol. *111*, 599–606.

Solsona, C., Innocenti, B., and Fernandez, J.M. (1998). Regulation of exocytotic fusion by cell inflation. Biophys. J. *74*, 1061–1073.

Somasundaram, B., Norman, J.C., and Mahaut-Smith, M.P. (1995). Primaquine, an inhibitor of vesicular transport, blocks the calcium-release-activated current in rat megakaryocytes. Biochem. J. *309*, 725–729.

Sutton, R.B., Fasshauer, D., Jahn, R., and Brunger, A.T. (1998). Crystal structure of a SNARE complex involved in synaptic exocytosis at 2.4 Å resolution. Nature *395*, 347–353.

Tamori, Y., Hashiramoto, M., Araki, S., Kamata, Y., Takahashi, M., Kozaki, S, and Kasuga, M. (1996). Cleavage of vesicle-associated membrane protein (VAMP)-2 and cellubrevin on GLUT4-containing vesicles inhibits the translocation of GLUT4 in 3T3-L1 adipocytes. Biochem. Biophys. Res. Commun. *220*, 740–745.

Van Aelst, L., and D'Souza-Schorey, C. (1997). Rho GTPases and signaling networks. Genes Dev. *11*, 2295–2322.

Van den Berghe, N., Barros, L.F., van Mackelenbergh, M.G., and Krans, H.M. (1996). *Clostridium botulinum* C3 exoenzyme stimulates GLUT4-mediated glucose transport, but not glycogen synthesis, in 3T3-L1 adipocytes—a potential role of rho? Biochem. Biophys. Res. Commun. *229*, 430–439.

Weimbs, T., Mostov, K.E., Lows, S.H., and Hofmann, K. (1998). A model for structural similarity between different SNARE complexes based on sequence relationships. Trends Cell Biol. *8*, 260–262.

Xu, T., Binz, T., Niemann, H., and Neher, E. (1998). Multiple kinetic components of exocytosis distinguished by neurotoxin sensitivity. Nat. Neurosci. *1*, 192–200.

Yao, Y., and Tsien, R.Y. (1997). Calcium current activated by depletion of calcium stores in *Xenopus* oocytes. J. Gen. Physiol. *109*, 703–715.

Yao, Y., Choi, J., and Parker, I. (1995). Quantal puffs of intracellular Ca^{2+} evoked by inositol trisphosphate in *Xenopus* oocytes. J. Physiol. *482*, 533–553.

Zampighi, G.A., Loo, D.D.F., Kreman, M., Eskandari, S., and Wright, E.M. (1999). Functional and morphological correlates of connexin50 expressed in *Xenopus laevis* oocytes. J. Gen. Physiol. *113*, 507–523.

Hypothesis

Electrostatic attraction at the core of membrane fusion

M. Montal*

Department of Biology, University of California San Diego, La Jolla, CA 92093, USA

Received 5 January 1999

Abstract SNARE proteins appear to be involved in homotypic and heterotypic membrane fusion events [Söllner et al. (1993) Nature 362, 318–324]. The crystal structure of the synaptic SNARE complex exhibits a parallel four-helical bundle fold with two helices contributed by SNAP-25, a target SNARE (t-SNARE), and the other two by a different t-SNARE, syntaxin, and a donor vesicle SNARE (v-SNARE), synaptobrevin. The carboxy-terminal boundary of the complex, predicted to occur at the closest proximity between the apposed membranes, displays a high density of positively charged residues. This feature combined with the enrichment of negatively charged phospholipids in the cytosolic exposed leaflet of the membrane bilayer suggest that electrostatic attraction between oppositely charged interfaces may be sufficient to induce dynamic and discrete micellar discontinuities of the apposed membranes with the transient breakdown at the junction and subsequent reformation. Thus, the positively charged end of the SNARE complex in concert with Ca^{2+} may be sufficient to generate a transient 'fusion pore'.

Key words: SNARE protein; Electrostatic attraction; Membrane fusion

1. Introduction

Neurons communicate with each other by means of neurotransmitters. Membrane fusion is essential for synaptic transmission, a process by which neurotransmitters are released from excited nerve terminals [1]. Recently, the crystal structure of a SNARE complex, a key entity involved in the specific recognition and ultimately fusion of synaptic vesicles with the neuronal plasma membrane, was described [2]. The complex is formed by the specific interaction between segments of three proteins: synaptobrevin-II, a vesicle associated protein, and syntaxin-1A and SNAP-25B, two distinct proteins anchored to the plasma membrane. The clostridial botulinum and tetanus neurotoxins proteolytically cleave these three proteins consequently preventing vesicle fusion and thereby abrogating transmitter release [3]. The SNARE complex folds into a parallel four-helical bundle with a left handed superhelical twist [2,4]: two helices are contributed by a molecule of the t-SNARE SNAP-25, the other two by synaptobrevin and syntaxin. Such a structure may bring into juxtaposition the surfaces of the apposed vesicle and plasma membrane bilayers to facilitate fusion. How this may happen is not known, however, Ca^{2+} is required and other proteins may catalyze and confer additional specificity to the process [5,6]. Here, we focus on highlighting a number of features of this fascinating structure that may provide clues to understand how it mediates bilayer fusion.

2. Electrostatic attractions between oppositely charged interfaces and fusion

A key finding emerged from electrostatic calculations that showed a conspicuous enrichment of positively charged residues at the carboxy-terminal end of the complex [2]. This boundary is assigned to be at the membrane-anchored end of the complex, and therefore, at the minimum distance between the apposed membranes. It is known that negatively charged lipids are preferentially distributed in the inner leaflet of the bilayer plasma membrane [7]. It is also well recognized that Ca^{2+} and highly basic polypeptides interact with negatively charged lipids to induce a lamellar to hexagonal phase transition with the consequent generation of local micellization foci and, if propagated, the breakdown of the bilayer structure [7–10]. And it is well established that acidic lipids are required for the insertion into and translocation across bilayers of a number of channel-forming proteins, conspicuous among them diphtheria [11] and tetanus [12] toxins, colicin [13] and Bcl-2 family proteins [14]. It appears therefore, that electrostatic interaction energy between oppositely charged interfaces might drive discrete micellizations of the apposed membranes with the transient breakdown of the hydrophobic membrane barrier and the consequent release of the transmitter. Thus, the positively charged end of the SNARE complex in concert with Ca^{2+} may be sufficient to generate a transient 'fusion pore'. This hypothesis could be tested using purified SNARE proteins reconstituted into separate bilayer vesicles of defined phospholipid composition [15]. This model system has demonstrated that SNARE proteins are necessary and sufficient for fusion in the absence of other protein components, albeit at a low rate and efficiency [15].

3. Acidic phospholipids and Ca^{2+} ions as mediators of fusion

Another striking feature of the SNARE complex is the occurrence of four shallow grooves at the surface of the helical bundle [2]. Such grooves, particularly those present at the basic charged end of the complex, may provide specific binding pockets for acidic lipids. There is structural evidence for such lipid binding pockets: the crystal structure of a type IIβ phosphatidylinositol phosphate kinase reveals an extensive flat basic surface well suited for the interfacial binding of phosphoinositides and catalysis [16]. The crystal structure of the annexin XII hexamer displays a prominent concave disc with numerous surface exposed Ca^{2+} ions on the perimeter [17].

*Fax: (1) (619) 534 0931.
E-mail: montal@biomail.ucsd.edu

PII: S0014-5793(99)00269-0

Presumably, these Ca^{2+} ions mediate annexin binding to phosphatidylserine, its insertion into membranes and lead to channel formation and membrane fusion [18].

Specific protein-lipid interactions are considered key events in viral fusion mechanisms and the analogy to the SNARE coil-coiled complex has been drawn [15]. The recent identification of a mitochondrial v-SNARE [19] combined with the abundance of acidic lipids in mitochondrial membranes [7] raise the intriguing possibility that SNAREs could be at the fusion interface between mitochondria and other organelles, as it appears to be between yeast vacuoles [20,21]. It would be interesting to examine in molecular detail if the electrostatic attraction between oppositely charged interfaces is sufficient to induce dynamic and discrete micellar discontinuities of the apposed membranes with the transient breakdown at the junction and subsequent reformation. Attention to Ca^{2+} as a mediator of protein-lipid interactions at membrane fusion interfaces is worth revisiting in view of the new structural information.

Acknowledgements: Our research is supported by grants from the U.S. Public Health Service (GM-49711, GM-56538), the Department of the Army Medical Research (DAMD 17-98-C-8040), and the U.S. Army Research Office (DAAG55-98-1-0106).

References

[1] Söllner, T., Whiteheart, S.W., Brunner, M., Erdjument-Bromage, H., Geromanos, S., Tempst, P. and Rothman, J.E. (1993) Nature 362, 318–324.
[2] Sutton, R.B., Fasshauer, D., Jahn, R. and Brunger, A.T. (1998) Nature 395, 347–353.
[3] Montecucco, C. and Schiavo, G. (1995) Q. Rev. Biophys. 28, 423–472.
[4] Poirier, M.A., Xiao, W., Macosko, J.C., Chan, C., Shin, Y.-K. and Bennett, M.K. (1998) Nature Struct. Biol. 5, 765–769.
[5] Shao, X., Li, C., Fernandez, I., Zhang, X., Südhof, T.C. and Rizo, J. (1997) Neuron 18, 133–142.
[6] Rettig, J., Heinemann, C., Ashery, U., Sheng, Z.-H., Yokoyama, C.T., Catterall, W.A. and Neher, E. (1997) J. Neurosci. 17, 6647–6656.
[7] De Kruijff, B. (1997) Nature 386, 129–130.
[8] Sherwood, D. and Montal, M. (1975) Biophys. J. 15, 417–434.
[9] Montal, M. (1972) J. Membr. Biol. 7, 245–266.
[10] Siegel, D.P. and Epand, R.M. (1997) Biophys. J. 73, 3089–3111.
[11] Donovan, J.J., Simon, M.I. and Montal, M. (1982) Nature 298, 669–672.
[12] Gambale, F. and Montal, M. (1988) Biophys. J. 53, 771–783.
[13] Zakharov, S.D., Lindeberg, M., Griko, Y., Salamon, Z., Tollin, G., Prendergast, F.G. and Cramer, W.A. (1998) Proc. Natl. Acad. Sci. USA 95, 4282–4287.
[14] Schendel, S.L., Xie, Z., Oblatt-Montal, M., Matsuyama, S., Montal, M. and Reed, J.C. (1997) Proc. Natl. Acad. Sci. USA 93, 5113–5118.
[15] Weber, T., Zemelman, B.V., McNew, J.A., Westermann, B., Gmachl, M., Parlati, F., Söllner, T.H. and Rothman, J.E. (1998) Cell 92, 759–772.
[16] Rao, V.D., Misra, S., Boronenkov, I.V., Anderson, R.A. and Hurley, J.H. (1998) Cell 94, 829–829.
[17] Luecke, H., Chang, B.T., Maillard, W.S., Schlapfer, D.D. and Haigler, H.T. (1995) Nature 378, 512–515.
[18] Langen, R., Isas, J.M., Hubbell, W.L. and Haigler, H.T. (1998) Proc. Natl. Acad. Sci. USA 95, 14060–14065.
[19] Isenmann, S., Khew-Goodall, Y., Gamble, J., Vadas, M. and Wattenberg, B.W. (1998) Mol. Biol. Cell 9, 1649–1660.
[20] Ungermann, C., Sato, K. and Wickner, W. (1998) Nature 396, 543–548.
[21] Peters, C. and Mayer, A. (1998) Nature 396, 575–580.

THE JOURNAL OF BIOLOGICAL CHEMISTRY
Vol. 273, No. 51, Issue of December 18, pp. 34214–34221, 1998
Printed in U.S.A.

Assembly of a Ternary Complex by the Predicted Minimal Coiled-coil-forming Domains of Syntaxin, SNAP-25, and Synaptobrevin

A CIRCULAR DICHROISM STUDY*

(Received for publication, June 18, 1998, and in revised form, October 1, 1998)

Jaume M. Cànaves and Mauricio Montal‡

From the Department of Biology, University of California San Diego, La Jolla, California 92093-0366

The assembly of target (t-SNARE) and vesicle-associated SNAP receptor (v-SNARE) proteins is a critical step for the docking of synaptic vesicles to the plasma membrane. Syntaxin-1A, SNAP-25, and synaptobrevin-2 (also known as vesicle-associated membrane protein, or VAMP-2) bind to each other with high affinity, and their binding regions are predicted to form a trimeric coiled-coil. Here, we have designed three peptides, which correspond to sequences located in the syntaxin-1A H3 domain, the C-terminal domain of SNAP-25, and a conserved central domain of synaptobrevin-2, that exhibit a high propensity to form a minimal trimeric coiled-coil. The peptides were synthesized by solid phase methods, and their interactions were studied by CD spectroscopy. In aqueous solution, the peptides were unstructured and showed no interactions with each other. In contrast, upon the addition of moderate amounts of trifluoroethanol (30%), the peptides adopted an α-helical structure and displayed both homomeric and heteromeric interactions. The interactions observed in ternary mixtures induce a stabilization of peptide structure that is greater than that predicted from individual binary interactions, suggesting the formation of a higher order structure compatible with the assembly of a trimeric coiled-coil.

The assembly of the synaptic core complex is essential for Ca^{2+}-dependent neuroexocytosis. This early event in the secretory cascade is then followed by the priming and vesicle fusion steps (1–6). According to the SNARE[1] model, docking of synaptic vesicles to the plasma membrane is a critical step that involves the formation of a ternary complex by the v-SNARE synaptobrevin (also known as vesicle-associated membrane protein, or VAMP), and two t-SNAREs: SNAP-25 and syntaxin (7–9). Reconstitution of the v-SNARE synaptobrevin into lipid vesicles and the two t-SNAREs, SNAP-25 and syntaxin, into a distinct vesicle pool has provided evidence that the formation of a ternary complex is sufficient to join the independent vesicle pools and lead to fusion of the apposed bilayer membranes (10).

Understanding the interactions between the proteins of the trimeric complex in a simplified model may outline new ways to control its assembly and dissociation or to modulate the conformational changes that are presumably necessary for the progression from the docking step to the subsequent phases in the secretory process. The structural domains that appear to be implicated in the protein-protein interactions between SNAP-25, synaptobrevin, and syntaxin show a high propensity for the formation of α-helices (11–15). Secondary structure analysis shows that the periodic distribution of hydrophobic amino acids is consistent with a coiled-coil organization (2, 11, 12, 14, 15). Fluorescence energy transfer experiments (12) and electron microscopy (15) further indicate that synaptobrevin and syntaxin are aligned in parallel in the context of a ternary coiled-coil.

To investigate the postulated coiled-coil interactions between the proteins that constitute the docking complex in a minimal model, we have applied the principles involved in the formation of stable coiled-coils (16) to design three peptides corresponding to predicted coiled-coil-forming domains in SNAP-25, synaptobrevin-2, and syntaxin-1A. We have used CD spectroscopy to determine the secondary structure of these peptides and their interactions in binary and tertiary mixtures. Our findings are consistent with the assembly of the predicted ternary complex.

EXPERIMENTAL PROCEDURES

Reagents—HPLC grade trifluoroacetic acid, trifluoroethanol (TFE), ethanedithiol, thioanisol, phenol, and acetonitrile were purchased from Aldrich. Methyl *tert*-butyl ether was from Fisher. HPLC columns were from Vydac (Hesperia, CA). L-Amino acids and protected derivatives used for peptide synthesis were made by Calbiochem. Benzoic anhydride was obtained from Sigma. All other reagents for peptide synthesis and resins were from Applied Biosystems (Foster City, CA).

Peptide Synthesis and Purification—Peptides SN (human brain SNAP-25-(181–206)), SB (human brain synaptobrevin-2-(40–67)), ST (human brain syntaxin-1A-(191–218)), and SN_{RD} (scrambled SN peptide sequence: ESDNDTRAIKITQAGSMKRMGLNAKE) were produced using solid phase peptide synthesis. Synthesis started with a *p*-hydroxymethyl phenoxy methyl polysterene resin and was carried out using the Fastmoc® Fmoc strategy on an Applied Biosystems peptide synthesizer model 431A (Foster City, CA) according to a single coupling plus capping protocol. Cleavage from the resin and removal of all protecting groups was accomplished by using trifluoroacetic acid cleavage as described (17). Crude peptides were precipitated from the trifluoroacetic acid mixture in cold methyl *tert*-butyl ether and centrifuged, the supernatant was discarded, and the remaining methyl *tert*-butyl ether was removed under high vacuum at 0 °C for 3 h. Samples of crude peptide (10–20 mg) were dissolved in 0.1% trifluoroacetic acid, applied to a semipreparatory column (Vydac, C-18), and eluted at a flow rate of 3 ml/min with a linear gradient of 90% acetonitrile in 0.1% trifluoroacetic acid. Eluted peaks were monitored by absorbance measurements at 214 nm, pooled, and lyophilized. Peptide purity was assessed by RP-HPLC in an analytical column (Vydac, C-18).

Secondary and Tertiary Structure Predictions—Propensities of peptides to adopt a coiled-coil structure were estimated using two different

* This work was supported by U.S. Army Medical Research and Materiel Command Grants DAMD 17-93-C-3100 and DAMD 17-98-C-8040 (to M. M.) and a grant from the Dystonia Medical Research Foundation (to J. M. C.). The costs of publication of this article were defrayed in part by the payment of page charges. This article must therefore be hereby marked "*advertisement*" in accordance with 18 U.S.C. Section 1734 solely to indicate this fact.

‡ To whom correspondence should be addressed: Dept. of Biology, University of California San Diego, 9500 Gilman Dr., La Jolla, CA 92093-0366. Tel./Fax: 619-534-0931; E-mail: montal@biomail.ucsd.edu.

[1] The abbreviations used are: SNARE, SNAP receptor; v-SNARE, vesicle SNARE; t-SNARE, target SNARE; BoNT, botulinum neurotoxin; SNAP-25, synaptosomal associated protein of 25 kDa; TFE, trifluoroethanol; HPLC, high pressure liquid chromatography.

programs: Coils and Paircoil. The Coils program uses the Lupas algorithm (18, 19). Sequences were compared with an unweighted MTIDK matrix (18) using 14- and 28-residue scanning windows. The second program uses the Berger algorithm (20), which is more stringent. Both methods are based on the relative frequency of occurrence of amino acids at each position (a–g) of the coiled-coil heptad repeat. Secondary structure predictions were performed using the SOPMA method (21, 22) and the AGADIR program (23).

CD Measurements—CD measurements were carried out on a modified Cary 61 (24) or an AVIV model 202 spectropolarimeter. The original Pockel cell and Cary linear polarizer in the Cary 61 were replaced with a 50-kHz photoelastic modulator (Hinds International, FS-5/PEM-80) and a MgF_2 linear polarizer (AVIV Inc.). The phase-detected output of the original end-on photomultiplier and preamplifier were integrated using an Egg Princeton Applied Research model 128A lock-in amplifier. System automation and multiple scan averaging were accomplished with an IBM PC-compatible computer interfaced directly to both the Cary 61 and the 128A amplifier. Constant N_2 flushing was employed. Spectra were measured at 195–250 nm using a 0.05-cm cell, a 1-nm bandwidth, a 0.3-ms time constant, and a cell temperature of 25 °C. All recordings were performed in 10 mM sodium phosphate buffer, pH 7.4, 100 mM NaCl, with or without TFE, unless otherwise indicated. Twenty scans were averaged for every spectrum. Base line subtraction, conversion of measured rotations to mean residue ellipticity $[\theta]$ ($deg \cdot cm^2 \cdot dmol^{-1}$) (25), and filtering of the spectra using a fast fourier transform filter were performed using the Microcal Origin 3.5 program. The percentage of α-helical content was estimated directly from the molar residue ellipticity at 222 nm as described by Chen *et al.* (26). Percentages of secondary structures were also estimated using the neural network-based K2 algorithm (27). To evaluate the spectral changes induced by peptide-peptide interactions in mixtures, the non-interacting spectra were calculated from the individual spectra using the equation,

$$[\theta]_{theo} = \Sigma(c_i \cdot n_i \cdot [\theta]_i)/\Sigma(c_i \cdot n_i) \quad \text{(Eq. 1)}$$

where c_i denotes the molar peptide concentrations, n_i represents the peptide lengths in number of residues, and $[\theta]_i$ values are observed mean residue ellipticities.

RESULTS AND DISCUSSION

Peptide Design

Basic Criteria for the Design of the Minimal Predicted Coiled-coil-forming Peptides—The sequences of the peptides synthesized from selected regions from human SNAP-25 (peptide SN), synaptobrevin-2 (peptide SB), and syntaxin-1A (peptide ST) are shown in Fig. 1*A*. Sequence selection was based on six criteria: 1) information about the minimal domains of SNAP-25, synaptobrevin, and syntaxin involved in protein-protein interactions in the core complex (1–5, 28); 2) botulinum neurotoxins (BoNTs) cleavage sites and their effects on neurotransmitter release (29–37); 3) sequence specificity of peptides inhibitors of neurotransmitter release (38–44); 4) effects of point mutations on the process of secretion and endocytosis (4, 11, 44–47); 5) predictions of secondary structure formation of coiled-coil structures; and 6) a minimum length for a stable parallel coil peptide of ~28 residues, or 4 heptad repeats (48, 49).

Design of the SN Peptide—The region of SNAP-25 interacting with synaptobrevin-2 has been localized between residue 41 and the C-terminal residue (2, 4). The segment from residue 181 to the C terminus is necessary for the SNAP-25-synaptobrevin interaction (3). Peptides corresponding to the 20 and 26 C-terminal residues, the latter analogous to the SNAP-25 segment released after cleavage by BoNT E, inhibit neurotransmitter release with IC_{50} values of 10 and 0.25 μM, presumably by preventing the docking of synaptic vesicles (40, 43).

The C-terminal region of SNAP-25 delimited by residues 169 and 206 displays a high propensity (99%) to form coiled-coil structures. Two distinct domains are predicted: one from position 166 to 187 (62%), and the second from position 189 to the C terminus (55%). Accordingly, the 26-residue peptide corresponding to the C-terminal segment of SNAP-25, hereafter designated as SN, was selected based on the fact that it is nearly 4 heptads long, it exhibits high propensity to form coiled-coils, and it is an efficient inhibitor of neurotransmitter release (Fig. 1*A*, *Peptide SN*).

Design of the ST Peptide—Similar considerations were used in the design of a potentially coiled-coil-forming peptide from syntaxin-1A. The region between positions 194 and 261 is necessary for the interaction with synaptobrevin-2 and SNAP-25 (2, 3, 5). The segment necessary for interaction with SNAP-25 has been located between residues 199 and 267 (1) and further delimited to residues 199–220 (4). All of these studies confine the SNAP-25 binding region on syntaxin to the N-terminal portion of the H3 domain (residues 191–266) (2, 4), and a putative minimal SNAP-25 binding domain (residues 189–220) has been identified (11, 44). Coiled-coil predictions using the sequence of human syntaxin revealed a region between positions 199 and 214 with high probability (78%) of coiled-coil formation.

Syntaxin-1A mutants containing point mutations (4, 11, 44) at the a and d repeats of a predicted coiled-coil show reduced SNAP-25 binding, supporting the involvement of this region in the interaction with SNAP-25 (Fig. 1*B*). Peptides corresponding to the predicted coiled-coil-forming region of syntaxin-1A have also been shown to inhibit neurotransmitter release (11, 42, 44). Given these considerations, the selected 4-heptad synthetic peptide corresponding to human syntaxin spanned from residue 191 to 218 (Fig. 1*A*, *Peptide ST*).

Design of the SB Peptide—The region of synaptobrevin-2 between positions 27 and 96 interacts with both SNAP-25 and syntaxin-1A in the core complex (3, 28). Synaptobrevin-2 contains a conserved domain between residues 57 and 88, with high propensity (95%) to form coiled-coils, and two distinct subdomains (28–42 and 52–72). Deletion of the region spanning from residue 41 to 50 abolishes endocytosis (45), and mutants lacking the segments 41–50 or 51–60 do not to bind to SNAP-25 and syntaxin-1A. The mutants with deletion of segment 31–38 show weak binding to t-SNAREs, whereas the deletion of segments 61–70 or 71–80 results in poor binding to syntaxin while maintaining the interactions with SNAP-25 (47). Moreover, a single mutation (M46A) inhibits endocytosis by 80% and reduces binding to syntaxin-1A and SNAP-25 (45, 46). Taken together, this information suggests that the region delimited by positions 40 and 60 is involved in the ternary interactions that result in the assembly of the docking complex; therefore, the peptide synthesized encompassed 4 heptads from position 40 (Fig. 1*A*, *Peptide ST*).

Design of the SN_{RD} Control Peptide—A control peptide corresponding to the scrambled sequence of the selected SNAP-25 peptide was also synthesized. Randomized sequences were generated, their secondary structures were predicted using the SOPMA method, and the sequences with an α-helical content similar to the original sequence were run against the Prosite data base. A peptide with the same functional sites but without the heptad periodicity was synthesized (sequence shown under "Experimental Procedures"), and it was shown to be pharmacologically inactive. The SN_{RD} peptide, at variance to SN, did not affect Ca^{2+}-dependent release in chromaffin cells.

Secondary structure predictions using the SOPMA method (21, 22) indicate that all three peptides may form stable α-helices in the context of a whole protein structure. Predicted helicities for SN, SB, and ST peptides were 62, 96, and 86%, respectively, when considered integrated in the protein, in contrast to 42, 57, and 67% as isolated peptides. The behavior of the isolated peptides in an aqueous environment was predicted by using the AGADIR algorithm (23). This program uses

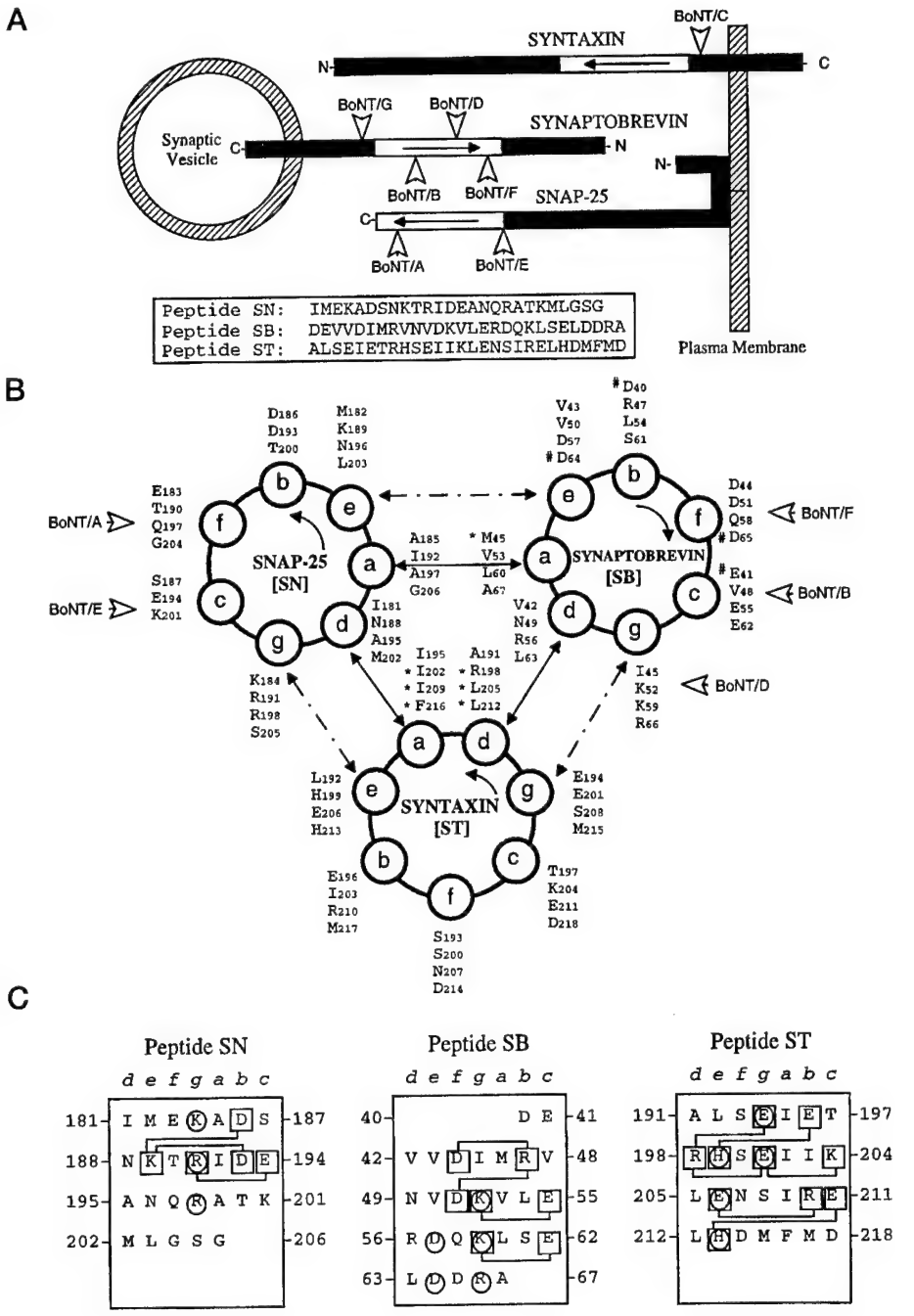

FIG. 1. **Model of a minimal trimeric coiled-coil using selected sequences from SNAP-25, synaptobrevin-2, and syntaxin-A.** *A*, schematic representation of the relative location of SNAP-25, synaptobrevin-2, and syntaxin-A in the synaptic terminal (*black boxes*). The *white boxes* represent the segments corresponding to the synthetic peptides SN, SB, and ST, respectively. The relative size of the proteins and synthetic peptides are not to scale. The amino acid sequences of the SN, SB, and ST peptides are given in the *box*. *B*, triple helical coiled-coil model of the segments of SNAP-25, synaptobrevin-2, and syntaxin-A represented by the synthetic peptides SN, SB, and ST, respectively. The sequences have a heptad pattern of residues (designated as *a–g*), where *a* and *d* are usually hydrophobic and *e* and *g* are frequently charged. *Solid arrows* denote hydrophobic interactions in the core of the complex, whereas *broken arrows* refer to potential ionic interactions, as described in detail in *C*. Mutations known to disrupt the interactions between proteins (*) are located in the hydrophobic core. Mutations known not to interfere in the assembly of the complex (#) are all located outside the hydrophobic core. Most of the charged residues are located in the outer shell of the complex (positions *b*, *c*, and *f*). *Hollow arrows* in *A* and *B* show the relative location of Botulinum neurotoxin cleavage sites, which are all accessible on the surface of the complex. *C*, potential interactions between charged residues of peptides SN, SB, and ST. Charged residues in positions *e* and *g* or at $i + 3$- or $i + 4$-positions can form intramolecular (*squares*) or intermolecular (*circles*) salt bridges that contribute to the overall stability of the trimeric complex.

statistical mechanics to consider short range interactions between residues at different pH and temperature. Given the size of our peptides, they are predicted to be unstructured (4% for SN, 3% for SB, and 2% for ST peptide, respectively) under aqueous conditions. Thus, considering both sets of data, we infer that these peptides can adopt α-helical structures only in the context of the intact protein and, therefore, that the presence of helicity-inducing conditions may be necessary to mimic the secondary structure of the peptides in the cytosol. TFE, a hydrophilic and hydrogen-bonding solvent, has been widely used to stabilize marginally stable α-helical structures in potentially α-helical peptides (48, 50–53). TFE is not limited to promoting helix formation, since it has also been shown to stabilize β-turns and even β-strands (54, 55). Notwithstanding, TFE-induced α-helical conformation in fragments of proteins known to be β-sheet in the native context has been documented (56–63). Therefore, caution must be exercised in inferring structure from CD data of peptides in the presence of TFE, particularly with regard to the extent that it represents the native structure in the context of the intact protein from which the peptide sequences were selected.

Trimeric Coiled-coil Model

Theoretical Considerations—A model of one of the trimeric conformers of the selected peptides forming a coiled-coil structure is shown in Fig. 1*B*. Given the helical wheel representation, residues at the *a*- and *d*-positions stabilize the structure by hydrophobic interchain interactions. According to this model, the synaptobrevin-2 residue Met^{45}, which upon mutation inhibits endocytosis, would be located in the hydrophobic core, where such a change would be predictably disruptive. The mutations in syntaxin that reduce its binding to SNAP-25 would also be located in positions *a* and *d* (residues denoted with an *asterisk* in Fig. 1*B*). Interestingly, the cleavage sites for

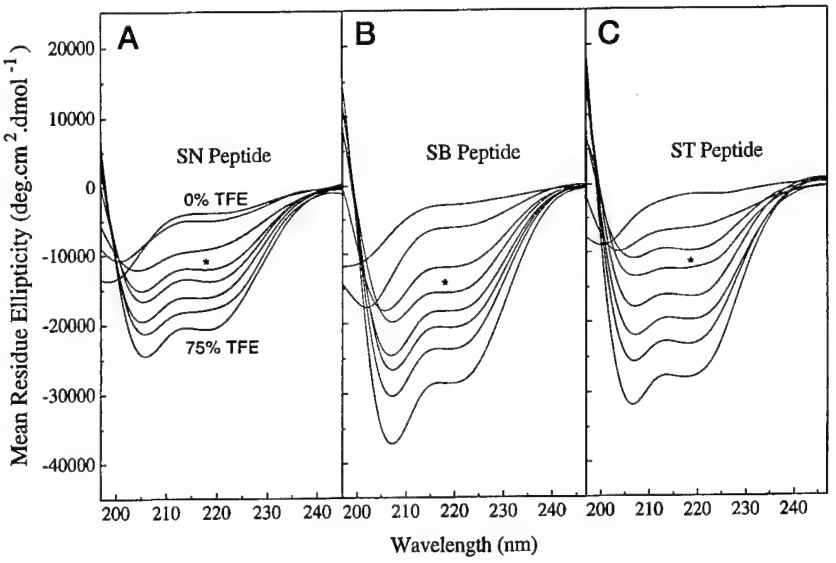

FIG. 2. **CD spectra of the synthetic peptides at different TFE concentrations.** *A*, SN peptide; *B*, SB peptide; *C*, ST peptide. Spectra were recorded in 10 mM sodium phosphate, pH 7.4, 100 mM NaCl, in the presence of increasing concentrations of TFE. Peptide concentration was 30 μM. TFE concentrations used were 10, 20, 30 (*), 40, 50, 65, and 75%.

five of the seven BoNT serotypes (BoNT A, B, D, E, and F) are found in the model peptides, and all are in surface locations potentially accessible to the BoNT proteases.

Interchain interactions of *e*- and *g*-positions mediated by charged residues also contribute to the stability of a coiled-coil (64). There are 12 charged residues in positions *e* and *g*; accordingly, inter- or intrahelical ionic interactions could synergistically contribute to the stability of the coil (Fig. 1*C*). Polar residues implanted in the hydrophobic core are potentially disruptive, although strategic placement can facilitate correct oligomerization arrangements (65). In the model, the core contains only two charged residues: Arg^{198} (peptide ST) could establish an intramolecular salt bridge with either Glu^{194} or Glu^{201} (Fig. 1*B*), and Arg^{56} (peptide SB) would be at a suitable distance to interact with the glutamate residues in position *g* of the ST peptide and form an intermolecular linkage (Fig. 1*B*).

In the outer layer (positions *b*, *c*, and *f*), 14 negatively and 3 positively charged residues would be exposed. This arrangement of negative charges mostly in the surface is consistent with observations by Regazzi *et al.* (47) that substitutions of negatively charged residues of synaptobrevin-2 do not alter function (66) (Fig. 1*B*).

Circular Dichroism Results—In aqueous media, all peptides (alone or in mixtures) were unstructured, and neither increasing peptide concentration nor changing pH, ionic strength, or divalent cation concentration increased the α-helical content. Typical single-stranded polypeptides generally do not form stable α-helices in aqueous solution and require the additional stabilization of less polar solvents (67, 68); therefore, we resorted to the use of the helix-promoting solvent TFE.

In the presence of increasing concentrations of TFE (Fig. 2, *A–C*), there was a significant increase in the α-helical content. The minimal concentration at which the peptides underwent a transition from mostly unstructured to partially structured was approximately 30%. At that concentration, the α-helical contents of the SNAP-25, synaptobrevin, and syntaxin peptides were 31, 44, and 32%, respectively. At the maximum concentration of TFE used (75%), the α-helical contents of the peptides were 59, 87, and 85%, respectively. TFE increases the α-helical content, while it disrupts tertiary and quaternary structures stabilized by hydrophobic interactions (69); therefore, it was imperative to use a concentration of TFE low enough to marginally stabilize the secondary structure of monomeric peptides while still allowing the expression of tertiary interactions. Notwithstanding the disrupting effects of TFE on the tertiary structure of oligomeric complexes, peptide-peptide interactions producing stable oligomers have been documented at concentrations of TFE as high as 50% (70). Interestingly, the TFE concentration used in our experiments (30%) has been reported to yield for numerous peptides secondary structures that compare favorably with those of the native systems (71–73).

Equimolar ternary mixtures SN/SB/ST in aqueous solution showed no interaction between the non-α-helical peptides (not shown). In the presence of TFE, the spectrum of the SN/SB/ST mixture (Fig. 3*E*, *solid line*) was significantly different from a noninteracting spectrum (Fig. 3*E*, *dashed line*) calculated from the three individual CD spectra (Fig. 3*A*). The expected α-helicity from the calculated spectrum was 35%, whereas the α-helicity from the experimental spectrum was 46%; *i.e.* a 31% net increase over the predicted value. The ratios between the intensities of the bands at 222 and 208 nm were 0.76 for the calculated and 0.80 for the experimental spectrum, respectively. This larger $\Theta_{222}/\Theta_{208}$ ratio is consistent with an increase in coiling.

The 31% net increase in helicity observed in the experimental ternary mixture spectrum with respect to the prediction could arise from the occurrence of distinct binary complexes in the mixture. Equimolar binary mixtures SN/SB, SN/ST, and SB/ST in aqueous solution showed no interaction between the peptides (not shown). In the presence of 30% TFE, the SN and SB peptides did not interact in binary mixtures (Fig. 3*B*). The helicity of the experimental spectrum was identical to that predicted by the noninteracting calculated spectrum (36%). In contrast, spectra from binary mixtures SB/ST (Fig. 3*C*) and SN/ST (Fig. 3*D*) indicated that both pairs of peptides interact under these experimental conditions. In each case, the α-helical content calculated from the experimental spectra was ~15% greater than expected for a noninteracting mixture. Predicted helicities were 34 and 33%, respectively, for the SB/ST and SN/ST mixtures, whereas the experimental values were 39 and 38%, *i.e.* 15% higher than expected for noninteracting mixtures.

Increasingly higher peptide concentration in equimolar mixtures of the SN, SB, and ST peptides in the presence of 30% TFE (Fig. 4*A*) also results in an increase in helicity and therefore a stabilization of the complex. Increasing the individual peptide concentrations from 10 to 30 μM results in an increase in helicity from 46 to 54%. It is noticeable that the three spectra define a unique isodichroic point, consistent with the occur-

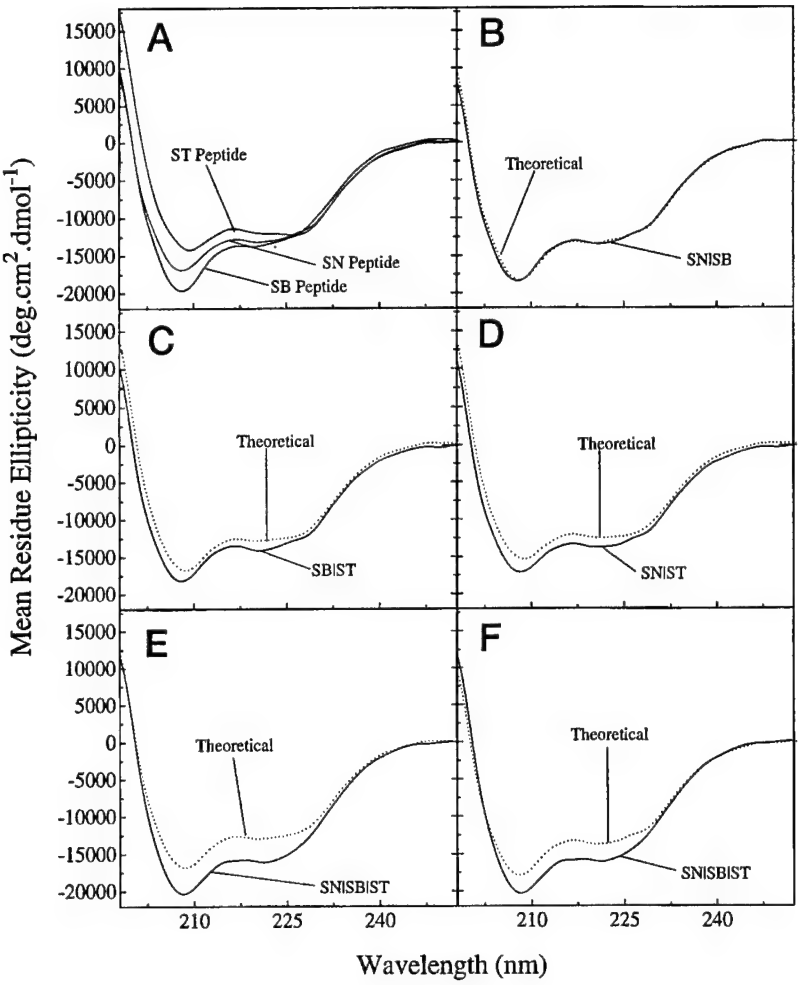

FIG. 3. **CD spectra of binary and ternary mixtures of synthetic peptides SN, SB, and ST.** Experimental (*solid line*) and calculated (*dashed line*) noninteracting spectra are shown for each mixture as well as recordings corresponding to the same peptide mixture after a 24-h incubation at 5 °C. *A*, individual spectra of SN, SB, and ST peptides used to determine the calculated noninteracting spectra; *B*, SN/SB mixture; *C*, SB/ST mixture; *D*, SN/ST mixture; *E*, SN/SB/ST ternary mixture; *F*, comparison between the spectrum of the ternary mixture after a 24-h incubation and the spectrum calculated from the summation of the binary spectra. Peptide concentration was 30 μM for each peptide. Spectra were recorded in 10 mM sodium phosphate, pH 7.4, 100 mM NaCl, with 30% TFE.

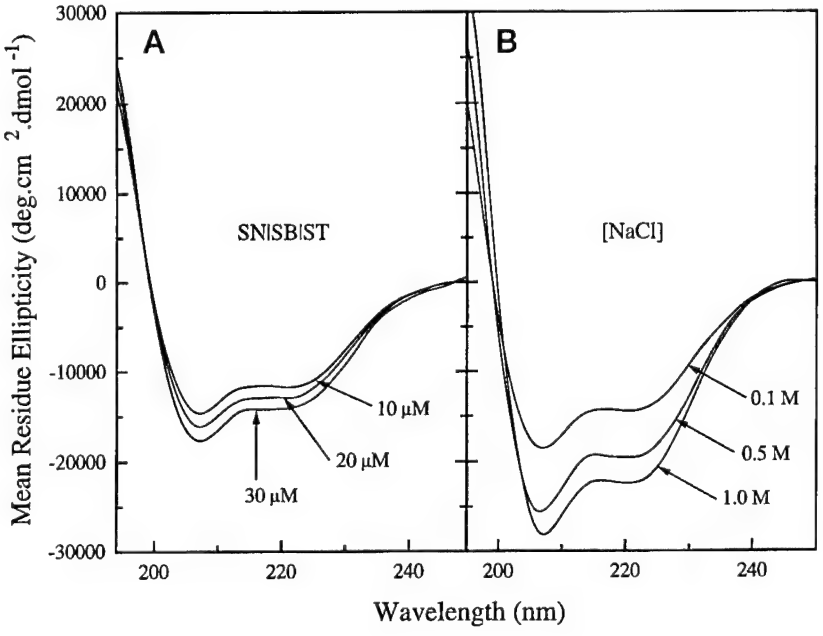

FIG. 4. **CD spectra of ternary mixtures of the SN, SB, and ST peptides as function of peptide concentration and ionic strength.** *A*, CD spectra of equimolar mixtures of SN, SB, and ST peptides, at individual peptide concentrations of 10, 20, and 30 μM. Spectra were recorded in 10 mM sodium phosphate, pH 7.4, 100 mM NaCl, with 30% TFE; *B*, effect of increasingly higher concentrations of NaCl on the secondary structure of equimolar ternary mixtures of SN, SB, and ST peptides at individual peptide concentrations of 30 μM. Spectra were recorded in 10 mM sodium phosphate, pH 7.4, 30% TFE. NaCl concentrations used were 0.1, 0.5, and 1 M.

rence of a single specific complex. When equimolar ternary mixtures are exposed to higher concentrations of NaCl in the presence of 30% TFE (Fig. 4*B*), there is a remarkable increase in the helicity (from 55% at 0.1 M NaCl to 72% at 0.5 M and 81% at 1 M). This feature is consistent with hydrophobic peptide-peptide interactions as suggested by the model (Fig. 1*B*). The increased α-helical content with increasing ionic strength is in accordance with data for coiled-coil peptides and can be explained by the increased strength of the hydrophobic interactions as the polarity of the medium is increased (69).

Whereas the spectra of all three peptides were independent of the peptide concentration in aqueous solution (Fig. 5, *A–C*),

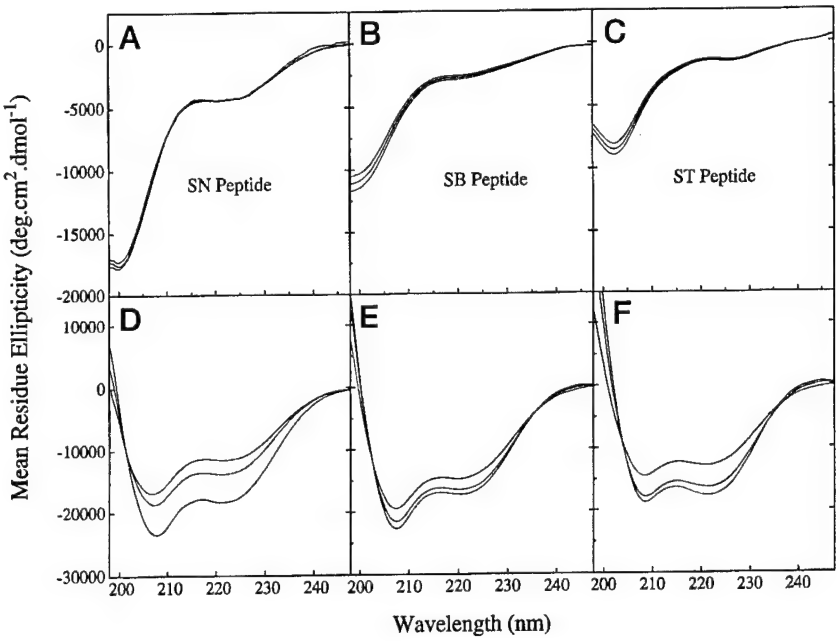

FIG. 5. **CD spectra of the synthetic peptides at increasingly higher concentrations in the absence or presence of TFE.** *A*, SN peptide; *B*, SB peptide; and *C*, ST peptide in aqueous solution. *D*, SN peptide; *E*, SB peptide; and *F*, ST peptide in 30% TFE. Peptide concentrations were 30, 60, and 90 μM, respectively. Spectra were recorded in 10 mM sodium phosphate, pH 7.4, 100 mM NaCl, with or without 30% TFE.

in the presence of 30% TFE the increase in peptide concentration resulted in a concomitant increase in the α-helical content, as indicated by the increase in negative ellipticity at 222 nm (Fig. 5, *D–F*). Helicity increased from 30 to 53% for SN, from 41 to 49% for SB, and from 35 to 51% for ST. This is consistent with the fact that peptides with α-helical structures that are dependent on dimerization or oligomerization show an augmentation of α-helical content as the peptide concentration is increased (74). This presumably arises because the equilibrium between monomeric peptide (in the form of random coil) and coiled-coil dimer is shifted toward the formation of the coiled-coil dimer, which increases the α-helical content of the peptide (65).

Higher peptide concentrations induced a moderate increase in the ratio between the peaks at 222 and 208 nm ($\Theta_{222}/\Theta_{208}$): from 0.68 to 0.78 for SN; from 0.75 to 0.77 for SB; and from 0.88 to 0.94 for ST. The ratio between the intensities of the bands at 222 and 208 nm may be regarded as a measure for the extent of coiling of α-helices around each other. The 222-nm CD band is mainly responsive to the α-helical content, whereas the band at 208 nm is sensitive to whether the α-helix is monomeric or is involved in tertiary contacts with other α-helices (75–77). Therefore, this is an additional criterion for the formation of stable coiled-coil structures. Each set of curves defined a unique isodichroic point, consistent with a single monomer-dimer equilibrium, which indicated that the oligomerization observed was sequence-specific and presumably stabilized by a concerted set of ion pairs in a defined spatial arrangement.

The ratio of the 222- to the 208-nm peak is an operational index to detect the presence of pure coiled-coils. For peptides stabilized at low TFE concentrations, an equilibrium between monomeric and multimeric states is anticipated, resulting in a profile intermediate between a pure coiled-coil and a predominantly monomeric situation. Given that the peptides exhibit a relatively low α-helical content and that there is a substantial fraction of peptide in monomeric form, the formation of homomeric or heteromeric arrays arising from interhelical interactions would result in an α-helical content of the mixtures larger than that expected from a spectrum calculated from the individual spectra (Fig. 3*A*).

To address the question of whether the increase in α-helicity observed in the ternary mixture could be accounted for by mere binary interactions between the SN, SB, and ST peptides, the calculated spectrum predicted from the sum of SN/ST and SB/ST interactions was calculated (Fig. 3*F*, *dashed line*). The experimental spectrum obtained from the ternary mixture (Fig. 3*F*, *solid line*) showed an α-helical content (46%) considerably higher than expected from a mixture of dimers (38%), suggesting the presence of ternary or higher order interactions.

The specificity of the interactions observed in binary mixtures was tested using mixtures of the SN, SB, and ST peptides with the SN_{RD} control peptide (Fig. 6). The SN_{RD} peptide was unstructured in aqueous solution, and in the presence of 30% TFE its α-helical content was similar to that of the SN peptide (spectrum not shown). Equimolar mixtures of SN_{RD} and SN (SN/SN_{RD}) showed no difference between the spectrum calculated for a noninteracting mixture and the experimental spectrum (Fig. 6*A*). Similarly, spectra obtained from SB/SN_{RD} and ST/SN_{RD} binary mixtures showed no difference with respect to the calculated noninteracting spectra (Fig. 6, *B* and *C*). The slight differences observed in the figure are not statistically significant as assessed using a Student's *t* test on the nonfiltered spectra. In the case of mixtures assayed in the presence of 30% TFE, the situation is the same: there is no interaction between SN, SB, or ST and the control peptide (Fig. 6, *D–F*). This indicates that the interactions observed upon increasing peptide concentration or mixing with other peptides, either in binary or ternary mixtures, is sequence-specific.

Conclusion

Our study identifies a minimal entity that opens a new perspective for the study of the molecular interactions between SNAP-25, synaptobrevin, and syntaxin. Three distinct synthetic peptides patterned after the sequences of the putative coiled-coil-forming domains of the main components of the docking and fusion complex self-assemble into a complex that exhibits spectral characteristics consistent with a coiled-coil structure. A synthetic coiled-coil ternary complex provides a basis for further developments: 1) the ternary complex appears suitable for both crystallization and NMR spectroscopy that, in due turn, may yield a high resolution structure of the fusion core complex; 2) it represents a conceptual framework to assist in the design and test of new peptide inhibitors of neurotransmitter release; 3) it provides leads for the design of small molecule peptidomimetic drugs; and 4) it may be valuable to generate specific antibodies to block neurotransmitter release.

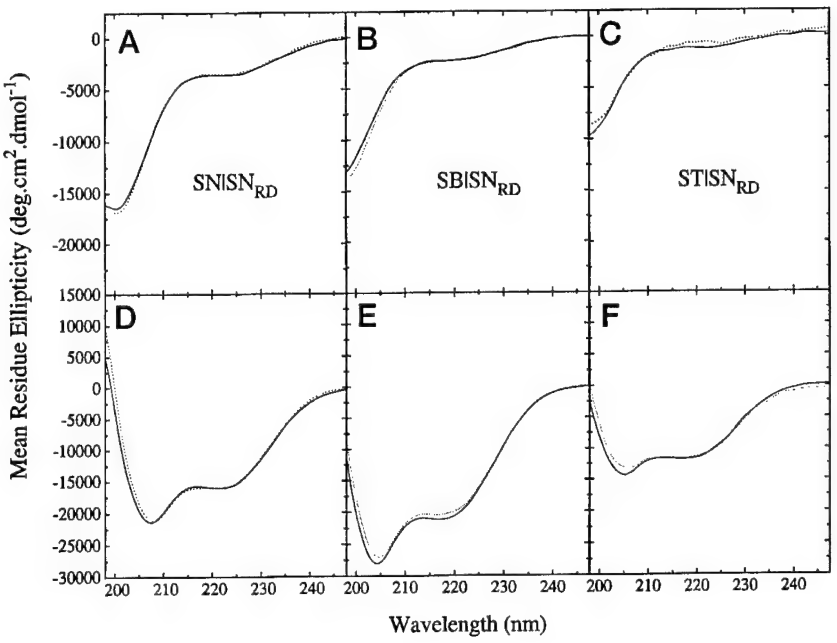

FIG. 6. **CD spectra of binary mixtures of synthetic peptides SN, SB, and ST and the control peptide SN_{RD}.** *A*, SN/SN_{RD} mixture; *B*, SB/SN_{RD} mixture; and *C*, ST/SN_{RD} mixture in aqueous solution. *D*, SN/SN_{RD} mixture; *E*, SB/SN_{RD}; and *F*, SB/SN_{RD} mixture in 30% TFE. Experimental (*solid line*) and calculated (*dashed line*) noninteracting spectra are shown for each binary mixture. Peptide concentration was 30 μM. Spectra were recorded in 10 mM sodium phosphate, pH 7.4, 100 mM NaCl, with or without 30% TFE.

Indeed, the synthetic peptides that, as shown here, participate in the assembly of the ternay complex in fact mimic the action of *Clostridial* neurotoxins (40, 43). Therefore, our findings may lead to the development of peptide-based agents that may be used as potential therapy in spastic neuromuscular disorders, substituting or complementing the current treatment with BoNTs.

Acknowledgments—We thank Professor Murray Goodman and Dr. Joseph Taulane for the use of the Cary 61 CD spectrometer and Dr. Susan S. Taylor for the use of the AVIV 202 CD spectrometer.

Note Added in Proof—After submission of this manuscript, two papers reported the structure of the SNARE complex as a parallel four-helix bundle determined by x-ray crystallography (Sutton R. B., Fasshauer, D., Jahn, R., and Brunger, A. T. (1998) *Nature* **395,** 347–353) and by electron paramagnetic resonance spectroscopy (Poirier, M. A., Xiao, W., Macosko, J. C., Chan, C., Shin, Y.-K., and Bennett, M. K. (1998) *Nat. Struct. Biol.* **5,** 765–769). The results of our study are consistent with the high resolution structure of the SNARE complex.

REFERENCES

1. Calakos, N., Bennet, M. K., Peterson, K. E., and Scheller, R. H. (1994) *Science* **263,** 1146–1149
2. Chapman, E. R., An, S., Barton, N., and Jahn, R. (1994) *J. Biol. Chem.* **269,** 27427–27432
3. Hayashi, T., McMahon, H., Yamasaki, S., Binz, T., Hata, Y., Sudhof, T. C., and Niemann, H. (1994) *EMBO J.* **13,** 5051–5061
4. Kee, Y., Lin, R. C., Hsu, S. C., and Scheller, R. H. (1995) *Neuron* **14,** 991–998
5. Hayashi, T., Yamasaki, S., Nauenburg, S., Binz, T., and Niemann, H. (1995) *EMBO J.* **14,** 2317–2325
6. Sudhof, T. C. (1995) *Nature* **375,** 645–653
7. Sollner, T., Whiteheart, S. W., Brunner, M., Erdjument-Bromage, H., Geromanos, S., Tempst, P., and Rothman, J. E. (1993) *Nature* **362,** 318–324
8. Sollner, T., Bennett, M. K., Whiteheart, S. W., Scheller, R. H., and Rothman, J. E. (1993) *Cell* **75,** 409–418
9. Rothman, J. E., and Sollner, T. (1997) *Science* **276,** 1212–1213
10. Weber, T., Zemeelman, B., McNew, J. A., Westermann, B., Gmachl, M., Parlati, F., Sollner, T., and Rothman, J. E. (1998) *Cell* **92,** 759–7772
11. Zhong, P., Chen, Y. A., Tam, D., Chung, D., Scheller, R. H., and Miljanich, G. P. (1997) *Biochemistry* **36,** 4317–4326
12. Lin, R. C., and Scheller, R. H. (1997) *Neuron* **19,** 1087–1094
13. Gerst, J. E. (1997) *J. Biol. Chem.* **272,** 16591–16598
14. Fasshauer, D., Bruns, D., Shen, B., Jahn, R., and Brunger, A. T. (1997) *J. Biol. Chem.* **272,** 4582–4590
15. Hanson, P. I., Roth, R., Morisaki, H., Jahn, R., and Heuser, J. E. (1997) *Cell* **90,** 523–535
16. O'Shea, E. K., Lumb, K. J., and Kim, P. S. (1993) *Curr. Biol.* **3,** 658–667
17. King, D. S., Fields, C. G., and Fields, G. B. (1990) *Int. J. Pept. Protein Res.* **36,** 255–266
18. Lupas, A., Van Dyke, M., and Stock, J. (1991) *Science* **252,** 1162–1164
19. Lupas, A. (1996) *Methods Enzymol.* **266,** 513–525
20. Berger, B., Wilson, D. B., Wolf, E., Tonchev, T., Milla, M., and Kim, P. S. (1995) *Proc. Natl. Acad. Sci. U. S. A.* **92,** 8259–8263
21. Geourjon, C., and Deleage, G. (1994) *Protein Eng.* **7,** 157–164
22. Geourjon, C., and Deleage, G. (1995) *Comp. Appl. Biosci.* **11,** 681–684
23. Munoz, V., and Serrano, L. (1997) *Biopolymers* **41,** 495–509
24. Feng, Y., Melacini, G., Taulane, J. P., and Goodman, M. (1996) *J. Am. Chem. Soc.* **118,** 10351–10358
25. Schmid, F. X. (1989) in *Protein Structure: A Practical Approach* (Creighton, T. E., ed) pp. 251–286, IRL Press, Oxford
26. Chen, Y. H., Yang, J. T., and Chau, K. H. (1974) *Biochemistry* **13,** 3350–3359
27. Andrade, M. A., Chacon, P., Merelo, J. J., and Moran, F. (1993) *Protein Eng.* **6,** 383–390
28. Archer, B. T., III, Ozcelik, T., Jahn, R., Francke, U., and Sudhof, T. (1990) *J. Biol. Chem.* **265,** 17267–17273
29. Binz, T., Blasi, J., Yamasaki, S., Baumeister, A., Link, E., Sudhof, T. C., Jahn, R., and Niemann, H. (1994) *J. Biol. Chem.* **269,** 1617–1620
30. Blasi, J., Chapman, E. R., Link, E., Binz, T., Yamasaki, S., De Camilli, P., Sudhof, T. C., Niemann, H., and Jahn, R. (1993) *Nature* **365,** 160–163
31. Foran, P., Lawrence, G. W., Shone, C. C., Foster, K. A., and Dolly, J. O. (1996) *Biochemistry* **35,** 2630–2636
32. Schiavo, G., Santucci, A., DasGupta, B. R., Mehta, P. P., Jontes, J., Benfenati, F., Wilson, M. C., and Montecucco, C. (1993) *FEBS Lett.* **335,** 99–103
33. Schiavo, G., Rosetto, O., Catsicas, S., Polverino de Laureto, P., DasGupta, B. R., Benfenati, F., and Montecucco, C. (1993) *J. Biol. Chem.* **268,** 23784–23787
34. Schiavo, G., Shone, C. C., Bennet, M. K., Scheller, R. H., and Montecucco, C. (1995) *J. Biol. Chem.* **270,** 10566–10570
35. Williamson, L. C., Halpern, J. L., Montecucco, C., Brown, J. E., and Neale, E. A. (1996) *J. Biol. Chem.* **271,** 7694–7699
36. Yamasaki, S., Baumeister, A., Binz, T., Blasi, J., Link, E., Cornille, F., Roques, B., Fykse, E. M., Sudhof, T. C., Jahn, R., and Niemann, H. (1994) *J. Biol. Chem.* **269,** 12764–12772
37. Yamasaki, S., Binz, T., Hayashi, T., Szabo, E., Yamasaki, N., Eklund, M., Jahn, R., and Niemann, H. (1994) *Biochem. Biophys. Res. Commun.* **200,** 829–835
38. Cornille, F., Deloye, F., Fournie-Zaluski, M. C., Roques, B. P., and Poulain, B. (1995) *J. Biol. Chem.* **270,** 16826–16832
39. Gutierrez, L. M., Canaves, J. M., Ferrer-Montiel, A. V., Reig, J. A., Montal, M., and Viniegra, S. (1995) *FEBS Lett.* **372,** 39–43
40. Gutierrez, L. M., Viniegra, S., Rueda, J., Ferrer-Montiel, A. V., Canaves, J. M., and Montal, M. (1996) *J. Biol. Chem.* **272,** 2634–2639
41. Hunt, J. M., Bommert, K., Charlton, M. P., Kistner, A., Haberman, E., Augustine, G. J., and Betz, H. (1994) *Neuron* **12,** 1269–1279
42. Martin, F., Salinas, E., Vazquez, J., Soria, B., and Reig, J. A. (1996) *Biochem. J.* **320,** 201–205
43. Ferrer-Montiel, A. V., Gutierrez, L. M., Apland, J. P., Canaves, J. M., Gil, A., Viniegra, S., Adler, M., and Montal, M. (1998) *FEBS Lett.* **435,** 84–88
44. Kee, Y., and Scheller, R. H. (1996) *J. Neurosci.* **16,** 1975–1981
45. Grote, E., and Kelly R. B. (1996) *J. Cell Biol.* **132,** 537–547
46. Hao, J. C., Salem, N., Peng, X. R., Kelly, R. B., and Bennet, M. K. (1997) *J. Neurosci.* **17,** 1596–1603
47. Regazzi, R., Sadoul, K., Meda, P., Kelly, R. B., Halban, P. A., and Wollheim, C. B. (1996) *EMBO J.* **15,** 6951–6959
48. Hodges, R. S., Zhou, N. E., Kay, C. M., and Semchuk, P. D. (1990) *Peptide Res.* **3,** 123–137
49. Marmorstein, R., Carey, M., Ptashne, M., and Harrison, S. C. (1992) *Nature* **356,** 408–414
50. Nelson, J. W., and Kallenbach, N. R. (1986) *Proteins* **1,** 211–217
51. Nelson, J. W., and Kallenbach, N. R. (1990) *Biochemistry* **28,** 5256–5261
52. Dyson, H. J., Merutka, G., Waltho, J. P., Lerner, R. A., and Wright, P. E. (1992) *J. Mol. Biol.* **226,** 795–818
53. Dyson, H. J., Savre, J. R., Merutka, G., Shin, H. C., Lerner, R. A., and Wright,

P. E. (1992) *J. Mol. Biol.* **226,** 819–835
54. Blanco, J. F., and Serrano, L. (1995) *Eur. J. Biochem.* **230,** 634–649
55. Narayanan, U., Keiderling, T. A., Bonora, G. M., and Toniolo, C. (1986) *J. Am. Chem. Soc.* **108,** 2431–2437
56. Dong, A., Matsuura, J., Manning, M. C., and Carpenter, J. F. (1998) *Arch. Biochem. Biophys.* **355,** 275–281
57. Arunkumar, A. I., Kumar, T. K. S., and Yu, C. (1997) *Biochim. Biophys. Acta* **1338,** 69–76
58. Jayaraman, G., Kumar, T. K. S., Arunkumar, A. I., and Yu, C. (1996) *Biochem. Biophys. Res. Commun.* **222,** 33–37
59. Luidens, M. K., Figge, J., Breese, K., and Vajda, S. (1996) *Biopolymers* **39,** 367–376
60. Schonbrunner, N., Wey, J., Engels, J., Georg, H., and Kiefhaber, T. (1996) *J. Mol. Biol.* **260,** 432–445
61. Hamada, D., and Goto, Y. (1997) *J. Mol. Biol.* **269,** 479–487
62. Najbar, L. V., Craik, D. J., Wade, J. D., Salvatore, D., and McLeish, M. J. (1997) *Biochemistry* **36,** 11525–11533
63. MacPhee, C. E., Perugini, M. A., Sawyer, W. H., and Howlett, G. J. (1997) *FEBS Lett.* **416,** 265–268
64. Zhou, N. E., Kay, C. M., and Hodges, R. S. (1994) *Protein Eng.* **7,** 1365–1372
65. Adamson, J. G., Zhou, N. E., and Hodges, R. S. (1993) *Curr. Opin. Biotechnol.* **4,** 428–437
66. Pellizzari, R., Rosetto, O., Lozzi, L., Giovedi, S., Johnson, E., Shone, C. C., and Montecucco, C. (1996) *J. Biol. Chem.* **271,** 20353–20358
67. Bierzynski, A., Kim, P. S., and Baldwin, R. L. (1982) *Proc. Natl. Acad. Sci. U. S. A.* **79,** 2470–2474
68. Brown, J. E., and Klee, W. A. (1971) *Biochemistry* **10,** 470–476
69. Lau, S. Y. M., Taneja, A. K., and Hodges, R. S. (1984) *J. Biol. Chem.* **259,** 13253–13261
70. Vinogradov, A. A., Mari, F., Humphreys, R. E., and Wright G. E. (1996) *Int. J. Pept. Protein Res.* **47,** 467–476
71. Munoz, V., Serrano, L., Jimenez, M. A., and Rico, M. (1995) *J. Mol. Biol.* **247,** 648–669
72. Blanco, F. J., Ortiz, A. R., and Serrano, L. (1997) *Folding Design* **2,** 123–133
73. Ramirez-Alvarado, M., Serrano, L., and Blanco, F. J. (1997) *Protein Sci.* **6,** 162–174
74. Zhou, N. E., Kay, C. M., and Hodges, R. S. (1992) *J. Biol. Chem.* **267,** 2664–2670
75. Zhou, N. E., Zhu, B. Y., Kay, C. M., and Hodges, R. S. (1992) *Biopolymers* **32,** 419–426
76. Cooper, T. M., and Woody, R. W. (1990) *Biopolymers* **30,** 657–676
77. Greenfield, N. J., and Hitchcock-DeGregori, S. E. (1995) *Biochemistry* **34,** 16797–16805

FEBS Letters 429 (1998) 78–82

FEBS 20336

Structural stabilization of botulinum neurotoxins by tyrosine phosphorylation

José A. Encinar[a], Asia Fernández[a], José A. Ferragut[a], José M. González-Ros[a], Bibhuti R. DasGupta[b], Mauricio Montal[c], Antonio Ferrer-Montiel[c,*]

[a]*Department of Neurochemistry, University Miguel Hernández, Cl Monóvar sln (Poligono de Carrús), E-03206 Elche (Alicante), Spain*
[b]*University of Wisconsin, Madison, WI 53706, USA*
[c]*Department of Biology, University of California at San Diego, La Jolla, CA 92093-0366, USA*

Received 20 March 1998; revised version received 28 April 1998

Abstract **Tyrosine phosphorylation of botulinum neurotoxins augments their proteolytic activity and thermal stability, suggesting a substantial modification of the global protein conformation. We used Fourier-transform infrared (FTIR) spectroscopy to study changes of secondary structure and thermostability of tyrosine phosphorylated botulinum neurotoxins A (BoNT A) and E (BoNT E). Changes in the conformationally-sensitive amide I band upon phosphorylation indicated an increase of the α-helical content with a concomitant decrease of less ordered structures such as turns and random coils, and without changes in β-sheet content. These changes in secondary structure were accompanied by an increase in the residual amide II absorbance band remaining upon H-D exchange, consistent with a tighter packing of the phosphorylated proteins. FTIR and differential scanning calorimetry (DSC) analyses of the denaturation process show that phosphorylated neurotoxins denature at temperatures higher than those required by non-phosphorylated species. These findings indicate that tyrosine phosphorylation induced a transition to higher order and that the more compact structure presumably imparts to the phosphorylated neurotoxins the higher catalytic activity and thermostability.**

Key words: Protein structure; Protein folding; Metalloprotease; Fourier transform infrared; Exocytosis

1. Introduction

Botulinum neurotoxin (BoNT), considered the most potent neurotoxin and the sole cause of the neuroparalytic disease botulism, blocks acetylcholine release at the neuromuscular junction and thus produces flaccid paralysis in skeletal muscles [1,2]. Because of the extremely selective mode of action, inhibition of neurotransmitter release, BoNT is now an important therapeutic agent in the treatment of several neurological disorders associated with uncontrolled muscular contractions or spasms [3].

BoNT (serotypes A–G) is produced by the bacterium *Clostridium botulinum* as a single chain of 150 kDa which undergoes proteolytic cleavage yielding a fully active dichain protein composed of a 100-kDa heavy chain (HC) and a 50-kDa light chain (LC), linked by a disulfide bond. The neurotoxin first binds to a specific neuronal surface receptor, is internalized by receptor-mediated endocytosis, and the LC is then translocated to the cytosol, where it acts [1,4]. The LCs are Zn^{2+}-dependent metalloproteases that selectively cleave proteins involved in targeting and fusion of presynaptic vesicles with the plasma membrane [1,4–6]. The result is induction of nerve dysfunction by inhibiting Ca^{2+}-evoked neurotransmitter release.

The long lasting paralytic effects exerted by BoNT in botulism or in its therapeutic application suggest that these proteins are highly stable inside neurons at 37°C. This stability contrasts with the in vitro thermolability of pure BoNT implying structural difference(s) between the in vivo and in vitro forms [7,8]. Our discovery that tyrosine phosphorylation of BoNTs increases both their catalytic activity and thermal stability [7], suggests that significant changes in protein conformation may ensue, as reported for the phosphorylation of other proteins [9]. We examined this question by FTIR spectroscopy to monitor structural changes produced by phosphorylation of two neurotoxin serotypes, BoNT A and BoNT E, and differential scanning calorimetry to investigate the effect on their thermal denaturation process. Tyrosine phosphorylation of BoNT A and E increased their α-helix content, as evidenced from the conformationally-sensitive amide I bands [10]. The increment in structural order was accompanied by an increase in the absorbance of the amide II band remaining upon H-D exchange, suggesting that the phosphorylated neurotoxins are structurally more compact and less accessible to the solvent than the non-phosphorylated forms. Furthermore, the phosphorylation-induced structural change promoted a stabilization of the folded proteins that was reflected in an increase in the temperature at which the phosphorylated neurotoxins denature.

2. Materials and methods

Deuterium oxide (D_2O, 99.9% by atom) was purchased from Sigma. Centrifugal filter device Biomax-50K was from Millipore, Bedford, MA, USA. Recombinant Src kinase (specific activity 900 000 U/mg) was from Upstate Biotechnology, Lake Placid, NY, USA.

2.1. Phosphorylation of BoNT A and E

BoNT A and E were purified and tyrosine phosphorylated as described [7,11,12]. Briefly, 1 mg of neurotoxins in 500 μl of 20 mM HEPES (pH 7.4), 20 mM $MgCl_2$, 1 mM EGTA, 2 mM dithiothreitol, 0.5 mM ATP were incubated with 30 units of Src kinase for 90 min at 30°C. Non-phosphorylated and phosphorylated neurotoxins were kept at −80°C until used. Non-phosphorylated neurotoxin refers to samples in which ATP was omitted. Tyrosine phosphorylation was monitored by Western immunoblotting using a anti-phosphotyrosine monoclonal antibody (clone 4G10, UBI) as described [7]. To quantify tyrosine phosphorylation as mol Pi/mol neurotoxin a 40-μl aliquot of the phosphorylation reaction was supplemented with 5 μCi of [γ-^{32}P]ATP (3000 Ci/mmol). Phosphorylated neurotoxins were bound to phosphocellulose filters (SpinZyme, Pierce) and washed with 0.75%

*Corresponding author. Fax: (34) 6) 665 86 80.
E-mail: aferrer@umh.es

PII S0014-5793(98)00571-7

phosphoric acid. Phosphocellulose filters were immersed and equilibrated in scintillation fluid and the radioactivity was counted.

2.2. Infrared spectroscopy

BoNTs aqueous buffer was exchanged for deuterated buffer by subjecting the samples to two centrifugation cycles in a Biomax-50K filter, followed by incubation in D_2O-based buffer (10 mM HEPES buffer, pH 7.0, 130 mM KCl, 30 mM NaCl) for 2 h at ~20°C and, thereafter, another round of centrifugation cycles. Each sample of BoNTs (20 μl, at 8 mg/ml) was placed between a pair of CaF_2 windows separated by a 50-μm thick mylar spacer in a Harrick Ossining demountable cell. Spectra were recorded on a Nicolet 520 instrument equipped with a DTGS detector and the sample chamber was continuously purged with dry air. A minimum of 600 scans per sample were taken, averaged, apodized with a Happ-Genzel function and Fourier-transformed to give a nominal resolution of 2 cm^{-1} [13]. Three spectra at 20°C of each BoNT sample were recorded. Temperature was kept constant with a circulating water bath. Contribution of buffer spectra was subtracted and the resulting spectra used for analysis.

2.3. Determination of secondary structure components

Protein secondary structure components were quantified from curve-fitting analysis by band decomposition of the original amide I band after spectra smoothing [14,15]. Spectrum smoothing was carried out applying the maximum entropy method, assuming that noise and bandshape follow a normal distribution [14]. The minimum bandwidth was set to 12 cm^{-1} [14]. The resulting spectra possess a signal/noise ratio better than 4500:1. Derivation of IR spectra was performed using a power of 3, breakpoint of 0.3, and Fourier self-deconvolution was performed using a Lorenztian bandwidth of 18 cm^{-1} and a resolution enhancement factor (k) of 2.0 [16,17]. To quantify the secondary structure, the number and position of the absorbance band components were taken from the deconvoluted spectra, the bandwidth was estimated from the derived spectra, and the absorbance height from the original spectra [14]. The iterative curve-fitting process was performed in CURVEFIT running under SpectraCalc (Galactic Industries Corp., Salem, NH, USA). The number, position and bandshape were kept fixed during the first 200 iterations. The fittings were further refined by allowing the band positions to vary for 50 additional iterations. The goodness of fit between experimental and theoretical spectra was assessed from the χ^2 values (1×10^{-5}–4.5×10^{-5}). The area of the fitted absorbance band components was used to calculate the percent of secondary structure [13–18].

2.4. Differential scanning calorimetry

Differential scanning calorimetry (DSC) was performed on a Microcal MC-2 microcalorimeter, as described [19]. The difference in the heat capacities between 1-ml aliquots of BoNTs at 1 mg/ml (contained in the 'sample' cell of the instrument) and buffer alone ('reference' cell) were recorded by raising the temperature at a constant rate of 90°C/h.

3. Results and discussion

3.1. The helical content of BoNTs increases upon phosphorylation

The conformationally-sensitive amide I infrared absorbance band of BoNT A and E after tyrosine-specific phosphorylation (~0.5 mol Pi/mol toxin) were compared with non-phosphorylated neurotoxins. At this phosphorylation stoichiometry, both the LC and HC are similarly phosphorylated, and the activity and stability of the neurotoxins is augmented [7]. The original and the deconvoluted spectra of control and phosphorylated BoNTs samples are shown in Fig. 1. Tyrosine phosphorylation of BoNT A and E notably affected the spectral shape of the amide I band (Fig. 1, dashed lines). Although phosphorylated neurotoxins show the maxima observed in non-phosphorylated samples, the relative intensities of specific bands appear altered, suggesting that tyrosine phosphorylation modulates the relative content of secondary structural components. The individual components may be discerned upon application of resolution-enhancement and band-narrowing techniques [14,15]. Band-narrowing deconvolution of the amide I band showed that BoNT A and BoNT E exhibit maxima at approximately 1690, 1680, 1668, 1652, 1640, 1630 and 1615 cm^{-1}. Whereas the 1615-cm^{-1} component corresponds to amino acid side chain vibration, all the other maxima are assigned to vibration of the carbonyl group in peptide bonds within different secondary structural motifs [10]. The 1630-cm^{-1} component is assigned to β-structure, the 1640-cm^{-1} component to random structure, the 1652-cm^{-1} component to α-helix, the 1690- and 1668-cm^{-1} components to turns, and the 1680-cm^{-1} band includes contributions from

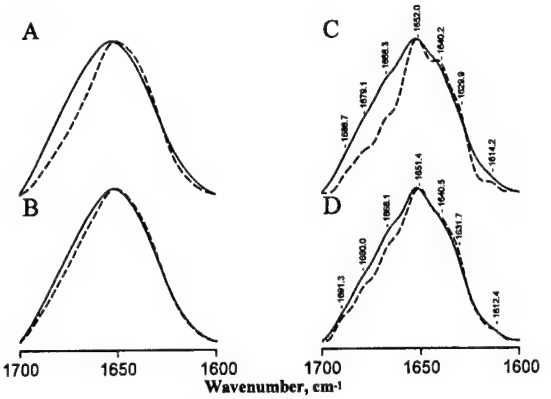

Fig. 1. Tyrosine phosphorylation modulates the secondary structure content of BoNT A and E. Infrared amide I band region of the original (A,B) and deconvoluted spectra (C,D) of BoNTA (A,C) and BoNT E (B,D) from control (solid line) and tyrosine phosphorylated samples (dashed line). Neurotoxins (8 mg/ml) were in D_2O medium prepared from 10 mM HEPES, pH 7.0, 130 mM KCl and 30 mM NaCl. Spectra were taken at 20°C and corrected from the buffer contribution by subtracting the spectrum characteristic of the buffer. Three spectra were acquired for each BoNT sample. Fourier self-deconvolution was carried out with a Lorentzian band of 18 cm^{-1} half-width, and a resolution enhancement factor of 2.0.

Table 1
Denaturation temperatures of non-phosphorylated and phosphorylated BoNTs

	BoNT A		BoNT E	
	Control	Phosphorylated	Control	Phosphorylated
T_d (°C) DSC[a]	51.1	53.0	50.5	53.2
T_d (°C) FT-IR[b]	50.5	53.5	51.3	55.1

[a]Denaturation temperatures were obtained from the DSC thermograms as the temperature at which the transition endotherm peaks [27,28]. Because of the need of large amounts of protein for DSC analysis, measures correspond to a single experiment.
[b]Denaturation temperatures correspond to the inflexion point of the sigmoidal curve obtained when the changes in the width at half-height of the amide I absorbance band are plotted as a function of the temperature (Fig. 4). Values correspond to three independent measurements. Experimental error is ≤10%.

turns as well as from the (0,π) β-sheet vibration band [10,20–22]. The secondary structures of non-phosphorylated and phosphorylated BoNTs were quantified using a maximum entropy method that reduces spectral noise providing a more accurate estimate of secondary structure [14,15]. Fig. 2 illustrates band-fitting analysis of the original amide I band of non-phosphorylated BoNT A (Fig. 2A) and BoNT E (Fig. 2B) and the corresponding phosphorylated species (Fig. 2C,D). Note that BoNT A shows a higher content of α-helix than BoNT E (Fig. 2E), consistent with other reports [23]. Upon phosphorylation, the α-helix content of BoNT A increased from 36% to 50% (Fig. 2E), and for BoNT E it augmented from 26% to 43% (Fig. 2E). This increment in α-helical structure was concomitant with a ≈40% decrease in less ordered structures such as turns (1668 cm^{-1}) and/or random coils (1640 cm^{-1}), without altering the β-sheet content (Fig. 2E). Therefore, these findings indicate that tyrosine phosphorylation promotes a disorder-to-order transition in the neurotoxin structure.

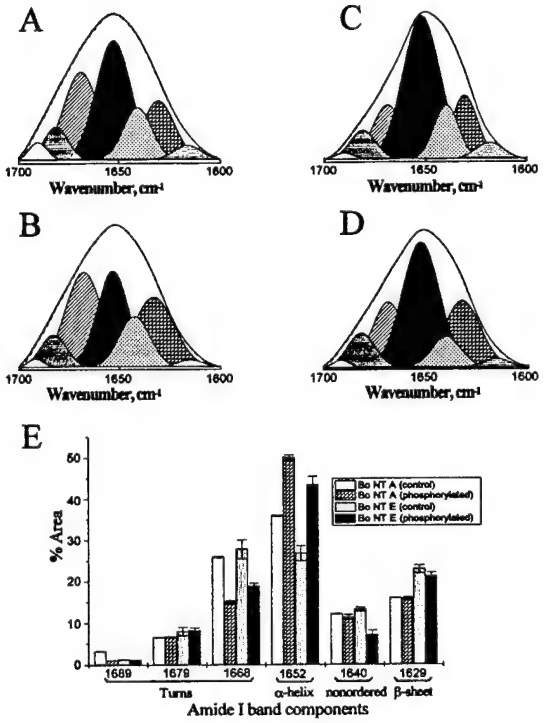

Fig. 2. Tyrosine phosphorylation increases the percent of α-helix secondary structure. Band-fitting analysis of the infrared amide I band of BoNT A (A,C) and BoNT E (B,D) from control (A,B) and phosphorylated samples (C,D). Each panel shows representative results from band-fitting analysis of BoNTs secondary structure. The discontinuous trace, superimposed on the original spectra, denotes the theoretical curve resulting from the contribution of all individual components, which are displayed as gaussian distributions under the spectra. E: Calculated percentages of all different components of the secondary structure of control and tyrosine phosphorylated BoNT A and BoNT E. Secondary structure elements were calculated by band decomposition and curve-fitting of the original amide I band after spectra smoothing [14,15]. Other conditions were as in legend to Fig. 1.

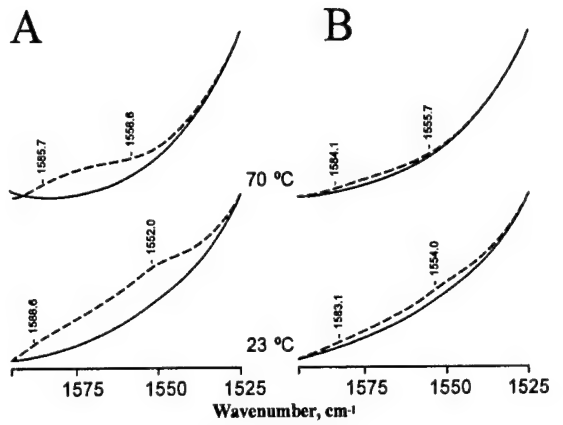

Fig. 3. Tyrosine phosphorylation of BoNT A and E promotes tighter packing. Phosphorylation-dependent changes in the amide II (1595–1525 cm^{-1} region) band of BoNT A (A) and BoNT E (B) remaining upon H-D exchange. Solid lines denote non-phosphorylated samples, and dashed lines indicate tyrosine-phosphorylated proteins. H-D exchange was carried out by 2-h incubation of samples in D_2O-based buffer followed by two washes with Biomax-50K centrifugal filters. The IR spectra were recorded in D_2O medium at the indicated temperatures during a heating cycle of 2.5 h. Protein concentration was 8 mg/ml. Contribution of buffer spectrum was subtracted.

3.2. The compactness of the BoNTs increases upon phosphorylation

The amide II band in proteins originates primarily from N-H bending in the peptide backbone [24,25]. Its residual intensity remaining after D_2O exchange arises from those NH groups unable to undergo H-D exchange and, therefore, it reports on the inaccessibility of the protein core to the solvent which, in turn, indicates the compactness of the protein [24,25]. Replacement of H_2O by D_2O from the non-phosphorylated neurotoxin resulted in the virtual disappearance of the amide II absorbance band centered at 1550 cm^{-1} (Fig. 3, lower panels, solid lines). Phosphorylated species, however, exhibited a substantial residual amide II band absorbance (Fig. 3, lower panels, dashed lines), which partly remained even after heating at 70°C (Fig. 3, upper panels). These results indicate a hindrance of H-D exchange in phosphorylated BoNTs, presumably because of the increased compactness of the structure. Taken together, the spectral changes in the amide I and the amide II upon phosphorylation suggest that the non-exchangeable hydrogens correspond to those involved in the newly generated α-helical structure.

3.3. The thermal stability of BoNTs increases upon phosphorylation

Non-phosphorylated neurotoxins displayed minor alterations on the spectral shape of the amide I band upon increasing the temperature up to 70°C (Fig. 4, solid lines). In contrast, for tyrosine-phosphorylated BoNTs the appearance of two components at 1618 and 1685 cm^{-1} (Fig. 4, dashed lines), which correspond to interactions between extended chains, was detected. This observation has been interpreted as a consequence of aggregation of thermally unfolded proteins [13,25–27]. The heat-induced denaturation process was irreversible as evidenced by the lack of recovery of the initial

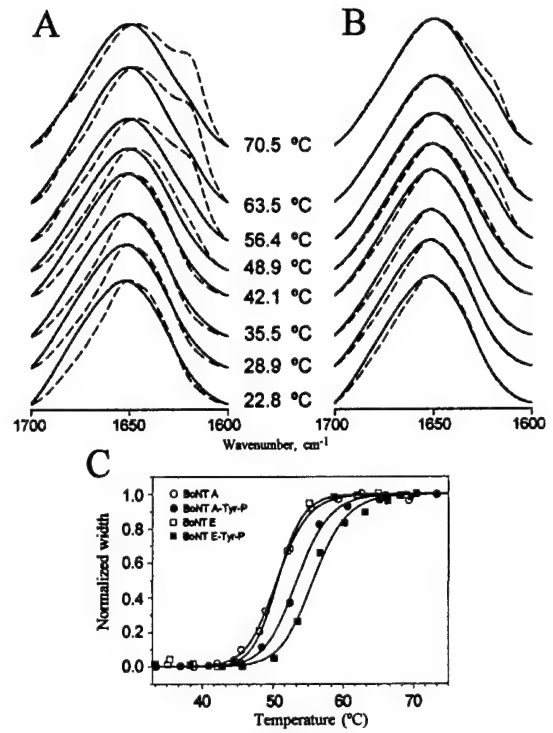

Fig. 4. Tyrosine phosphorylation increases the thermostability of BoNT A and BoNT E. Temperature dependence of the amide I band of BoNT A (A) and BoNT E (B) for control (solid line) and phosphorylated (dashed line) proteins. IR spectra were recorded in D_2O medium at the indicated temperatures during a heating cycle of 2.5 h. C: To determine the denaturing temperature, changes in the width at half-height of the amide I band were measured, normalized and plotted as a function of the temperature at which the spectrum was recorded. The data were described by the logistic equation:

$$\frac{w}{w_{max}} = \frac{1}{1+\left(\frac{T}{T_d}\right)^n}$$

where w denotes the width at half-height of the amide I band, w_{max} the maximal width at half-height, n the slope of the sigmoid, T the temperature, and T_d the denaturing temperature which corresponds to the inflexion point of the sigmoidal curve. Experimental data were fitted to the logistic equation with a non-linear least-squares regression algorithm using MicroCal ORIGIN version 2.8 (Microcal, Amherst). Solid lines depict the best fit to a sigmoidal curve. Denaturing temperatures are listed in Table 1.

spectral shape upon cooling the heated samples back to 20°C (data not shown).

The temperature-dependent changes in the width at half-height of the amide I IR band, plotted as a function of the temperature, display a sigmoidal shape with an inflexion point that corresponds to the denaturation temperature (Fig. 4C) [27]. Accordingly, BoNT A was found to denaturate at 50.5°C and BoNT E at 51.1°C, while phosphorylated BoNT A denatured at 53.5°C, and BoNT E at 55.1°C, i.e. 3–5°C higher than non-phosphorylated neurotoxins (Fig. 4C). The increased thermal stability was also detected by DSC, which measures directly the energetics of the heat-induced denaturation [28]. DSC demonstrated that phosphorylation induced a thermal stabilization, which was manifested as an increase of 2–3°C of the melting temperature (Table 1). These findings indicate that tyrosine phosphorylation of botulinum neurotoxins induces a conformation characterized by higher thermostability.

3.4. *Structural basis of the functional modulation of BoNTs by tyrosine phosphorylation*

Our findings show that tyrosine phosphorylation induces a disorder-to-order structural transition characterized by a significant increase in α-helical content with a decrease in less ordered structures. Consequently, phosphorylated BoNTs exhibit tighter packing than the non-phosphorylated species and denature at temperatures higher than those required for non-phosphorylated neurotoxins. The induction of structural order favors side chain interactions by hydrogen bond formation, an enthalpic gain. Higher order also augments the compactness of the protein, which presumably decreases the number of cavities, an entropic gain [9,29]. This mechanism to increase protein stability resembles that proposed to account for the extreme stability of thermophile enzymes, which are highly ordered and tightly packed structures [30]. We suggest that the more compact structure may account for the augmentation of the LC catalytic activity produced by tyrosine phosphorylation [7]. However, we cannot exclude a contribution of the HC to the structural changes observed in this study. Hence, additional studies are needed to determine the structural modulation of each neurotoxin chain by tyrosine phosphorylation.

Acknowledgements: This work was supported by grants from the Spanish DGICYT 95PM-0108 to (J.M.G.-R.) and PB93-0934 (to J.A.F.), the DAMD 17-93-C-3100 from the US Army Medical Research and Material Command (to M.M.), and an unrestricted generous gift from Athena Neurosciences (to B.R.D.G.). J.A.E. is recipient of a predoctoral fellowship from the Ministerio de Educación y Ciencia of Spain.

References

[1] Montecucco, C. and Schiavo, G. (1994) Molec. Microbiol. 13, 1–8.
[2] Ahnert-Hilger, G. and Bigalke, H. (1995) Prog. Neurobiol. 46, 83–96.
[3] Jankovic, J. and Hallett, M. (Eds.) (1994) Therapy with Botulinum Toxin, Marcel Dekker, New York, NY.
[4] Montecucco, C., Papini, E. and Schiavo, G. (1994) FEBS Lett. 346, 92–98.
[5] Jahn, R. and Südhof, T.C. (1994) Annu. Rev. Neurosci. 17, 219–246.
[6] Südhof, T.C. (1995) Nature 375, 645–653.
[7] Ferrer-Montiel, A.-V., Canaves, J.M., DasGupta, B.R., Wilson, M.C. and Montal, M. (1996) J. Biol. Chem. 271, 18322–18325.
[8] Kitamura, M., Sakaguchi, S. and Sakaguchi, G. (1969) J. Bacteriol. 98, 1173–1178.
[9] Johnson, L.N. and Barford, D. (1993) Annu. Rev. Biophys. Biomol. Struct. 22, 199–232.
[10] Braiman, M.S. and Rothschild, K.J. (1988) Annu. Rev. Biophys. Biophys. Chem. 17, 541–570.
[11] Sathyamoorthy, V. and DasGupta, B.R. (1985) J. Biol. Chem. 260, 10461–10466.
[12] Ferrer-Montiel, A.V., Montal, M.S., Díaz-Muñoz, M. and Montal, M. (1991) Proc. Natl. Acad. Sci. USA 88, 6418–6422.
[13] Fernández-Ballester, G., Castresana, J., Arrondo, J.L.R., Ferragut, J.A. and González-Ros, J.M. (1992) Biochem. J. 288, 421–426.
[14] Echabe, I., Encinar, J.A. and Arrondo, J.L.R. (1997) Biospectroscopy 3, 469–475.

[15] Bañuelos, S., Arrondo, J.L.R., Goñi, F.M. and Pifat, G. (1995) J. Biol. Chem. 270, 9192–9196.
[16] Moffatt, D.J., Kaupinnen, J.K., Cameron, D.G., Mantsch, H.H. and Jones, R.N. (1986) Computer Programs for Infrared Spectroscopy, NHCC Bulletin 18, National Research Council of Canada, Ottawa.
[17] Moffat, D.J. and Mantsch, H.H. (1992) Methods Enzymol. 210, 192–200.
[18] Surewicz, W.K., Mantsch, H.H. and Chapman, D. (1993) Biochemistry 32, 389–394.
[19] Artigues, A., Villar, M.T., Ferragut, J.A. and González-Ros, J.M. (1987) Arch. Biochem. Biophys. 258, 33–41.
[20] Arrondo, J.L.R., Mantsch, H.H., Mullner, N., Pikula, S. and Martonosi, A. (1987) J. Biol. Chem. 262, 9037–9043.
[21] Krimm, S. and Bandekar, J. (1986) Adv. Prot. Chem. 38, 181–364.
[22] Byler, D.M. and Susi, H. (1986) Biopolymers 25, 469–487.
[23] Singh, B.R., Wasacz, F.M., Strand, S., Jakobsen, R.J. and Das-Gupta, B.R. (1990) J. Protein Chem. 9, 705–713.
[24] Zhang, Y.P., Lewis, R.N.A.H., Hodges, R.S. and McEllaney, R.N. (1992) Biochemistry 31, 11572–11578.
[25] Baezinger, I.E. and Méthot, N. (1985) J. Biol. Chem. 270, 29129–29137.
[26] Surewicz, W.K., Leddy, J.J. and Mantsch, H.H. (1990) Biochemistry 29, 8106–8111.
[27] Castresana, J., Fernández-Ballester, G., Fernándes, A.M., Laynez, J.L., Arrondo, J.L.R., Ferragut, J.A. and González-Ros, J.M. (1992) FEBS Lett. 314, 171–175.
[28] Freire, E., Osdol, W.W., Mayorga, O.L. and Sanchez-Ruiz A, J.M. (1990) Annu. Rev. Biophys. Biophys. Chem. 19, 159–188.
[29] Shaw, A. and Bot, R. (1996) Curr. Opin. Struct. Biol. 6, 546–550.
[30] Szilagyi, A. and Zavodszky, P. (1995) Protein Eng. 8, 779–789.

FEBS Letters 435 (1998) 84–88

FEBS 20774

The 26-mer peptide released from SNAP-25 cleavage by botulinum neurotoxin E inhibits vesicle docking

Antonio V. Ferrer-Montiel[1,2,a], Luis M. Gutiérrez[b], James P. Apland[c], Jaume M. Canaves[a], Anabel Gil[b], Salvador Viniegra[b], Jennifer A. Biser[c], Michael Adler[c], Mauricio Montal[a,*]

[a]*Department of Biology, University of California San Diego, 9500 Gilman Dr, La Jolla, CA 92093-0366, USA*
[b]*Departamento de Neuroquímica, Instituto de Neurociencias and Facultad de Medicina, Universidad Miguel Hernández, San Juan, Spain*
[c]*Neurotoxicology Branch, U.S. Army Medical Research Institute of Chemical Defense, 3100 Ricketts Point Road, Aberdeen Proving Ground, MD 21010-5425, USA*

Received 3 August 1998

Abstract **Botulinum neurotoxin E (BoNT E) cleaves SNAP-25 at the C-terminal domain releasing a 26-mer peptide. This peptide product may act as an excitation-secretion uncoupling peptide (ESUP) to inhibit vesicle fusion and thus contribute to the efficacy of BoNT E in disabling neurosecretion. We have addressed this question using a synthetic 26-mer peptide which mimics the amino acid sequence of the naturally released peptide, and is hereafter denoted as ESUP E. This synthetic peptide is a potent inhibitor of Ca^{2+}-evoked exocytosis in permeabilized chromaffin cells and reduces neurotransmitter release from identified cholinergic synapses in in vitro buccal ganglia of *Aplysia californica*. In chromaffin cells, both ESUP E and BoNT E abrogate the slow component of secretion without affecting the fast, Ca^{2+}-mediated fusion event. Analysis of immunoprecipitates of the synaptic ternary complex involving SNAP-25, VAMP and syntaxin demonstrates that ESUP E interferes with the assembly of the docking complex. Thus, the efficacy of BoNTs as inhibitors of neurosecretion may arise from the synergistic action of cleaving the substrate and releasing peptide products that disable the fusion process by blocking specific steps of the exocytotic cascade.**

Key words: SNARE hypothesis; Neurosecretion; Exocytosis; Synaptic transmission; Protein-protein interaction

1. Introduction

A widely held view considers that the process of vesicle fusion with the plasma membrane which occurs during neuronal exocytosis is mediated by SNARE proteins [1–5]. This family of membrane proteins provides a specific means of pairing vesicles (v-SNAREs) with target (t-SNAREs) membranes [1–5]. *Clostridial* neurotoxins are metalloproteases that cleave specific components of the v-SNARE and t-SNARE and abolish neurotransmitter release. Botulinum neurotoxins (BoNT) B, D, F, and G, and the structurally related tetanus toxin specifically cleave VAMP at different sites [6,7]; BoNT A and E cleave SNAP-25 at the C-terminus [8,9], and BoNT C cuts syntaxin and SNAP-25 [10,11]. Proteolysis of each of these substrates produces a truncated protein and releases a peptide product [6–11]. It has been proposed that these peptide products may also prevent the formation of the core complex and thereby abrogate Ca^{2+}-triggered exocytosis [12,13]. This hypothesis is supported by the finding that truncated fusion proteins and synthetic peptides that mimic the amino acid sequence of segments from synaptotagmin [14,15], SNAPs [16], synaptobrevin [17], syntaxin [18], Ca^{2+} channels [19], and SNAP-25 [12,13,20] are specific inhibitors of neurosecretion. In particular, a 20-mer peptide encompassing the C-terminal domain of SNAP-25 blocked exocytosis by inhibiting vesicle docking in permeabilized chromaffin cells [12,13]. The term ESUP (excitation-secretion uncoupling peptide) was coined to highlight this inhibitory activity [12]. Although these results suggest that peptide products resulting from substrate cleavage by BoNTs may block vesicle fusion, experimental support to substantiate this notion is still limited.

Here, we show that a 26-mer peptide corresponding to the amino acid sequence of the peptide product released by BoNT E cleavage of SNAP-25, referred to as ESUP E, efficiently and selectively blocks Ca^{2+}-evoked exocytosis in chromaffin cells and neurotransmitter release in *Aplysia* cholinergic synapses. Our results are consistent with the notion that ESUP E prevents vesicle docking by interfering with the assembly of the synaptic ternary complex formed by SNAP-25, VAMP and syntaxin.

2. Material and methods

2.1. Reagents

[^{3}H]Noradrenaline was from DuPont-NEN (Boston, MA). t-Boc and Fmoc amino acids, with standard side chain protecting groups, were obtained from Applied Biosystems (Foster City, CA), NovaBiochem (La Jolla, CA) or Peninsula Laboratories (Belmont, CA). Solvents, reagents and resins for peptide synthesis were obtained from Applied Biosystems (Foster City, CA), Percoll from Pharmacia, collagenase (EC 3.4.24.3) from Boehringer Mannheim (Germany), anti-SNAP-25 mAb (clone SM81) from Sternberger (Baltimore, MD), anti-syntaxin mAb (clone HPC1) from Sigma (St. Louis, MO) and anti-VAMP Ab from Stressgen (Canada). Agarose-conjugated protein G was from Pierce (Rockford, IL). BoNTs were kindly provided by Drs. B.R. DasGupta and M. Goodnough (University of Wisconsin). All other reagents were of analytical grade from Sigma.

*Corresponding author. Fax: (1) (619) 534-0931.
E-mail: montal@biomail.ucsd.edu

[1]A.V.F.-M. and L.M.G. contributed equally to this work.

[2]Present address: Centro de Biología Molecular y Celular, Universidad Miguel Hernández, C/ Monóvar s/n, 03206 Elche, Spain.

Abbreviations: BoNT, botulinum neurotoxin; SNAP-25, synaptosomal associated protein of 25 kDa; ESUP, excitation-secretion uncoupling peptide; VAMP, vesicle associated membrane protein; SNARE, SNAP receptor; v-SNARE, vesicle-SNARE; t-SNARE, target-SNARE; NSF, *N*-ethylmaleimide-sensitive fusion protein; SNAP, soluble NSF attachment protein; IPSC, inhibitory postsynaptic current; ACh, acetylcholine

PII: S0014-5793(98)01012-6

2.2. Peptide synthesis and purification

ESUP E (SNAP-25 [181–206]: IMEKADSNKTRIDEANQRATKMLGSG) and ESUP E^{RDM} (ESDNDTRAIKITQAGSMKRMGLNAKE) were synthesized by Fastmoc Fmoc chemistries in an Applied Biosystems 431A automated solid-phase peptide synthesizer, cleaved and purified as described [12,13].

2.3. Activation of BoNT E

The single chain BoNT E in 25 mM HEPES was converted to the 'nicked' di-chain form by treatment with 0.3 mg/ml trypsin XI for 30 min at 37°C, followed by incubation with 0.5 mg/ml soybean trypsin inhibitor for 15 min at room temperature. Aliquots of the nicked toxin were frozen at −80°C, then thawed and treated with 1 mM dithiothreitol (DTT) immediately before use to expose the active site of the light chain protease.

2.4. Chromaffin cell cultures and secretion assays

Chromaffin cell cultures were prepared from bovine adrenal glands by collagenase digestion and further separated from debris and erythrocytes by centrifugation on Percoll gradients as described [12,13]. Cells were maintained in monolayer cultures at a density of 625 000 cells/cm^2 and were used 3–6 days after plating. All the experiments were performed at 37°C. Secreted [^{3}H]noradrenaline was assayed in digitonin-permeabilized cells as described [12,13]. The CPM released from control cells under basal conditions was ~3000, and increased to ~11 000 when stimulated with 10 μM Ca^{2+}. The total number of counts obtained from detergent-permeabilized cells was ~110 000. Thus, the normalized basal release represents 3.5% of the total secretion, and the Ca^{2+}-evoked component accounts for ~10% of the total. Statistical significance was calculated using Student's *t*-test with data from ≥4 independent experiments.

2.5. Immunoprecipitation of the ternary complex SNAP-25/VAMP/syntaxin from solubilized rat brain synaptosomes

Rat brain synaptosomes were prepared from brain cortices as described [21]. Synaptosomes (100 μg) were solubilized in radioimmunoprecipitation assay buffer (50 mM Tris-HCl pH 7.4, 150 mM NaCl, 1% Nonidet P-40, 0.25% deoxycholate, 1 mM EGTA, 1 mM NaF, 1 mM Na_3VO_4, 1 mM phenylmethylsulfonyl fluoride and 5 mM iodoacetamide), incubated with or without 100 μM ESUPs for 2 h at 4°C, unless otherwise indicated. Insoluble material was removed by centrifugation at 10 000×*g* for 30 min at 4°C. Immunopurification of the ternary complex SNAP-25/VAMP/syntaxin from the soluble material was achieved by using an overnight incubation with anti-SNAP-25 monoclonal antibody (1 μg mAb/100 μg protein). Immunocomplexes were captured with agarose-conjugated protein G (100 μl, 50% slurry), and washed six times with 500 μl of radioimmunoprecipitation buffer at 4°C. Immunoprecipitates were dissolved with 50 μl of SDS-PAGE buffer, boiled 5 min, separated by SDS-PAGE and analyzed by immunoblotting. Blots were probed with the anti-SNAP-25 mAb, an anti-syntaxin mAb and an anti-VAMP Ab. Bands were visualized using the ECL system, and quantified using the public domain NIH Image program version 1.57 [13]. Data are given as mean ± S.E.M., with *n* (number of experiments) = 3.

2.6. Inhibition of neurotransmitter release in Aplysia synapses

Experiments were performed with neuronal preparations from the marine mollusc *Aplysia californica*. Intraneuronal inhibition of nerve-evoked release of acetylcholine (ACh) was measured at identified cholinergic synapses of *Aplysia* buccal ganglia [22,23]. The ganglia were surgically removed and pinned to the Sylgard lined bottom of an acrylic chamber, and the connective tissue capsule was excised. The soma of identified pre- and postsynaptic cholinergic neurons were impaled with glass microelectrodes (2–4 MΩ) filled with 2 M potassium acetate. Action potentials were evoked in presynaptic neurons by suprathreshold depolarizing stimuli applied at 0.1 Hz. Neurotransmitter release was assessed by measuring the amplitudes of inhibitory postsynaptic currents (IPSCs) in voltage-clamped follower neurons. Presynaptic potentials and postsynaptic currents were digitized and stored on a personal computer using pClamp software (Axon Instruments, Foster City, CA). Only responses that were not accompanied by spontaneous activity were analyzed. The preparation was superfused continuously at a rate of 1 ml/min with artificial sea water containing in mM: NaCl 480; KCl 10; $CaCl_2$ 10; $MgCl_2$ 20; $MgSO_4$ 30; $NaHCO_3$ 2.5; HEPES 10, at pH 7.8, maintained at room temperature. ESUP E and ESUP E^{RDM} (5 mM) were dissolved in 600 mM NaCl containing 1% (w/v) fast green FCF dye to aid in visualizing the volume injected. The solution was air pressure-injected into the presynaptic cell by micropipette. A maximum pressure of 60 psi was used to introduce an adequate volume of solution into the presynaptic cell as indicated by the appearance of intracellular dye. The volume of solution injected was ≤10% of the estimated cell volume, yielding a final intracellular peptide concentration ≤100 μM. BoNT E concentration in the micropipette was 3.3 μM.

3. Results and discussion

3.1. A peptide mimicking the 26-aa peptide fragment released by BoNT E cleavage of SNAP-25 blocks exocytosis

Cleavage of the C-terminus of SNAP-25 by BoNT E releases a 26-mer peptide that may block neurosecretion [12,13]. To test this hypothesis, we synthesized this 26-mer peptide (ESUP E) and assayed the presumed inhibitory activity on Ca^{2+}-evoked catecholamine release from digitonin-permeabilized chromaffin cells. ESUP E blocked noradrenaline

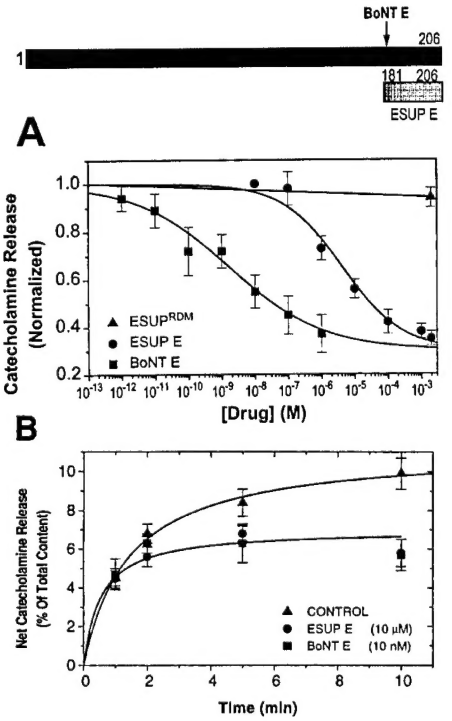

Fig. 1. ESUP E blocks Ca^{2+}-dependent catecholamine secretion from permeabilized chromaffin cells. Top: Schematic representation of SNAP-25 with the cleavage site for BoNT E. ESUP E represent the peptide product (aa 181–206) released by BoNT E cleavage of SNAP-25. Bottom: A: Concentration-dependent inhibition of Ca^{2+}-evoked catecholamine release from permeabilized chromaffin cells by BoNT E, ESUP E and ESUP E^{RDM}. Net release is given as mean ± S.E.M. with *n* (number of experiments performed in triplicate) = 4. Solid lines depict the best fit to the logistic equation: $B/B_{max} = 1/(1+([blocker]/IC_{50})^n)$, where B denotes the extent of block, B_{max} represents the maximal block; IC_{50} denotes the concentration of blocker (BoNT E or ESUP E) that produces half-maximal block, and n is the Hill coefficient of the blocking activity. For BoNT E the values were $IC_{50} = 1.8 \pm 1.3$ nM, n = 0.5; and for ESUP E, $IC_{50} = 250 \pm 75$ nM, n = 0.6. B: Time course of the net noradrenaline release (Ca^{2+}-stimulated minus basal) obtained in presence or absence of 100 μM ESUP E or 10 nM BoNT E.

release with an IC_{50}=250 ± 75 nM, and a maximal inhibition of ~70% (Fig. 1A). The ESUP inhibitory activity was similar to that elicited by BoNT E with respect to maximal inhibition (~70%) but was ~140-fold less efficient (BoNT E IC_{50}=1.8 ± 1.3 nM). The sequence specificity of ESUP activity was assessed by synthesizing a randomized version of the peptide (ESUP E^{RDM}), which was proven inert in blocking catecholamine release at concentrations up to 100 μM (Fig. 1A).

To identify the step of the exocytotic cascade blocked by ESUP E, we investigated its activity on the kinetics of the secretory process and compared it with that produced by BoNT E (Fig. 1B). Permeabilized cells were incubated with ESUP E or DTT-reduced BoNT E for 5 min, and secretion was evoked by Ca^{2+} pulses of different duration. Incubation of permeabilized chromaffin cells with 10 μM ESUP E or 10 nM BoNT E inhibited ~60% of catecholamine release, primarily by altering the slow phase of secretion (Fig. 1B), suggesting that the vesicle pools upstream of docking and priming steps are sensitive to the action of ESUP E and BoNT E [24–26]. These data indicate that the 26-mer peptide released by BoNT E cleavage of SNAP-25 is a potent and specific uncoupler of Ca^{2+}-evoked exocytosis, and suggest that the efficiency of BoNT E to disable the fusion process may arise from the combined action of cleaving a protein critical for the assembly of the fusion complex, and by releasing a small peptide which, in turn, may interfere with the formation of the complex.

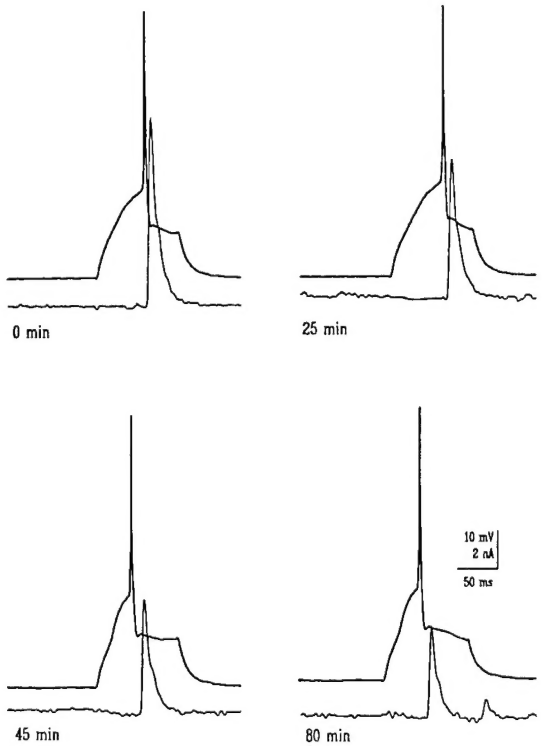

Fig. 2. ESUP E blocks ACh release by the presynaptic neuron in a cholinergic synapse in *Aplysia* buccal ganglia. ACh release was monitored as the amplitude of the IPSC (lower trace) elicited by an evoked action potential (upper trace) in the presynaptic neuron. Recordings show the decrement of the IPSC amplitude after injection of ESUP E into the presynaptic neuron at zero time.

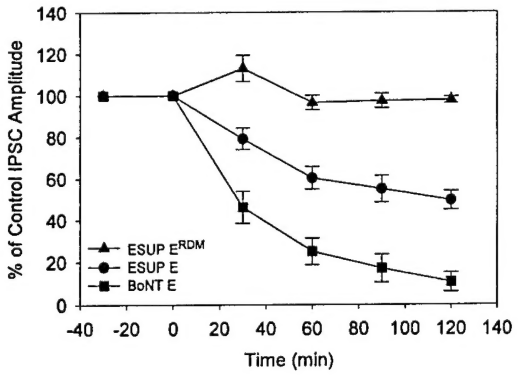

Fig. 3. ESUP E and BoNT E inhibit IPSC amplitude in *Aplysia* buccal ganglion synapses. Active ESUP E (n=10), the inactive random sequence ESUP E^{RDM} analog (n=8), or BoNT E (n=7) were injected into the presynaptic neuron at zero time. IPSC amplitude was inhibited after injection of active ESUP E and BoNT E but not by injection of the inactive analog. Mean ± S.E.M.

3.2. *ESUP E and BoNT E inhibit neurotransmitter release in Aplysia cholinergic synapses in vitro*

Release of ACh by the presynaptic neuron in response to electrically evoked action potentials was assessed from the amplitudes of the evoked IPSCs in a voltage-clamped postsynaptic neuron. Fig. 2 shows superimposed action potentials and IPSCs in a typical experiment. ESUP E was injected into the presynaptic neuron at zero time (top left panel), and the resultant decline of IPSC amplitude is shown at three successive time points. The IPSC amplitude declined to 52% of the control value 120 min after the injection of ESUP E. The decrease of IPSC amplitude was gradual and incomplete, typically requiring 2 h to reach a stable value of 30–70% of the control. The time course of the effect of peptides or toxin injection on IPSC amplitude is shown in Fig. 3. BoNT E, ESUP E or ESUP E^{RDM} were injected at time zero. The increase of IPSC amplitude immediately following the injection of ESUP E^{RDM} was not considered to be significant since such increases were a frequent consequence of pressure injection of any compound, and IPSC amplitudes typically returned to control values within 20 min. No further reduction of responses occurred in cells injected with the random-sequence control peptide, whereas IPSCs in cells injected with BoNT E and active ESUP E declined to a stable level over the ensuing 120 min.

The rate and extent of IPSC inhibition caused by BoNT E was greater than that produced by ESUP E: the amplitude was attenuated by 50% in 28 min and by 90% in 120 min by BoNT E, whereas inhibition by ESUP E was only 50% at 120 min. The more rapid and nearly complete IPSC decrement caused by BoNT E supports the concept that the inhibition caused by the toxin protease is a consequence of both a decrease in available SNAP-25 and an accumulation of cleavage products.

3.3. *ESUP E inhibits vesicle docking by interfering with the formation of the ternary complex comprising SNAP-25, VAMP, and syntaxin*

Since the C-terminal domain of SNAP-25 binds tightly to VAMP and syntaxin during vesicle docking, forming a highly stable ternary complex, it is conceivable that ESUP E blocks

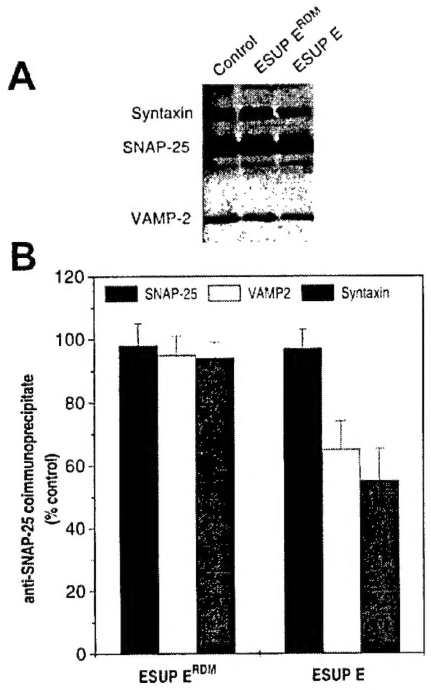

Fig. 4. ESUP E disrupts the interaction between SNAP-25, VAMP and syntaxin. A: Immunoprecipitates of the ternary complex SNAP-25/VAMP/syntaxin from rat brain synaptosomes incubated without (Control) or with 100 μM ESUP E or ESUP E^{RDM}. Immunocomplexes were analyzed using SDS-PAGE (4–20%) under non-reducing conditions, and immunoblotted with an anti-syntaxin mAb, anti-SNAP-25 mAb and anti-VAMP Ab. B: Data of three different experiments were quantified by image analysis, and values normalized with respect to that of control.

the docking process by competition with SNAP-25 for binding to the ternary complex. To examine this question, we studied the effect of ESUP E on the interaction of SNARE proteins in digitonin-permeabilized chromaffin cells. We did not observe coimmunoprecipitation of all the SNARE proteins with the anti-SNAP-25 mAb (data not shown), as reported by others [27]. We therefore turned to rat brain synaptosomes as an alternative preparation [3,20,28]. Since the SNARE complex forms spontaneously during synaptosome preparation and solubilization, we evaluated if ESUP E could displace SNAP-25 from the ternary complex and, therefore, dissociate the preformed aggregate or interfere with its assembly. The experimental protocol involved detergent solubilization of synaptosomes, incubation with ESUP E or ESUP E^{RDM}, immunopurification of the ternary complex using an anti-SNAP-25 mAb followed by separation of the components using SDS-PAGE. Immunoblots probed with specific antibodies raised against syntaxin, SNAP-25 and VAMP revealed the presence of the three proteins in the immunoprecipitate (Fig. 4A). Incubation with 100 μM ESUP E inhibited the coimmunoprecipitation of VAMP and syntaxin without affecting the immunopurification of SNAP-25.

A quantitative analysis of the immunoblots is shown in Fig. 4B. An excess of ESUP E inhibited the coimmunoprecipitation of VAMP by ~30% and of syntaxin by ~40%, whereas no effect was detected with ESUP E^{RDM}, in accord with expectations. The partial inhibition produced by ESUP E (100 μM) may be accounted for by its relatively low affinity (Fig. 1A). Nonetheless, the fact that a short peptide may interfere with the assembly or stability of an SDS-resistant complex is highly significant, and provides experimental support for the notion that ESUP E inhibits vesicle docking by preventing the formation of the essential ternary complex. These findings suggest that ESUP E may compete with SNAP-25 for binding to VAMP and interrupt the ensuing chain of protein-protein interactions that lead to vesicle fusion.

3.4. Molecular mechanism of ESUPs biological activity

The finding that the 26-mer peptide released from SNAP-25 cleavage by BoNT E mimics the inhibitory action of this neurotoxin on neurosecretion (Fig. 1), and on synaptic transmission (Figs. 2 and 3), provides support to the tenet that BoNTs abrogate vesicle fusion by the combined action of cleaving the substrate and releasing peptide products which block the docking or/and priming steps of the exocytotic cascade. The result that the ternary complex is specifically disrupted by an excess of ESUP E (Fig. 4) supports this view. The fact that the 20-mer ESUP A (SNAP-25 [187–206]: SNKTRIDEANQRATKMLGSG), corresponding to the C-terminal sequence of SNAP-25, arrests the ATP-dependent maturation of the secretory granules and promotes the accumulation of secretory vesicles near the plasma membrane is in accord with this notion [13]. Recent studies implicate the C-terminal segment of SNAP-25 encompassing residues 180–196 in vesicle docking and in a late post-docking step [29,30]. Our finding that ESUP E is a more efficient inhibitor of neurosecretion than ESUP A supports this conclusion. Thus, ESUPs mimicking specific protein domains provide novel tools to dissect their contribution to different steps of neurosecretion.

Acknowledgements: We thank B. R. DasGupta and M. Goodnough for purified BoNT E. This work was supported by Grants from the Spanish DGICYT PM-0110 (to S.V.), the US Army Medical Research and Materiel Command DAMD 17-93-C-3100 and DAMD 17-98-C-8040 (to M.M.), and a Postdoctoral Fellowship from the Dystonia Medical Research Foundation (to J.M.C.).

References

[1] Rothmann, J.E. (1994) Nature 372, 55–63.
[2] Matthews, G. (1996) Annu. Rev. Neurosci. 19, 219–233.
[3] Südhof, T.C. (1995) Nature 375, 645–653.
[4] Calakos, N. and Scheller, R.H. (1996) Physiol. Rev. 76, 1–29.
[5] Weber, T., Zemelman, B.V., McNew, J.A., Westermann, B., Gmachl, M., Parlati, F., Söllner, T.H. and Rothman, J.E. (1998) Cell 92, 759–772.
[6] Schiavo, G., Benfenati, F., Poulain, B., Rossetto, O., Polverino de Laureto, P., DasGupta, B.R. and Montecucco, C. (1992) Nature 359, 832–835.
[7] Yamasaki, S., Baumeister, A., Binz, T., Blasi, J., Link, E., Cornille, F., Rogues, B., Fykse, E.M., Sudhof, T.C., Jahn, R. and Niemann, H. (1994) J. Biol. Chem. 269, 12764–12772.
[8] Blasi, J., Chapman, E.R., Link, E., Binz, T., Yamasaki, S., De Camilli, P., Südhof, T.C., Niemann, H. and Jahn, R. (1993) Nature 365, 160–163.
[9] Schiavo, G., Santucci, A., DasGupta, B.R., Mehta, P.P., Jontes, J., Benfenati, F., Wilson, M.C. and Montecucco, C. (1993) FEBS Lett. 335, 99–103.
[10] Schiavo, G., Shone, C.C., Bennett, M.K., Scheller, R.H. and Montecucco, C. (1995) J. Biol. Chem. 270, 10566–10570.

[11] Williamson, L.C., Halpen, J.L., Montecucco, C., Brown, J.E. and Neale, E.A. (1996) J. Biol. Chem. 271, 7694–7699.
[12] Gutierrez, L.M., Canaves, J.M., Ferrer-Montiel, A.V., Reig, J.A., Montal, M. and Viniegra, S. (1995) FEBS Lett. 372, 39–43.
[13] Gutierrez, L.M., Viniegra, S., Rueda, J., Ferrer-Montiel, A.V., Canaves, J.M. and Montal, M. (1997) J. Biol. Chem. 272, 2634–2639.
[14] DeBello, W.M., Betz, H. and Augustine, G.J. (1993) Cell 74, 947–950.
[15] Geppert, M., Goda, Y., Hammer, R.E., Li, C., Rosahl, T.W., Stevens, C.F. and Südhof, T.C. (1994) Cell 79, 717–727.
[16] DeBello, W.M., O'Connor, V., Dresbach, T., Whiteheart, S.W., Wang, S.S.-H., Scheweizer, F.E., Betz, H., Rothman, J.E. and Augustine, G.J. (1995) Nature 373, 626–630.
[17] Cornille, F., Deloye, F., Fournie-Zaluski, M.-C., Roques, B.P. and Poulain, B. (1995) J. Biol. Chem. 270, 16826–16832.
[18] Martin, F., Salinas, E., Vazquez, J., Soria, B. and Reig, J.A. (1996) Biochem. J. 320, 201–205.
[19] Mochida, S., Sheng, Z.H., Baker, C., Kobayashi, H. and Catterall, W.A. (1996) Neuron 17, 781–788.
[20] Metha, P.P., Battenberg, E. and Wilson, M.C. (1996) Proc. Natl. Acad. Sci. USA 93, 10471–10476.
[21] Huttner, W.B., Schiebler, W., Greengard, P. and De Camilli, P. (1983) J. Cell Biol. 96, 1374–1378.
[22] Gardner, D. and Kandel, E.R. (1977) J. Neurophysiol. 40, 333–348.
[23] Poulain, B., Tauc, L., Maisey, E.A., Wadsworth, J.D.F., Mohan, P.M. and Dolly, J.O. (1988) Proc. Natl. Acad. Sci. USA 85, 4090–4094.
[24] Hay, J.C. and Martin, T.F.J. (1992) J. Cell Biol. 119, 139–151.
[25] Bittner, M.A. and Holz, R.W. (1992) J. Biol. Chem. 267, 16219–16225.
[26] Parsons, T.D., Coorssen, J.R., Horstmann, H. and Almers, W. (1995) Neuron 15, 1085–1096.
[27] Misono, H., Nishiki, T.-I., Sekiguchi, M., Takahashi, M., Kamata, Y., Kozaki, S., Ohara-Imaizumi, M. and Kumakura, K. (1996) Brain Res. 737, 351–355.
[28] Hayashi, T., Yamasaki, S., Nauenburg, S., Binz, T. and Niemann, H. (1995) EMBO J. 14, 2317–2325.
[29] Lawrence, G.W., Foran, P., Mohammed, N., DasGupta, B.R. and Dolly, J.O. (1997) Biochemistry 36, 3061–3067.
[30] Barnajee, A., Kowalchyk, J.A., DasGupta, B.R. and Martin, T.F.J. (1996) J. Biol. Chem. 271, 20227–20230.